Title
Investigating the transcriptional targets and role of physiological activation of the unfolded protein response in Saccharomyces cerevisiae

Author
Van Dalfsen, Kelsey

Publication Date
2018

Peer reviewed|Thesis/dissertation

Investigating the transcriptional targets and role of physiological activation of the unfolded protein response in *Saccharomyces cerevisiae*

By

Kelsey M. Van Dalfsen

A dissertation submitted in partial satisfaction of the

requirements for the degree of

Doctor of Philosophy

in

Molecular and Cell Biology

in the

Graduate Division

of the

University of California, Berkeley

Committee in charge:

Professor Gloria Brar, Chair
Professor Andrew Dillin
Professor Jasper Rine
Professor James Olzmann

Summer 2018

Abstract

Investigating the transcriptional targets and role of physiological activation of the unfolded protein response in *Saccharomyces cerevisiae*

by

Kelsey M. Van Dalfsen

Doctor of Philosophy in Molecular and Cell Biology

University of California, Berkeley

Professor Gloria Brar, Chair

The endoplasmic reticulum (ER) maintains a lumenal environment favorable for the folding of at least 30% of the cell's protein complement. ER quality control mechanisms, including chaperone systems, ensure proper protein folding in this compartment. However, the burden of misfolded proteins within the ER lumen can exceed the capacity of the ER folding machinery. In such instances of ER stress, a conserved pathway called the unfolded protein response (UPR^{ER}) is induced. The budding yeast *Saccharomyces cerevisiae* harbor only the most conserved branch of this pathway, at the crux of which is the cytoplasmic splicing of a translationally repressed mRNA encoding the transcription factor Hac1. Splicing of the *HAC1* mRNA is executed by a conserved ER-localized stress sensor and endonuclease, Ire1. Transcriptional targets of the UPR^{ER} in yeast include ER resident chaperones, ER associated decay (ERAD) machinery, and membrane biogenesis factors, which all serve to mitigate ER stress.

Despite conservation of this pathway, several key differences exist between UPR^{ER} signaling in budding yeast and metazoans. First, widespread gene repression is a component of the UPR^{ER} gene expression program in metazoans, but has previously not been appreciated to be an important aspect of UPR^{ER} signaling in budding yeast. Second, even though many of the mechanistic details of the pathway were first elucidated in budding yeast, physiological significance of the pathway has only been established in metazoans. This is in part because UPR^{ER} activation in budding yeast is generally achieved by external perturbation, such as via drug treatment. Furthermore, *hac1*Δ and *ire1*Δ cells do not exhibit severe phenotypes during vegetative yeast growth, suggesting that the UPR^{ER} may not play a crucial role under standard laboratory growth conditions. Based on our observations that budding yeast cells activate the UPR^{ER} during meiotic differentiation and recent findings that gene repression can occur through transcription of poorly translated alternate mRNA isoforms, I investigated whether and how pharmacological activation of the UPR^{ER} in budding yeast involves Hac1-dependent gene repression, and additionally sought to characterize the basis for and importance of meiotic physiological UPR^{ER} induction in yeast.

To capture a more nuanced view of the Hac1-dependent gene expression program during the UPR^{ER}, I generated deep, parallel gene expression datasets (measuring mRNA, translation, and protein levels). I found that a recently described mode of gene repression relying on the expression of long undecoded transcript isoforms (LUTIs) contributes to global proteome remodeling in response to ER stress. Namely, Hac1-dependent LUTI expression resulted in decreased protein levels of one set of targets, while Hac1-dependent transcription of canonical mRNAs resulted in increased protein levels of a separate set of targets. My findings elucidate how gene repression during UPR^{ER} can be achieved by the same transcription factor, Hac1, that has been previously associated with only gene activation. The same principle may be applicable to other transcriptionally driven stress response pathways.

To investigate the physiological UPR^{ER} induction seen in the absence of external perturbation during meiosis, I evaluated whether an intact UPR^{ER} is required for the meiotic program in budding yeast. I determined that having *HAC1* prior to and/or during meiotic entry is necessary for meiotic progression. I showed that while many key meiotic events were dispensable for meiotic UPR^{ER} induction, expression of the meiotic transcription factor Ndt80 was required. I developed strategies to identify transcriptional targets of the UPR^{ER} in meiosis, and used them to generate rich datasets allowing for physiological target identification, which will enable a better understanding of the meiotic function of UPR^{ER} activation.

Whether gene repression via the LUTI mechanism and/or physiological induction as part of the meiotic program are conserved characteristics of the UPR^{ER} remains to be determined. However, my findings resolve two of the discrepancies between UPR^{ER} signaling in budding yeast and metazoans, elucidating a mechanism by which gene repression is achieved and characterizing a physiological context in which the pathway is activated in budding yeast.

This dissertation is dedicated to Albert John Van Dalfsen
1933-2014

Table of Contents

List of figures

List of tables

Acknowledgements

There are many people without whom this would not have been possible. First, thank you to my advisor, Gloria Brar, for giving me the chance to work on exciting scientific questions in a fun environment, all while being very supportive. I am grateful for the opportunity to work in your lab and for all you have taught me. I am also appreciative of the support I received from Elçin Ünal, Christiane Brune, Leon Chan, and Chris Mugler, in addition to all of the graduate students, post-docs, technicians, and undergrads in the BrÜn Lab. Many people in the lab became great friends, and all were a pleasure to work with. A special thanks to the three undergraduate students I worked with – Clarence Yeung, Crystal Zhong, and Tia Cheunkarndee- for bearing with me as I figured out how to be a mentor and for their assistance with various aspects of my work, and to Tina Sing for her helpful comments on this dissertation.

I am grateful to Andy Dillin, James Olzmann, and Jasper Rine for their time and advice. My thesis committee provided lots of direction, and my meetings were always very intellectually stimulating.

Graduate school had its ups and downs. The ups were made possible and the downs were made bearable by friendships with some pretty outstanding people. Thank you to the MCB entering class of 2013, and especially WNDCOT. Many of my best memories from graduate school were made with Sarah and Evan Gilbertson and Joe, Ella, Tater Tot, and Luna Ireland. You guys became my family here, and it's hard to think about leaving Berkeley because of you. Thanks to Madeleine Jensen and Rebecca Lamothe for being great friends and supportive roommates, and making the best cake I've ever had. I'm grateful to Ross Pedersen for his friendship and support, especially in the home stretch.

Thanks also to my family, who were all extremely supportive. I appreciate Bill and Smidty Schripsema for taking me sailing, introducing me to Hartford Winery, and giving me a place to go on holidays – all of which provided much needed breaks from graduate school. Katie Schripsema was a frequent source of support for me, and I'm grateful she was always there. I thank my brother and sister-in-law, Sam and Dana, for coming to visit and for flying me home from time to time, as well as being great friends. My niece and nephew, Evelyn and Henry, were both born while I was in graduate school. It was really hard to be far away while they were so little, but on tough days in the lab, watching videos of those two or FaceTiming them never failed to cheer me up and put things into perspective. Thanks to my parents, Gary and Jill, for always being there for me and carrying me to the finish line when I needed it. I am not exaggerating when I say that I could not have done this without you.

Chapter 1: An introduction to the endoplasmic reticulum unfolded protein response (UPR^{ER}) in *Saccharomyces cerevisiae*

The function of a protein is determined by the 3-dimensional shape it adopts via a process called protein folding. Different subcellular environments provide specialized conditions favorable for protein folding, often housing a specific class of proteins called chaperones that aid in the proper folding of other proteins. One important location of protein folding in the cell is the lumen of the endoplasmic reticulum (ER). Over 30% of a cell's proteins are folded in the environment of the ER lumen (Brodsky and Skach, 2011), where chaperones are concentrated to assist polypeptides in achieving the proper folded state. Under certain conditions, however, the demand for chaperones by misfolded and unfolded proteins outweighs the supply, and the result is a state of ER stress that requires a specialized cellular response to be mitigated. This introductory chapter reviews how proteins are folded in the ER under normal conditions and what happens when protein folding in the ER goes awry. The primary focus is on the ER unfolded protein response (UPR^{ER}) pathway of the budding yeast *Saccharomyces cerevisiae*. First, I will provide an overview of protein folding in the ER lumen. Next, I will discuss the mechanisms involved in responding to ER stress. I will provide a historical perspective of the UPR^{ER}, as well as a current view of its mechanism in budding yeast. I will close with a discussion of the physiological activation and roles for this pathway.

1.1 Protein folding in the ER lumen

Most proteins destined to be secreted, expressed at the cell surface, or housed in a variety of intracellular organelles are translated across the ER membrane and folded within the ER lumen. The ER serves as the beginning of a trafficking system for these proteins to reach their ultimate destination, but also provides a folding environment favorable for them to adopt the conformation needed to carry out their functions. Ensuring proper protein folding within the ER lumen is challenging, as the very high concentration of proteins (100mg/mL [Gardner et al., 2013]) within the compartment poses a serious aggregation risk. The following sections highlight how proper folding in the ER lumen is achieved during normal, unstressed conditions.

1.1.1 Getting to the ER: co-translational translocation

Most of the proteins present in the ER lumen (either permanently or en route to another location) are transported across the ER membrane through the process of co-translational translocation (Voorhees and Hegde, 2016). Nascent peptides that will cross the ER membrane by the canonical co-translational translocation pathway are marked for this fate by exposed signal sequences on the nascent chain, which are poorly defined but generally include a short track of hydrophobic residues (Goder and Spiess, 2003). Once the signal sequence emerges from the ribosome, the signal recognition particle (SRP) stalls translation by binding the ribosome-nascent chain complex (RNC) (Akopian et al., 2013). The SRP-bound RNC is then brought to the SRP

receptor (SR), which is present at the ER membrane and is adjacent to a protein channel called the translocon (Jomaa et al., 2017). On the ER membrane, the RNC is passed from SRP to the translocon (Sec1 or Ssh1 in budding yeast [Jiang et al., 2008]) and translation resumes, proceeding across the ER membrane.

1.1.2 Chaperones in the ER lumen

Chaperone proteins play important roles in facilitating co-translational translocation, preventing aggregation, and promoting proper folding of nascent polypeptides. Three of the most important classes of chaperones for folding in the ER lumen are the heatshock proteins (Hsps), the thiol oxidoreductases, and the lectin chaperones.

The most well-characterized class of Hsps in the ER lumen includes members of the Hsp70 family. Hsp70s in the budding yeast ER lumen include BiP (also known as Kar2 in yeast) and Lhs1 (Normington et al., 1989; Baxter et al., 1996), with BiP being the most famous and well-studied chaperone of the ER lumen. Like all Hsp70s, BiP tightly binds its clients in an ADP-bound state and releases them in an ATP-bound state (Mayer and Bukau, 2005). Iterative cycles of BiP binding and release help to pull nascent polypeptides through the translocon and into the ER lumen, and additionally allow for "shielding" of aggregation-prone exposed hydrophobic stretches, allowing the nascent protein to fold without being impacted by the crowded environment of the ER lumen (Mayer and Bukau, 2005). Proper functioning of Hsp70s requires the action of Hsp40s (J-proteins), both for facilitating interactions with client proteins as well as for stimulation of Hsp70s' ATP hydrolysis (Laufen et al., 1999). In yeast, the major J-proteins in the ER lumen are Sec63, Scj1, and Jem1 (Silberstein et al., 1998). The importance of lumenal Hsp70 systems in budding yeast is exemplified by the fact that BiP/*KAR2* (an Hsp70) and *SEC63* (a J-protein) are essential for viability.

Thiol oxidoreductases such as the protein disulfide isomerase Pdi1 contribute to the ER lumen's oxidative environment and catalyze disulfide bond formation (Brodsky and Skach, 2011). Disulfide bonds between cysteine residues in proteins are acquired by a thiol-disulfide exchange reaction, in which two free thiols in the protein are replaced with a disulfide bond from a donor (for example, from the active site of Pdi1). Pdi1 requires the activity of Ero1, which provides Pdi1 with oxidizing equivalents (Pollard et al., 1998; Sevier and Kaiser 2010). Both *ERO1* and *PDI1* are essential for viability in budding yeast (Pollard et al., 1998; Farquhar et al., 1991).

Lectin chaperones, such as calnexin and calreticulin, also play important roles in protein folding in the ER lumen. It should be noted that budding yeast harbor only a calnexin homolog, Cne1 (Parlati et al., 1995), but they do contain other lectins outside of the calnexin/calreticulin family. Lectin chaperones interact with client proteins via glycan modifications (reviewed below) and also help prevent aggregation. Some evidence also suggests that interactions with lectin chaperones such as Cne1 may also influence the activity of protein disulfide isomerases (Kimura et al., 2005). *CNE1* and the genes encoding many other lectins are not essential in budding yeast, suggesting partially

overlapping functions and/or decreased importance of this chaperone class relative to the Hsp70s and thiol oxidoreductases.

1.1.3 Protein glycosylation and its role in folding in the ER

Most secretory proteins are modified by the addition of sugar chains called glycans (Pearse and Herbert, 2010). The most common glycan modification is *N*-linked glycosylation, in which an oligosaccharide is added to polypeptides via covalent linkage to asparagine residues. This reaction is carried out by membrane-bound oligosaccarhyltransferases (OSTs) that covalently attach pre-synthesized 14mers to nascent polypeptides (Pearse and Herbert, 2010). Additional enzymes subsequently trim this initial 14mer, and the length of the resulting glycan dictates interaction specificity with different members of the ER quality control machinery, such as the lectin chaperones. In addition to this role, *N*-linked glycosylation serves several other purposes. First, the hydrophilic glycans can mask aggregation prone hydrophobic stretches that would otherwise be left exposed. Second, the addition of the glycan can restrict the conformational space that the nascent polypeptide can explore, thus biasing it towards a folded state (Hanson et al., 2009; Shental-Bechor and Levy, 2008).

1.2 Protein misfolding and ER stress

Despite the conditions of the ER lumen being ideal for secretory protein folding, misfolding can still occur. This is problematic because a misfolded or aggregated protein cannot carry out its own cellular function and can impact the ability of other proteins to function, in some cases leading to cellular toxicity. To avoid these consequences, there are two major mechanisms by which a cell can deal with misfolded proteins: ER associated decay (ERAD) and the unfolded protein response (UPR^{ER}).

1.2.1 ERAD

When misfolded proteins are detected by chaperones such as Kar2 and lectins such as Yos9 and Htm1 (Kim et al., 2005) in the ER lumen, they are ubiquitinated and marked for ERAD. ERAD substrates are then retro-translocated back to the cytoplasm for proteasomal degradation. In yeast, this is mainly facilitated by the Doa10 and Hrd1 complexes, which each contain a namesake E3 ligase (Carvalho et al., 2006; Stevenson et al., 2016). Retro-translocation occurs through one or more channel type proteins, the identity of which is currently unknown but is most commonly thought to be Der1, Hrd1, or the Sec61 translocon itself (Cavarlho et al., 2006; Stenvenson et al., 2016).

1.2.2 The UPR^{ER}

Under certain conditions, the number of misfolded proteins can exceed the ER's capacity to properly fold or clear them via the chaperone and ERAD systems, which leads to ER stress. Conditions of ER stress prompt activation of the UPR^{ER} pathway, which serves to alter gene expression in order to restore homeostasis. In a general

sense, the UPR^{ER} functions to solve one of the major challenges of eukaryotic cells: namely, how membrane bound organelles communicate with the nucleus to ensure proper expression of genes required for each subcellular compartment. While there are many organelle-to-nucleus communication pathways, the UPR^{ER} is a particularly elegant one. In metazoans, it consists of three pathways that serve to monitor the status of the ER and convey information regarding protein folding and lipid homeostasis to the nucleus (reviewed in [Walter and Ron, 2011]). Budding yeast harbor only the most conserved branch of the UPR^{ER}, which depends on the sensor protein Ire1 and the transcription factor Hac1.

1.3 The UPR^{ER}: A historical perspective

In the 1980s, it became clear that protein folding played a role in intracellular transport when mutant versions of hemagglutinin (HA) were discovered to be retained in the ER lumen of mammalian cells, bound by BiP (Gething et al., 1986). Although BiP had not yet been fully characterized as a chaperone protein, it was generally considered to be the ER equivalent of Hsp70, a cytosolic chaperone protein (Munro and Pelham, 1986). It was observed that BiP was upregulated via increased mRNA levels when mutant HA was expressed. The fact that a putative chaperone was expressed at higher levels when a mutant client protein was expressed suggested a mechanism whereby the folding state of the ER was somehow monitored and relayed to the nucleus to tune the level of chaperone expression (Kozutsumi et al., 1988). This idea served as the basis for many experiments that ultimately led to the discovery of the UPR^{ER} and the elucidation of its mechanism.

Analysis of the promoter region of yeast BiP led to the identification of a 22 bp region that conferred transcriptional induction in response to ER stress, which was aptly named the unfolded protein response element, or UPRE (Mori et al., 1992). Electrophoretic mobility shift assays revealed that yeast extract prepared from cells experiencing ER stress contained a protein that bound to the UPRE. This led to a refined model in which a yet to be identified sensor protein sensed folding status, communicated it by activating a putative transcription factor via an unknown mechanism, and led to the downstream response of increased expression of chaperones via UPREs in their promoters (Mori et al.,1992; Kohno et al., 1993).

1.3.1 Discovery of the ER sensor protein, Ire1

The putative ER stress sensor protein, Ire1, was discovered by two independent studies in 1993 (Cox et al., 1993, Mori et al., 1993). Both relied on screens for genes that when mutated rendered cells incapable of expressing reporters regulated by UPRE-containing promoters in response to ER stress. Sequence analysis of the recovered gene, *IRE1*, suggested that this gene encoded an ER-localized serine/threonine kinase, which led to the hypothesis that the lumenal domain of Ire1 sensed a stress signal and the cytoplasmic kinase domain transmitted it, either directly to the nucleus or through the cytoplasm to activate a transcription factor (Cox et al., 1993).

1.3.2 Discovery of an Ire1-regulated transcription factor, Hac1

Even though multiple screens had identified *IRE1*, no study had identified the putative UPR^{ER} transcription factor. In 1996, a screen for high copy suppressors of *IRE1* deletion identified *HAC1*, a gene encoding a basic-leucine zipper transcription factor. Overexpression of *HAC1* resulted in constitutive activation of a reporter under the control of a UPRE-containing promoter (Cox and Walter, 1996). Extract from cells deleted for *HAC1* no longer showed ER stress-dependent UPRE binding activity, suggesting that *HAC1* encoded the long sought UPR^{ER} transcription factor. Interestingly, the Hac1 protein was only detected in cells carrying wild-type *IRE1* and experiencing ER stress, suggesting that Ire1 regulates *HAC1* expression during the UPR^{ER} (Cox and Walter 1996).

Despite the discovery of *HAC1*, there was still a major gap in the pathway - how was the regulation of *HAC1* achieved? One possible explanation was that *HAC1* was transcriptionally activated upon UPR^{ER} induction. To test this hypothesis, *HAC1* levels were analyzed by northern blot. Strikingly, this line of investigation revealed that upon UPR^{ER} induction, a faster migrating *HAC1* mRNA species was expressed. This smaller mRNA species was determined to be a spliced isoform of the *HAC1* message, as the 5' and 3' ends of the transcript were identical, but a 252 bp intervening sequence was missing in the UPR^{ER}-specific shorter mRNA species. Curiously, the putative splice sites did not conform to yeast splice consensus sites, suggesting that a non-canonical splicing mechanism was responsible for generating the shorter *HAC1* species. Further, if the 252 bp intervening sequence was removed genetically, the transcriptional response associated with ER stress was observed even in the absence of Ire1 activity (Cox and Walter, 1996). Later work showed that the unspliced *HAC1* message was cytoplasmically expressed, but translationally repressed (Chapman and Walter 1997). Critically, Ire1 had an endonuclease function that could specifically cleave the *HAC1* message, freeing it from the intron-derived translational repression with exon ligation facilitated by the tRNA ligase Rlg1 (Sidrauski et al., 1996; Sidrauski and Walter, 1997; Chapman and Walter, 1997).

1.4 A current view of UPR^{ER} activation and signaling in budding yeast

A current understanding of UPR^{ER} signaling (Figure 1.1) is detailed in the following sections.

1.4.1 Stress sensing by Ire1

There are several models for how Ire1 senses ER stress. One of the models posits that BiP binding to the lumenal surface of Ire1 represses Ire1 activation. Upon ER stress, the increased number of misfolded proteins in the ER lumen titrates BiP away from Ire1, releasing this inhibitory interaction (Bertolotti et al., 2000; Okamura et al., 2000). This model is supported by observations in metazoans, but it is inconsistent with data from yeast, where mutations abolishing the Ire1-BiP interaction do not show constitutive UPR^{ER} activation, a prediction of the model (Kimata et al., 2004).

A second model argues that misfolded proteins themselves activate Ire1. Evidence for this model includes the fact that the structure of dimerized Ire1 lumenal domains resembles that of the major histocompatibility complex groove, providing an ideal surface for peptide binding (Credle et al., 2005). More directly, model misfolded proteins such as CPY* interact with Ire1 in vivo and cause purified Ire1 to oligomerize in vitro

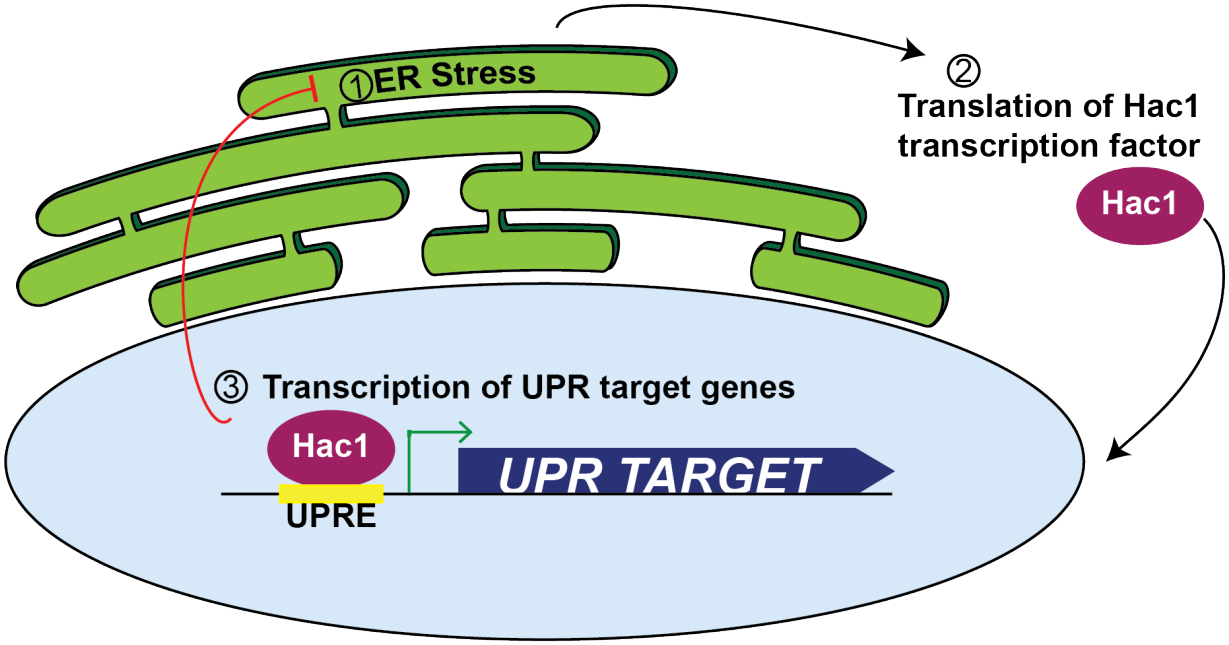

Figure 1.1. The UPR^{ER} in budding yeast. ER stress is sensed by the sensor protein, Ire1 (not shown), which results in expression of the Hac1 transcription factor. Hac1 goes into the nucleus to induce transcription of UPR^{ER} target genes, which commonly harbor unfolded protein response elements (UPREs) in their promoters. The collective action of UPR^{ER} target genes mitigates ER stress.

(Gardner and Walter, 2011; Promlek et al., 2011). Additionally, the lumenal domain of Ire1 can prevent aggregation of unfolded proteins in vitro, suggesting it binds to aggregation prone peptides (Kimata et al., 2007). More recently, peptides and unfolded proteins have been shown to interact with mammalian Ire1 in vitro, further supporting this model and suggesting conservation of this mechanism (Karagöz et al., 2017).

Currently, a model that integrates these two ideas is the most accepted and accommodates the observations made by several groups (reviewed in [Gardner et al., 2013]). This integrated view is one in which BiP binding/unbinding tunes the response to stress such that low levels of unfolded proteins fail to activate Ire1, but that ultimately the on/off state of Ire1 is governed by its binding to misfolded proteins (Figure 1.2). It is important to note that no endogenous protein has been shown to bind and activate Ire1, which would be a prediction of this model.

In addition to this integrated view, a separate mode of Ire1 activation has also been reported (Figure 1.2). Depriving yeast cells of inositol, a component of some

phospholipids, was suggested to promote Ire1 activation through an undefined mechanism for sensing membrane aberrancy, independent of a wild-type *IRE1* lumenal domain (Promlek et al., 2011). Lumenal domain-independent activation was also shown in response to membrane aberrancy in mammalian cells, suggesting this could be a conserved mechanism of ER stress sensing by Ire1 (Volmer et al., 2013). A juxta-membrane amphipathic helix was shown to be required for the proposed sensing of membrane aberrancy, and is thought to respond to alterations in lipid packing of the ER membrane (Halblieb et al., 2017). Perhaps changes in membrane composition could alter the propensity for Ire1 clustering (suggested in [Cohen et al., 2017]) and therefore promote activation independent of interactions between the lumenal domain and BiP or misfolded proteins.

Notably, these models are not mutually exclusive. It seems likely that Ire1 could be activated independently by interactions with misfolded proteins (which are buffered by BiP binding) and by membrane aberrancy (Figure 1.2), allowing for activation of the UPR^{ER} by a variety of stress signals.

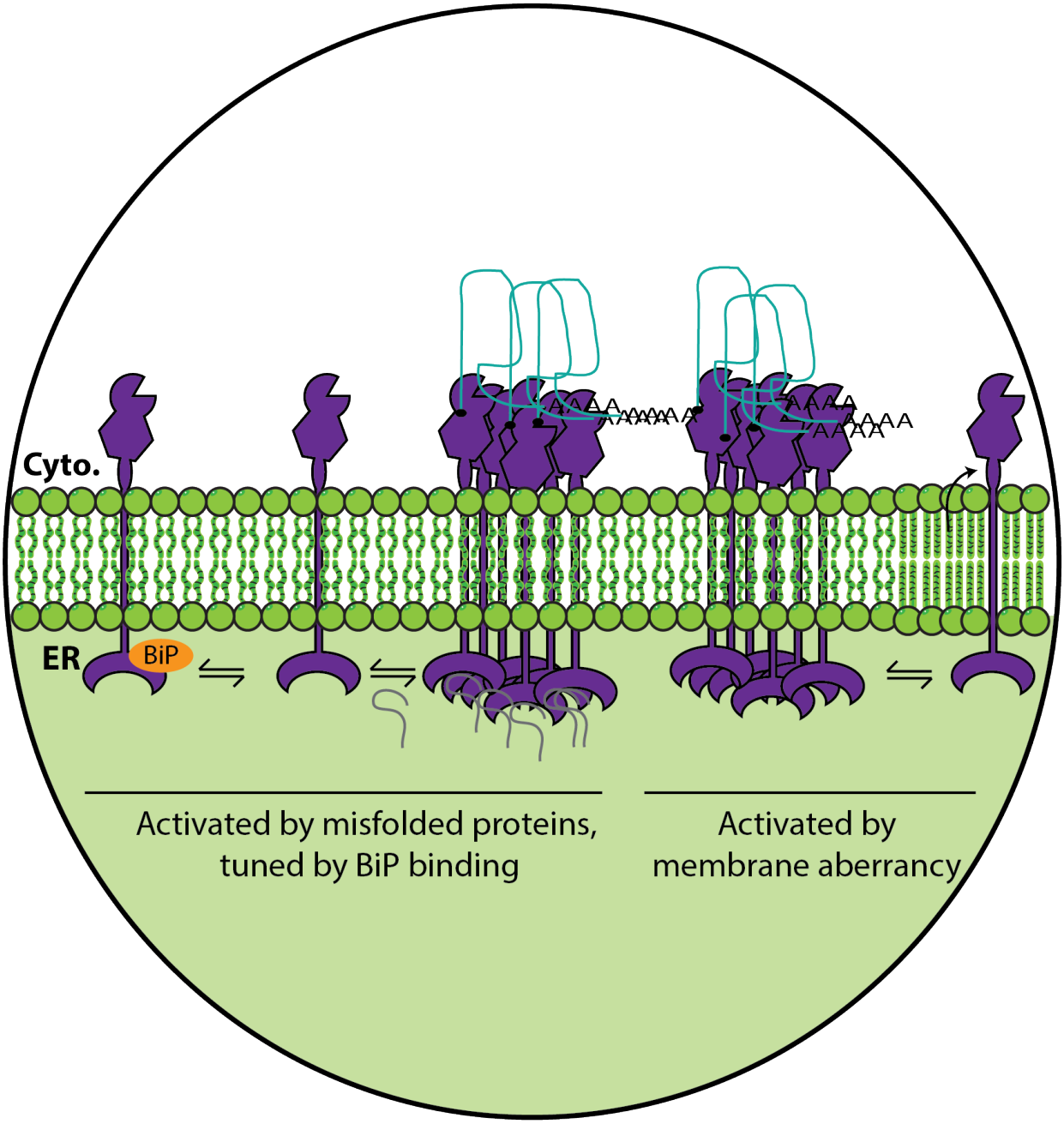

Figure 1.2. Ire1 activation in response to unfolded protein and membrane stress. In the absence of ER stress, Ire1 (purple) is in a monomeric, inactive state. Activation can occur by binding of misfolded proteins (grey), and is buffered by binding of BiP (orange). Alternatively, activation can occur by sensing membrane aberrancy (possibly detecting changes in lipid packing), dependent on the cytoplasmic linker region of Ire1. Upon activation, the *HAC1* transcript (teal) is recruited to Ire1 clusters for splicing.

1.4.2 Activation of Ire1

Upon sensing ER stress by one of the aforementioned mechanisms, Ire1 molecules cluster in the ER membrane, forming higher order oligomers (Shamu and Walter, 1996; Welihinda and Kaufman, 1996; Aragon et al., 2009). Oligomerization is required for activation of the Ire1 cytoplasmic kinase domain, which then carries out a trans-

autophosphorylation reaction (Shamu and Walter, 1996; Welihinda and Kaufman, 1996). The cytoplasmic endonuclease domain is activated in these oligomers as a result of oligomerization, as well as a conformational change that results from nucleotide binding. However, the phosphorylation event itself is dispensable for this activation (Papa et al., 2003; Korennykh et al., 2008).

Activation of the Ire1 endonuclease domain results in cleavage of the *HAC1* transcript as described in the following section. Though absent in budding yeast, activation of the endonuclease domain leads to an important additional function in fission yeast and metazoans called regulated Ire1-dependent decay (RIDD) (Maurel et al., 2014). RIDD results in the selective degradation of a subset of mRNAs that code for proteins that will be folded in the ER lumen (Hollien and Weissman, 2006). In this sense, the Ire1 branch of the UPR^{ER} in organisms other than budding yeast is considered to have both "positive" and "negative" targets, while in budding yeast it is generally considered only to have "positive" targets through Hac1-dependent transcription.

1.4.3 Splicing an inhibitory intron from the *HAC1* message

In order to mount a transcriptional response, Ire1 must splice an inhibitory intron from the *HAC1* message. This intron plays at least two important roles in the regulation of *HAC1*. First, the intron renders *HAC1* incapable of efficient translation through a base pairing interaction between the 5' UTR and intron (Chapman and Walter, 1997; Rüegsegger et al., 2001; Di Santo et al., 2016). While early reports claimed that the resulting translational repression was due to elongating ribosomes being blocked by this secondary structure, more recent evidence suggests that it is instead initiation of translation that is inhibited (Sathe et al., 2015; DiSanto et al., 2016).

Although the translational repression of *HAC1* is quite tight, occasionally leaky translation of the *HAC1* message occurs, necessitating the second important function of the *HAC1* intron. Recent evidence suggests that the intron plays a previously unrecognized additional repressive role by facilitating the turnover of the protein synthesized from the unspliced *HAC1* message. The c-terminus of the protein encoded by the intron-containing transcript appears to be a degron that facilitates an interaction between Hac1 and Duh1, an F-box protein that marks Hac1 for proteasomal degradation (DiSanto et al., 2016). Together, the translational repression mechanism and the "fail-safe" mechanism (coined by [DiSanto et al., 2016]) of intron-dependent accelerated protein degradation tightly regulate Hac1 levels in the absence of UPR^{ER} induction.

During ER stress, this repressive intron is removed to enable strong expression of the Hac1 protein. In order for this splicing event to be completed, several events have to occur. First, the *HAC1* message must be brought in close proximity to the activated Ire1 clusters located in the ER membrane. The 3' UTR of the *HAC1* message contains a conserved bipartite element within a 3' stem-loop required for the recruitment of *HAC1* to Ire1 clusters. (Aragon et al., 2009). This depends on Ire1 oligomerization, as well as a positive stretch of amino acids in the cytoplasmic linker region of Ire1, which is thought

to facilitate docking of the *HAC1* message at the ER (Aragon et al., 2009; Van Anken et al., 2014). Next, the 252 bp intron is cleaved out of the message by the Ire1 endonuclease via two independent cuts made at non-canonical splice sites in stem loops recognized by Ire1 (Sidrauski et al., 1996; Sidrauski and Walter, 1997; Gonzalez et al., 1999). The resulting 5' and 3' exons are then ligated by the tRNA ligase, Rlg1 (Sidrauski et al., 1996).

1.4.4 *HAC1* translation and nuclear function

Once translated, Hac1 can carry out its transcription factor function (Cox and Walter, 1996; Mori et al., 1996). Hac1 binds to UPREs (of which there are three types, UPRE-1, -2, and -3) in the promoters of UPR^{ER} targets (Mori et al., 1992; Kohno et al., 1993; Mori et al., 1996; Cox et al., 1996; Mori et al., 1998; Patil et al., 2004; Fordyce et al., 2012). Interestingly, over 50% of the reported UPR^{ER} targets do not contain one of these three motifs, and the most well-characterized motif (UPRE-1) is so ubiquitous in the genome that it is not significantly enriched in the target gene set (Patil et al., 2004), making computational target prediction difficult. It is possible that the reported targets that do not harbor one or more UPREs in their promoters could be indirect targets of the UPR^{ER}, or alternately that there are additional promoter elements that remain undiscovered.

An initial genome wide approach based on ORF microarray analyses with and without UPR^{ER} activation (Travers et al., 2000) identified close to 400 genes (representing ~6% of the yeast genome) as targets of Hac1 during the UPR^{ER}. These target genes are enriched for roles in translocation, glycosylation/modification, protein folding, protein degradation, vesicle trafficking/transport, lipid/inositol metabolism, vacuolar protein sorting, and cell wall biogenesis. While some of these targets are intuitive (for example chaperones like *KAR2*, *LHS1*, and *ERO1*, as well as membrane biogenesis genes and ERAD components), the roles of other targets remain unclear. Further, a study analyzing genes required for proper folding in the ER lumen identified approximately 400 genes, but the overlap between this gene set and the one identified in (Travers et al. 2000) was minimal, with only 56 genes shared between the two datasets (Jonikas et al., 2009). This result suggests that many of the reported UPR^{ER} targets do not play roles in maintaining the proper lumenal environment for protein folding.

The Hac1 transcription factor is recognized as the primary regulator of the UPR^{ER} gene expression program in budding yeast. Given that Hac1 is a transcriptional activator, this suggests that the UPR^{ER} in yeast mitigates ER stress primarily through positive regulation of gene expression (Travers et al., 2000). This is in contrast to other eukaryotes, which employ RIDD (discussed in section 1.4.2), as well as a mechanism for widespread downregulation of translation. Downregulation of translation in metazoans is achieved through inhibitory phosphorylation of the translation initiation factor eIF2α by another ER stress sensor, PERK (double-stranded RNA-activated protein kinase (PKR)–like ER kinase) (Walter and Ron, 2011). Why the UPR^{ER} in yeast would have almost exclusively positive targets while the UPR^{ER} in other organisms has clear positive and negative targets remains mysterious.

1.5 Experimental induction of the UPR^{ER}

The study of mechanistic details and transcriptional targets of the UPR^{ER} in yeast, as described in the previous sections, has traditionally depended on pharmacological induction of ER stress. In yeast, the UPR^{ER} is most commonly induced by the addition of dithiothreitol (DTT) or tunicamycin.

Addition of DTT reduces disulfide bonds, effectively breaking cysteine bridges and inducing misfolding (Braakman et al., 1992). Though the effects of DTT are not limited to the ER lumen, because the cytosol is already a reducing environment, the effects on protein folding by this mechanism are stronger in the ER.

Tunicamycin is an antibiotic used to induce protein misfolding in the ER. It blocks the activity of GlcNAc phosphotransferase, an enzyme involved in the formation of glycans used for *N*-linked glycosylation (Reviewed in [Esko et al., 2017]). As described in section 1.1.3, *N*-linked glycosylation plays an important role in folding. Therefore, inhibiting *N*-linked glycosylation by the addition of tunicamycin results in an increased burden of misfolded proteins in the ER lumen.

1.6 A physiological role for the UPR^{ER} in metazoans

While great advances have been made in the UPR^{ER} field using pharmacological induction of ER stress, understanding the biological function of the pathway is limited without study of its physiological induction in the absence of experimental perturbation. Although many of the mechanistic details of the UPR^{ER} were first elucidated in budding yeast, essentially all of the research on physiological roles for the pathway has been done in metazoans. Many of these roles are reviewed in (Rutkowski and Hegde, 2010; Frakes and Dillin, 2017). The following section highlights one example of the types of important processes in metazoans shown to rely on the UPR^{ER}.

1.6.1 B cell development

Immunoglobulin (Ig)-secreting plasma cells are derived from B-lymphocytes, and are professional secretory cells almost entirely filled with ER (Reimold et al., 2001; Iwakoshi et al., 2003). Ig proteins are translated at the ER and folded within the ER lumen. The burden on the quality control machinery in the ER of differentiating B cells as they begin to produce very high levels of Ig proteins is therefore very high. The UPR^{ER} is activated during this process (Gass et al., 2002), perhaps unsurprisingly, as there could be a point in the differentiation process at which Ig production would outpace ER folding capacity and therefore activate the UPR^{ER}. Further, the UPR^{ER} was reported to be required for this differentiation process, as it has been shown that *XBP1* (the metazoan ortholog of *HAC1*) is essential for plasma cell formation (Reimold et al., 2001). More recent work has shown that *XBP1* is required for efficient antibody production in mature plasma cells, but not their survival (Tellier et al, 2016). This further suggests that the role of the UPR^{ER} in B cells is related to Ig production.

However, strong UPR^{ER} activation in differentiating B cells is surprisingly independent of IgM production (Hu et al., 2009). This suggests an anticipatory mechanism whereby the folding capacity of the cell is expanded prior to the increase in demand. This type of model is also supported by work showing that some of the ER expansion observed during B cell differentiation precedes Ig production (van Anken, et al., 2003), as well as initial observations that *XBP1* splicing also precedes Ig production (Gass et al., 2002). Interestingly, UPR^{ER} activation has also been observed in pro-B cells (immune cell precursors differentiating into the B cells that may later differentiate into plasma cells) (Brunsing et al., 2008). This also suggests that the role of the UPR^{ER} in the B cell lineage is not dependent on Ig production.

1.7 Physiological activation of the UPR^{ER} in budding yeast

Very low levels of *HAC1* splicing (representing ~1-7% of the *HAC1* mRNA pool) have been reported in budding yeast when grown in optimal conditions (Bicknell et al., 2007; Schröder et al., 2000). This suggests that there could be a physiological role for this pathway, though the details of such a role remain to be elucidated. Additionally, such low levels of pathway induction severely limit experimental approaches to determine function and/or activation mechanism, leaving the physiological role for the UPR^{ER} in budding yeast largely unexplored. Interestingly, a more robust induction of the pathway was observed in budding yeast meiosis (Brar et al., 2012). The following sections provide a primer on meiosis in budding yeast, as well as an introduction to meiotic UPR^{ER} induction and the questions it raises.

1.7.1 Meiosis in budding yeast

Budding yeast cells sexually reproduce when cells of opposite mating types (**a** and **α**) fuse to form an **a/α** diploid that can undergo meiosis to generate four haploid spores. Meiosis is a specialized and conserved developmental program that includes two successive rounds of cell division following a single DNA replication event, resulting in the four haploid gametes. In budding yeast, meiosis is induced when the following conditions are met (reviewed in [van Werven and Amon, 2011]):

1) The cell contains both a and α mating information. This is because the a1-α2 repressor is critical to repress a negative regulator of the transcription factor required for meiotic entry, Ime1.
2) The protein kinase A (PKA) pathway is inhibited. PKA signaling inhibits expression of Ime1, so PKA signaling must be shutdown for proper Ime1 expression. To achieve this in the laboratory, budding yeast are starved for glucose.
3) The cell must be arrested in the G1 phase of the cell cycle. In the laboratory, this is most commonly achieved by nitrogen starvation to inhibit target of rapamycin (TOR) signaling.
4) The cell must be provided a non-fermentable carbon source and be respiration competent. This is because respiration is thought to promote Ime1 expression.

1.7.2 Evidence for UPR^{ER} activation in meiosis

Traditionally, study of the meiotic program has centered on chromosome segregation, with little focus on the complex cellular remodeling and organellar dynamics required to form healthy gametes. Importantly, it has been shown that in addition to modified chromosome segregation processes relative to mitotic growth, meiosis employs fundamentally different methods to segregate organelles (Suda et al., 2007). Through analysis of new protein synthesis throughout meiosis, a recent study (Brar et al., 2012) addressed the control of meiotic cellular remodeling. This temporal information about protein synthesis provided valuable clues as to the molecular effectors of cellular remodeling during this highly coordinated developmental program.

Interestingly, this work showed precisely timed induction of the UPR^{ER} during the meiotic program, suggesting that perhaps UPR^{ER} signaling could be an important aspect of cellular remodeling during meiosis. Two waves of meiotic *HAC1* splicing and translation were observed by northern blotting and ribosome profiling, respectively (Figure 1.3). The first wave of UPR^{ER} activation was stimulated very early in meiosis and is likely a response to the starvation conditions required to induce the meiotic differentiation program. It was estimated that this induction results in the splicing of approximately 10% of the *HAC1* mRNA pool (Brar et al., 2012). A second, stronger wave of induction (during which roughly ~50% of the *HAC1* pool is spliced) was observed approximately six hours after transfer to sporulation medium (corresponding to the end of the first meiotic segregation phase). Importantly, the pathway returns to the "off" state in between these two waves, without any change in media or external conditions. In matched *MAT**a**/MAT**a*** cells, unable to undergo meiosis due to absence of the a1-α2 repressor, the UPR^{ER} is constitutively induced at low levels in sporulation medium. The pattern of UPR^{ER} induction during meiosis (two waves, with a strong second wave) thus appears meiosis-specific.

Whether meiotic UPR^{ER} activation is present in other organisms remains to be determined, as meiosis is largely untapped with respect to investigation of the UPR^{ER}. However, evidence of spliced *XBP1* in late stages of *Xenopus* oogenesis suggests conservation of meiotic UPR^{ER} induction (Cao et al., 2006). It will be interesting to determine whether meiotic UPR^{ER} activation is conserved as the field continues to grow.

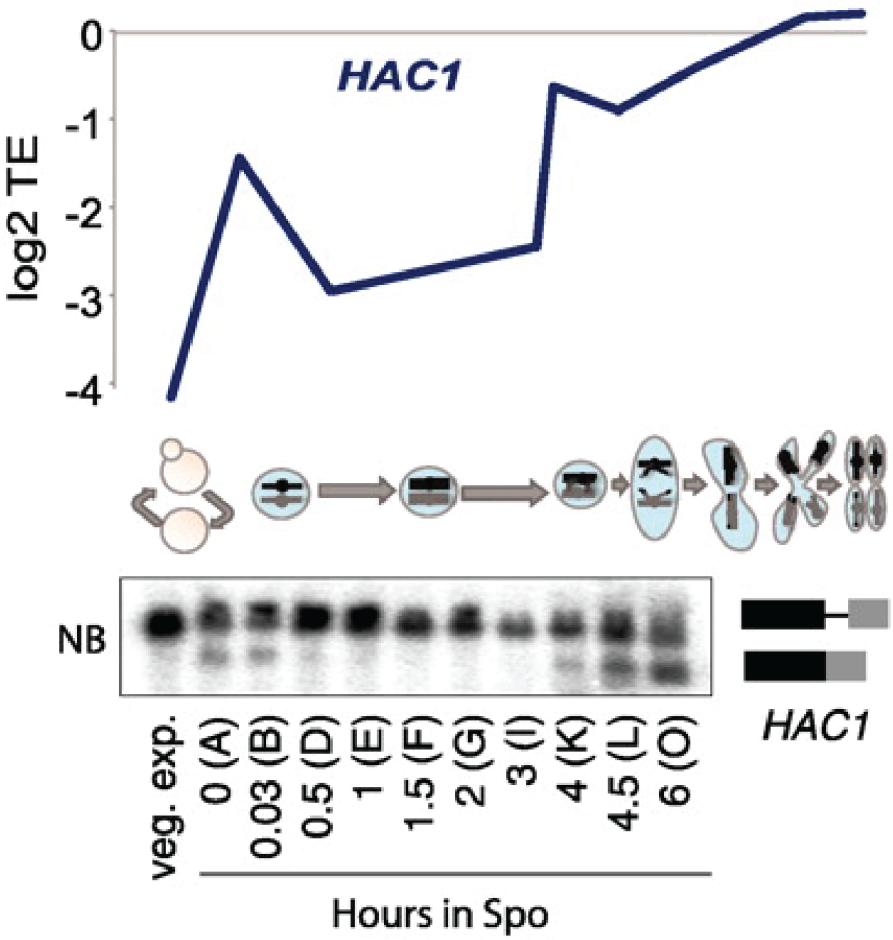

Figure 1.3 Induction of the UPR^{ER} during budding yeast meiosis. As cells progress through the meiotic divisions (left to right), the translation efficiency (top; ribosome profiling RPKM/mRNA-seq RPKM) of *HAC1* increases, suggesting *HAC1* is freed from its translational repression during meiosis. Translation of *HAC1* is correlated with an increased abundance of the spliced isoform (bottom; northern blot), suggesting this is a result of canonical UPR^{ER} activation. Reprinted with permission from (Brar et al., 2012).

1.7.3 Experimental avenues suggested by meiotic induction of the UPR^{ER}

Meiotic UPR^{ER} induction raises several important questions about physiological UPR^{ER} activation in budding yeast. First, little is known about the mechanism by which Ire1 is activated in the absence of an exogenous stimulus. Determining why meiotic cells activate the UPR^{ER} and how this activation is achieved could lead to insights regarding the physiological activation of this conserved pathway.

Additionally, transcriptional targets of UPR^{ER} signaling in budding yeast under physiological conditions are unknown. Identification of meiotic Hac1 targets could be important for understanding physiological UPR^{ER} signaling and its transcriptional

specificity, and could likely provide clues as to the role of UPR^{ER} induction in budding yeast meiosis.

The many tools available in yeast, including meiotic synchrony, make yeast meiotic UPR^{ER} induction a tractable context in which to study developmental UPR^{ER} signaling. UPR^{ER} components are required for many developmental processes, including organogenesis and B cell differentiation, suggesting that use of this historically stress-responsive pathway may be a general strategy employed by differentiating cells (Iwaki et al., 2009; Reimold et al., 2000; Iwakoshi et al., 2003). Therefore, insights gained through the study of meiotic UPR^{ER} induction have the potential to be broadly relevant to the role of the UPR^{ER} in developing cells.

1.8 Findings of the work presented in this dissertation

The following chapters of this dissertation explore the UPR^{ER} in budding yeast, focusing first on a re-evaluation of transcriptional targets of Hac1 during pharmacological induction of the pathway. Chapter 2 presents findings that Hac1 has a set of negative targets, whose protein products are repressed through a recently described non-canonical mode of gene regulation, relying on the production of long undecoded transcript isoforms (LUTIs). Chapter 3 explores meiotic UPR^{ER} induction, suggesting an intact UPR^{ER} during meiotic entry promotes meiotic success, evaluating meiotic events required for physiological UPR^{ER} activation, and developing strategies that can be applied to evaluate physiological targets of Hac1 during the UPR^{ER}.

Chapter 2: Global proteome remodeling during ER stress involves Hac1-driven expression of long undecoded transcript isoforms

This chapter is an adaptation of the following publication:

Van Dalfsen, K.M., Hodapp, S., Keskin, A., Otto, G.M., Berdan, C.A., Higdon, A., Cheunkarndee, T., Nomura, D.K., Jovanovic, M., Brar, G.A. (2018). Global proteome remodeling during ER stress involves Hac1-driven expression of long undecoded transcript isoforms. *Developmental Cell*, *46*.

2.1 Introduction

The endoplasmic reticulum unfolded protein response (UPR^{ER}) allows cells to respond to ER stress by activating a gene expression program that increases the folding capacity of the ER lumen. A conserved branch of this pathway relies on the Hac1 transcription factor (orthologous to XBP1 in metazoans) to allow cells to respond to aberrant protein folding within the ER (reviewed in [Han and Kaufman, 2017; Walter and Ron, 2011]). When ER protein folding is disrupted, such as through the addition of drugs including dithiothreitol (DTT) or tunicamycin (Tm), the resulting accumulation of misfolded proteins in the ER lumen promotes activation of the ER membrane-spanning kinase/endonuclease Ire1, which subsequently removes a translationally repressive cytoplasmically retained intron from the *HAC1* transcript through an atypical splicing event (Cox and Walter, 1996; Mori et al., 1996; Sidrauski et al., 1996). Spliced *HAC1* mRNA can be efficiently translated to produce a transcription factor (TF) that activates a set of target genes, the most well-studied of which play clear roles in increasing ER volume, folding capacity, and quality control. Included in this set of canonical Hac1 targets are chaperones, such as BiP (*KAR2* in yeast), protein disulfide isomerase (*PDI1* in yeast), lumenal Hsp70 (*LHS1*), as well as genes responsible for ER structure, lipid synthesis, and ER redox balance, like thiol oxidase (*ERO1*; reviewed in [Chapman et al., 1998]).

In metazoans, this gene expression program includes clear examples of gene downregulation, both through regulated Ire1-dependent decay (RIDD) and via global translational repression, which are both thought to function to decrease the secretory protein load (Walter and Ron, 2011). In budding yeast, however, the gene expression program is thought to almost exclusively involve transcriptional activation (Travers et al., 2000). An open reading frame (ORF) microarray study identified ~400 mRNAs that were induced in response to UPR^{ER} activation in a Hac1-dependent manner, some of which were known to have clear function in ER biology, but many of which were not and whose function in the UPR^{ER} remains mysterious (Travers et al., 2000). Given that mRNA sequence levels can be misleading predictors of gene expression output (Cheng et al., 2018; Maier et al., 2009), we hypothesized that some of the previously identified Hac1 transcriptional targets might actually be negatively regulated at the protein level,

thus allowing for coordination of gene activation and repression during the UPR^{ER} in budding yeast.

A recently defined mode of gene regulation is an attractive candidate for broadly mediating such coordination (Figure 2.1). This mechanism was shown to harness TF-driven synthesis of an ORF-encoding transcript to repress synthesis of the kinetochore protein Ndc80, a key event during meiotic differentiation in budding yeast (Chen et al., 2017; Chia et al., 2017). In short, it was found that *NDC80* has two transcription start sites (TSSs) that are activated by different TFs. Activation of the proximal TSS produces a canonical transcript that is translated to produce protein. Activation of the distal TSS results in synthesis of a 5' extended transcript that encodes the *NDC80* ORF, but the ORF is not expressed because of translation of uORFs in the extended 5' leader. Use of the distal TSS also represses use of the proximal TSS in cis by transcriptional interference. Effectively, as a result of this integrated mechanism, synthesis of the longer transcript halts Ndc80 protein production. This longer mRNA was termed a "LUTI", for long undecoded transcript isoform (Chen et al., 2017; Chia et al., 2017).

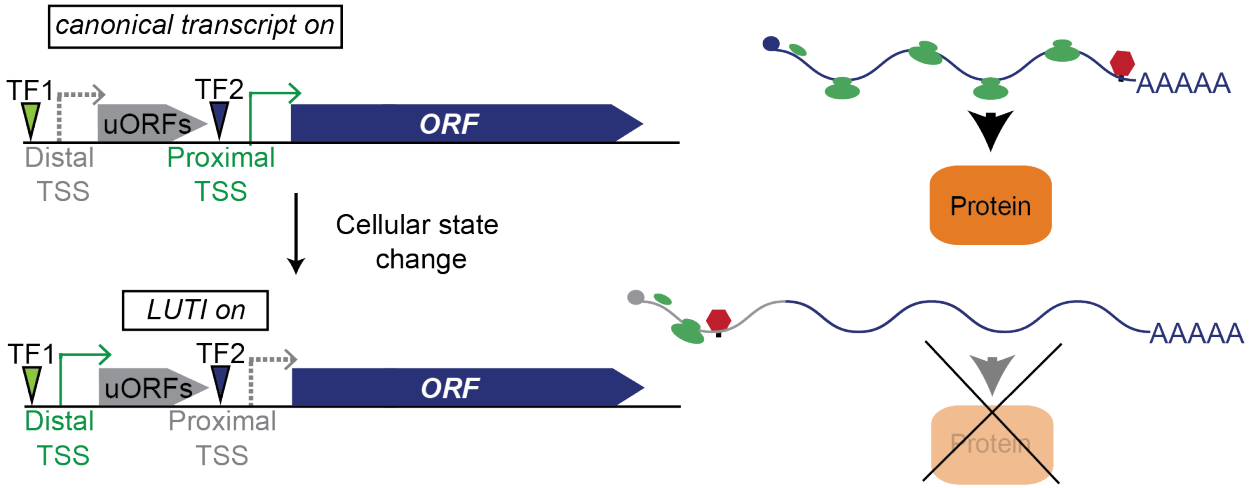

Figure 2.1 Schematic of LUTI-mediated repression of gene expression. When the LUTI-mRNA is off (top), TF2 drives transcription of a well-translated canonical mRNA. In contrast, when the LUTI-mRNA is on (bottom), TF1 drives transcription of a poorly translated extended mRNA. Transcription of the LUTI-mRNA prevents transcription of the canonical mRNA, ultimately resulting in decreased protein production.

Subsets of the hallmarks of LUTI-based regulation defined above were previously observed for several other genes (Law et al., 2005; Moseley et al., 2002; Sehgal et al., 2008; van Werven et al., 2012; Liu et al., 2015; Xie et al., 2016; Taggart et al., 2017; Shearwin et al., 2005), suggesting that use of this mechanism might be widespread, and could therefore possibly play a role in the UPR^{ER} gene expression program. Our lab recently found that LUTI-based regulation is common and responsible for setting protein levels of at least 380 genes as yeast cells progress through meiotic differentiation (Cheng et al., 2018). This work showed that the LUTI mechanism enables a single

meiotic TF to regulate two distinct sets of targets in a highly coordinated manner. The canonical set includes “positive” targets, whose transcription results in increased protein production, and the “negative” set includes LUTI targets, whose transcription leads to decreased protein production. While both sets of targets may exhibit increases in mRNA production, for genes that are regulated by the LUTI-based mechanism, overall mRNA levels are decoupled from protein levels. In fact, the 380 meiotic LUTI targets that we defined were found based on the signature of a poor, or even negative, correlation between mRNA and protein levels over time (Cheng et al., 2018; Otto and Brar, 2018). For these cases, it is the *type* of transcript produced rather than the amount that determines whether protein is synthesized.

Given the pervasiveness of LUTI-based regulation during budding yeast meiosis, it seemed possible that this mechanism might generally be used to coordinate gene up- and downregulation during cellular transitions such as the UPR^{ER}. If this were true, it might help to explain why many of the genes that are transcriptionally induced by the UPR^{ER} do not result in protein misfolding in the ER when deleted, and why—with few exceptions—roles in the UPR^{ER} remain undefined for most (Jonikas et al., 2009; Schuldiner and Weissman, 2013; Travers et al., 2000). Additionally, it would identify a mechanism of gene repression as part of the conserved Ire1/Hac1 branch of the UPR^{ER}.

Through analysis of deep, parallel gene expression datasets, we found examples of previously defined Hac1 targets that display *decreased* protein production as a result of UPR^{ER} activation. We expanded our study beyond previously defined targets to identify 15 LUTI targets of Hac1. To enable robust detection of Hac1 targets, we developed a version of this TF that can be conditionally degraded. Using cells carrying this conditional allele, as well as wild-type and *hac1*Δ cells, we performed thorough profiling of gene expression—measuring mRNA, translation, and protein levels in response to UPR^{ER} activation, with or without Hac1. This allowed us to holistically define the Hac1-dependent cellular response to UPR^{ER} activation, which we found involves coordinated up- and downregulation of distinct protein groups. We observed, as expected, that protein synthesis and levels of ER folding-related proteins are increased upon UPR^{ER} activation. We also observed downregulation of ribosomal genes, as well as of genes involved in aerobic respiration. In the case of the latter group, observed protein expression decreases were partly controlled by Hac1-induced transcription of LUTI targets. Perturbation of aerobic respiration was found to provide a growth advantage to UPR^{ER}-induced cells, suggesting a cellular function for UPR^{ER}-mediated gene downregulation, and raising the possibility that a shift in cellular metabolism is a core part of the UPR^{ER}, at least in yeast. Our results demonstrate that LUTI-based regulation is a broadly used mechanism by which transcription factors coordinate up- and downregulation of target genes during cellular state changes.

2.2 Results

2.2.1 Hac1 induces expression of LUTI targets, resulting in protein downregulation

To determine whether Hac1 induces LUTI-like repressive transcripts as part of the UPR^{ER}, we performed global gene expression measurements in wild-type and *hac1*Δ cells. We performed parallel mRNA-seq and ribosome profiling on untreated samples and those treated for 1 hr with either DTT or Tm to assay mRNA abundance and translation in response to UPR^{ER} activation (Figure 2.2). We reasoned that canonical Hac1 targets should show a Hac1-dependent increase in both mRNA and translation with DTT or Tm treatment. In contrast, Hac1 LUTI targets may show an increase in mRNA, but regardless of mRNA-level changes, should show a Hac1-dependent *decrease* in translation efficiency (TE; [ribosome footprint RPKM]/[mRNA RPKM]) with UPR^{ER} activation.

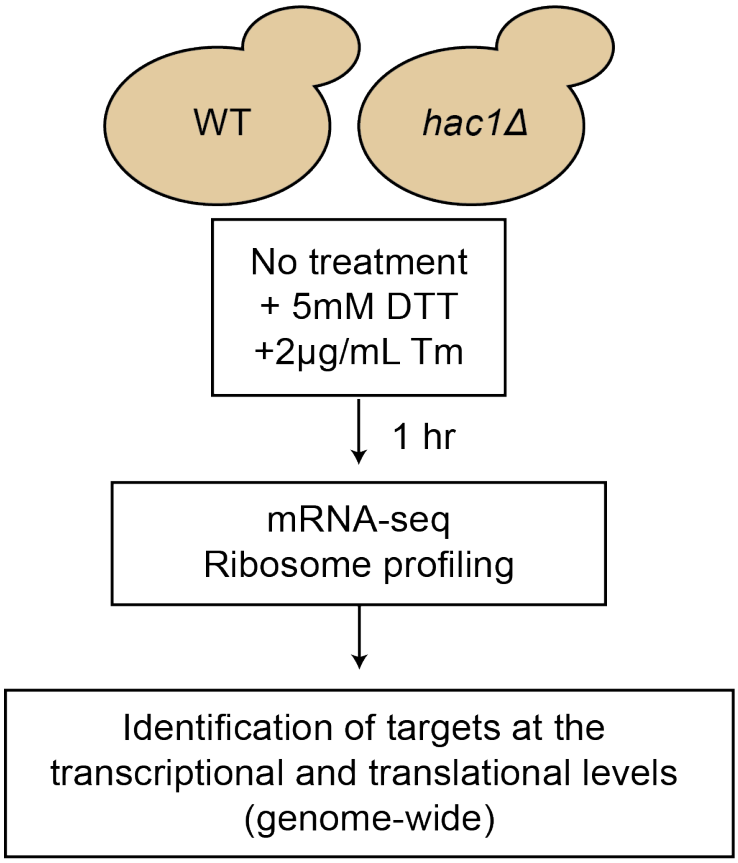

Figure 2.2. Schematic of wild-type/*hac1Δ* harvesting scheme. wild-type (BrÜn 1362) and *hac1Δ* (BrÜn 4431) cultures were grown in rich media alone, or that containing 5mM DTT or 2µg/mL Tm. Samples were collected after 1 hr of drug treatment, and matched extract was used for mRNA-sequencing and ribosome profiling analysis.

The set of transcripts reported to be induced by Hac1 based on microarray analyses (Travers et al., 2000) were also generally induced at the mRNA level in our dataset, dependent on *HAC1* (Figure 2.3). The most strongly upregulated transcripts included

the characterized UPR^{ER} targets *KAR2*, *ULI1*, *PDI1*, and *ERO1* (Figure 2.3; [Chapman et al., 1998; Metzger and Michaelis, 2008]).

When we evaluated translation levels (based on ribosome footprint density), we saw prominent induction of the best-characterized Hac1 targets, as expected (Figure 2.4). Overall, we identified 477 genes as showing a UPR^{ER}- and Hac1-dependent increase in translation of greater than 2-fold in this dataset. Genes in this group were strongly enriched for ER-localization and function, as expected (p-value for ER=2.64E-14; posttranslational protein targeting to membrane, translocation=1.33E-6; protein glycosylation=1.58E-5; note that this set is based on analysis of DTT data, but Tm treatment yields similar results; Tables 2.1, 2.2).

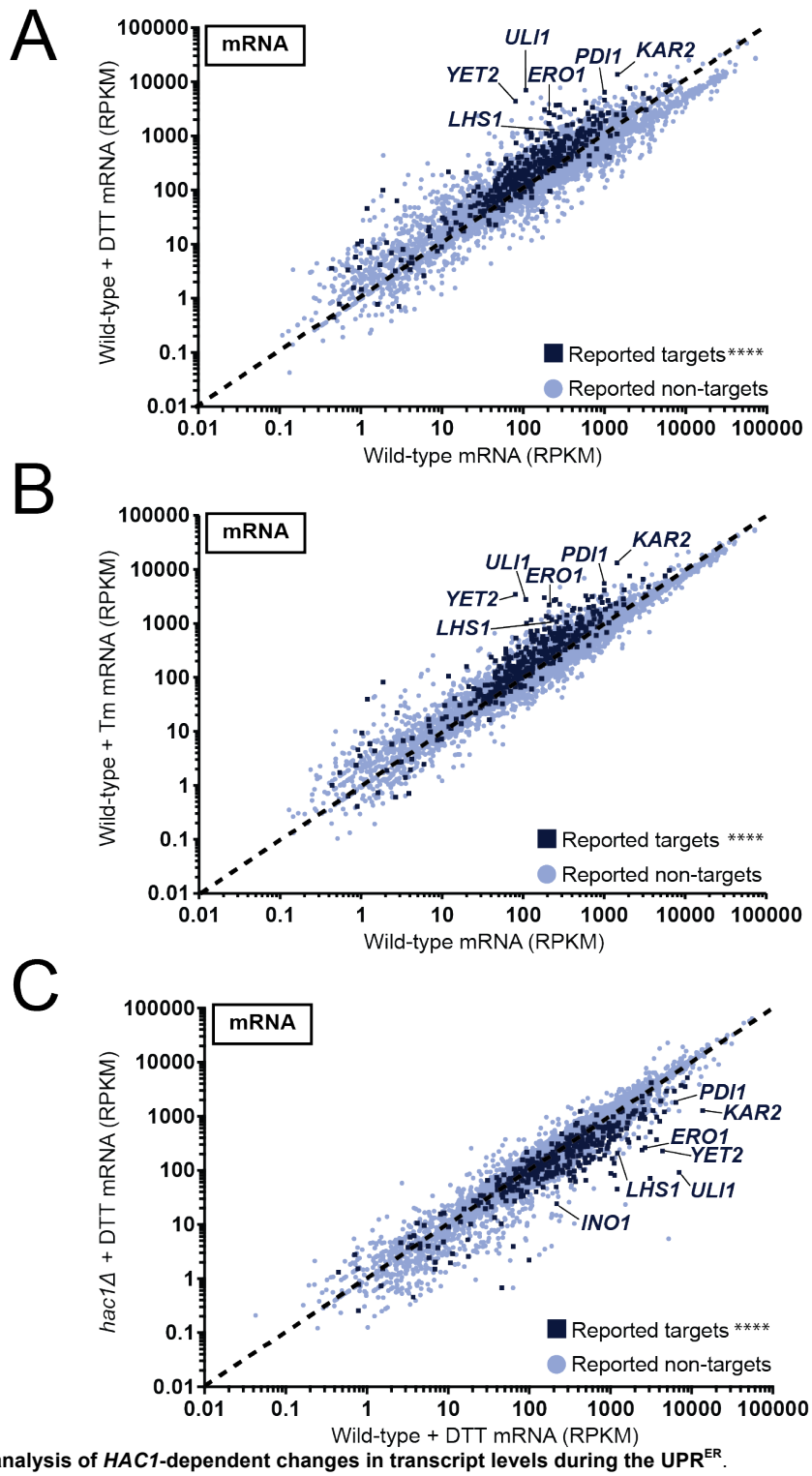

Figure 2.3. Global analysis of *HAC1*-dependent changes in transcript levels during the UPR^{ER}.
A) Comparison of mRNA levels (RPKMs) for each gene, as assayed by mRNA-seq, between wild-type cells (BrÜn 1362) treated with 5mM DTT and wild-type cells (BrÜn 1362) grown in rich media only.
B) Comparison of mRNA levels between wild-type cells (BrÜn 1362) treated with 2µg/mL Tm and wild-type cells (BrÜn 1362) grown in rich media only.
C) Comparison of mRNA levels between *hac1Δ* (BrÜn 4431) and wild-type cells (BrÜn 1362) treated with 5 mM DTT.
Note that for panels A-C, collection is described in Figure 2.2. Previously reported Hac1 targets (Travers et al., 2000) are shown with dark squares while all other genes are shown with light circles. Reported Hac1 targets were significantly (****p<0.0001) more likely to be upregulated upon UPR^{ER} induction than the full gene set.

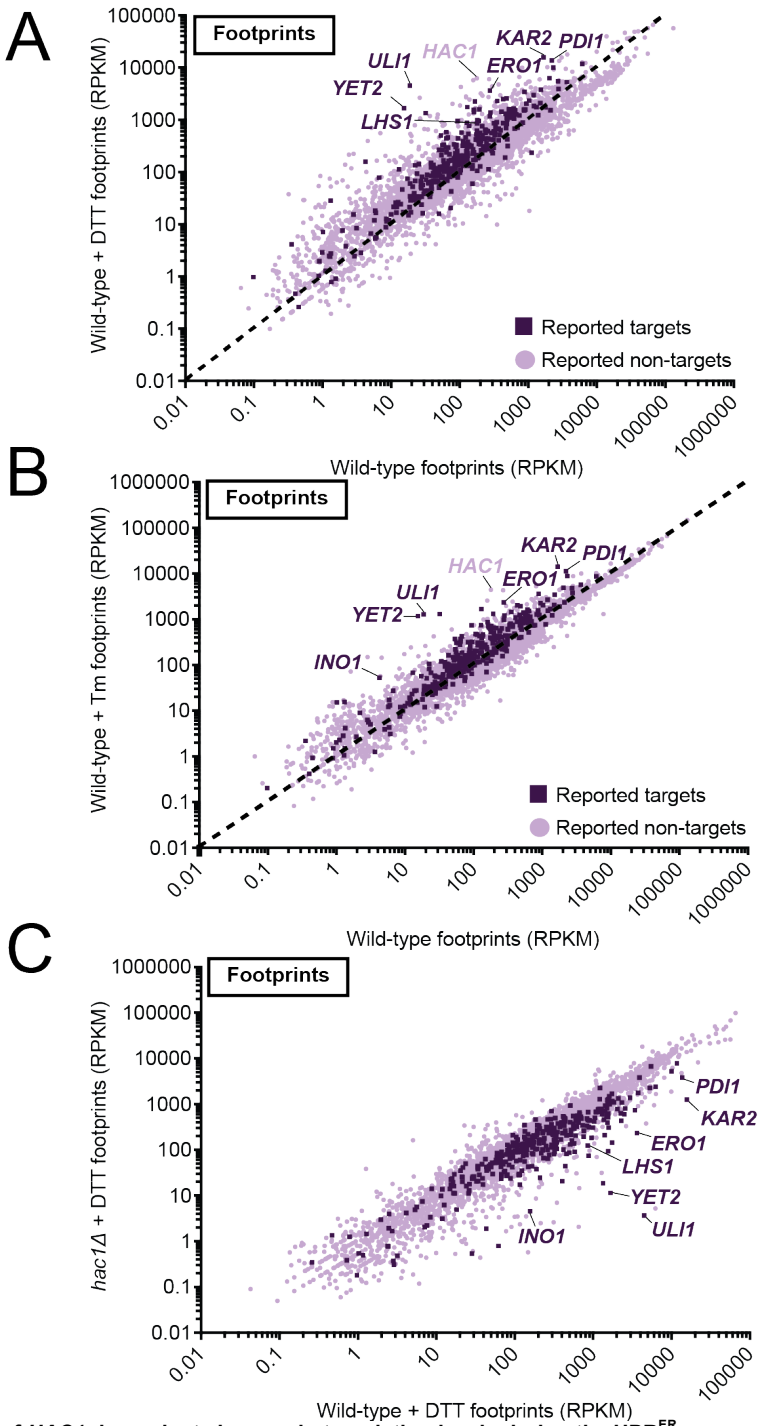

Figure 2.4. Analysis of *HAC1*-dependent changes in translation levels during the UPR^{ER}.
A) Comparison of translation levels (footprint RPKMs) for each gene, as assayed by ribosome profiling, between wild-type cells (BrÜn 1362) treated with 5mM DTT and wild-type cells (BrÜn 1362) grown in rich media only.
B) Comparison of translation levels between wild-type cells (BrÜn 1362) treated with 2µg/mL Tm and wild-type cells (BrÜn 1362) grown in rich media only.
C) Comparison of translation levels between *hac1Δ* (BrÜn 4431) and wild-type cells (BrÜn 1362) treated with 5 mM DTT.
Note that for panels A-C, collection is described in Figure 2.2. Previously reported Hac1 targets (Travers et al., 2000) are shown with dark squares while all other genes are shown with light circles. Reported Hac1 targets were significantly (****p<0.0001) more likely to be upregulated upon UPR^{ER} induction than the full gene set.

Biological process	p-value
protein localization to endoplasmic reticulum	3.58E-10
single-organism metabolic process	1.99E-07
posttranslational protein targeting to membrane, translocation	1.13269E-06
single-organism process	1.31535E-06
posttranslational protein targeting to membrane	1.04981E-05
protein targeting to ER	1.2165E-05
glycoprotein metabolic process	1.29573E-05
protein glycosylation	1.57638E-05
macromolecule glycosylation	1.57638E-05
establishment of protein localization to endoplasmic reticulum	1.84599E-05
glycoprotein biosynthetic process	3.43284E-05
response to endoplasmic reticulum stress	8.77364E-05
glycosylation	0.000144604
ERAD pathway	0.000271702
ER-associated ubiquitin-dependent protein catabolic process	0.000727358
protein targeting to membrane	0.00161035
oxidation-reduction process	0.015322006
single-organism catabolic process	0.017236996
transmembrane transport	0.019718658
cotranslational protein targeting to membrane	0.027334053
Cellular component	**p-value**
endoplasmic reticulum	2.64E-14
endoplasmic reticulum part	1.12E-13
endoplasmic reticulum membrane	2.56E-10
nuclear outer membrane-endoplasmic reticulum membrane network	3.88E-10
endomembrane system	2.02E-06
intrinsic component of membrane	2.80E-06
integral component of membrane	3.74E-06
membrane	7.23E-06
membrane part	3.38E-05
endoplasmic reticulum lumen	0.000136941
rough endoplasmic reticulum	0.002676583
rough endoplasmic reticulum membrane	0.002676583
endoplasmic reticulum Sec complex	0.006302302
Sec62/Sec63 complex	0.017368227
plasma membrane	0.039522841
Molecular function	**p-value**
catalytic activity	0.002236339
oxidoreductase activity	0.00443889
transmembrane transporter activity	0.041926906

active transmembrane transporter activity	0.044978514
heme binding	0.049463231
tetrapyrrole binding	0.049463231

Table 2.1. Gene ontology (GO) analysis for genes showing at least 2-fold enrichment in translation upon DTT treatment.

Biological process	p-value
single-organism metabolic process	6.97E-16
single-organism process	6.78E-12
cellular amino acid biosynthetic process	1.99E-11
alpha-amino acid biosynthetic process	5.85E-11
alpha-amino acid metabolic process	6.25E-11
small molecule biosynthetic process	4.80E-10
carboxylic acid metabolic process	1.72E-09
oxoacid metabolic process	1.81E-09
organic acid metabolic process	2.06E-09
cellular amino acid metabolic process	2.15E-09
small molecule metabolic process	1.27E-08
single-organism biosynthetic process	2.94E-08
organic acid biosynthetic process	4.50E-08
carboxylic acid biosynthetic process	4.50E-08
aspartate family amino acid biosynthetic process	3.38E-07
methionine biosynthetic process	9.39575E-05
aspartate family amino acid metabolic process	0.000125628
serine family amino acid metabolic process	0.000144999
sulfur amino acid biosynthetic process	0.000220233
single-organism catabolic process	0.000383734
response to organic substance	0.000413829
methionine metabolic process	0.000707317
response to endoplasmic reticulum stress	0.000848374
serine family amino acid biosynthetic process	0.003381465
multi-organism cellular process	0.003430676
response to unfolded protein	0.003622535
single-organism cellular process	0.004147036
sulfur amino acid metabolic process	0.005276639
conjugation with cellular fusion	0.008740976
conjugation	0.010296847
sulfur compound biosynthetic process	0.010842001
pyridine-containing compound metabolic process	0.011605604
oxidation-reduction process	0.014240952
pyridine nucleotide metabolic process	0.016326481
arginine biosynthetic process	0.017920256

ERAD pathway	0.026649695
homoserine metabolic process	0.028608569
arginine metabolic process	0.032555634
cellular response to organic substance	0.04068641
multi-organism process	0.043457014
response to chemical	0.045981574
response to topologically incorrect protein	0.046405287
Cellular component	**p-value**
endoplasmic reticulum	7.23E-07
plasma membrane	3.17993E-06
cell periphery	7.30999E-06
membrane	1.19191E-05
endoplasmic reticulum part	0.000432549
endomembrane system	0.00431358
storage vacuole	0.006142112
fungal-type vacuole	0.006142112
lytic vacuole	0.007124098
nuclear outer membrane-endoplasmic reticulum membrane network	0.012197167
intrinsic component of membrane	0.015364683
endoplasmic reticulum lumen	0.017353191
endoplasmic reticulum membrane	0.018169305
membrane part	0.034126491
intrinsic component of plasma membrane	0.036945303
Molecular function	**p-value**
catalytic activity	0.000125587
oxidoreductase activity	0.02567056

Table 2.2. Gene ontology (GO) analysis for genes showing at least 2-fold enrichment in translation levels upon Tm treatment.

Normalizing translation levels to mRNA levels allowed us to determine TEs across all annotated ORFs (Ingolia et al., 2009), enabling detection of Hac1-dependent TE shifts upon UPR^{ER} activation. Although UPR^{ER} activation has been reported to influence TEs of some genes (Krishnan et al., 2014; Labunskyy et al., 2014; Payne et al., 2008), little is known about the pervasiveness of or potential mechanisms behind such regulation. Rather, the UPR^{ER} has been defined primarily as a transcriptional response. Our data are consistent with this general model, with a clear cohort of UPR^{ER}-driven, Hac1-dependent upregulated transcripts seen (Figure 2.3). However, evidence for several dozen translationally regulated genes also emerged from our data. As expected, *HAC1* was one of the most strongly translationally upregulated genes upon DTT or Tm treatment (Figure 2.5A, 2.5B). An additional small subset of annotated Hac1 transcriptional targets seemed to show translational upregulation with UPR^{ER} activation, although the mechanistic basis for this remains unclear. The most prominent example was functionally uncharacterized ER-related gene *ULI1* (Metzger and Michaelis, 2008), which was also one of the most highly induced transcriptional targets of Hac1 (Figure 2.3). The large increase in *ULI1* TE seen upon DTT treatment may point to a new translational mechanism linked to UPR^{ER} activation (Figure 2.5).

Additionally, several annotated Hac1 targets appeared to show a Hac1-dependent decrease in TE upon UPR^{ER} activation (Figure 2.5). This type of TF-dependent TE drop is a hallmark of LUTI-based regulation during meiotic differentiation (Cheng et al., 2018). Because transcription of poorly-translated LUTI mRNAs decreases production of canonical well-translated transcript isoforms, TF-driven LUTI mRNA synthesis is detected in ribosome profiling datasets as translational repression (Cheng et al., 2018). We focused our attention on investigating *HNT1,* an annotated Hac1 target that consistently showed strong Hac1-and UPR^{ER}-dependent translational repression (Figure 2.5; [Travers et al., 2000]), by comparing its regulation to that of the most well-characterized Hac1 target, *KAR2*.

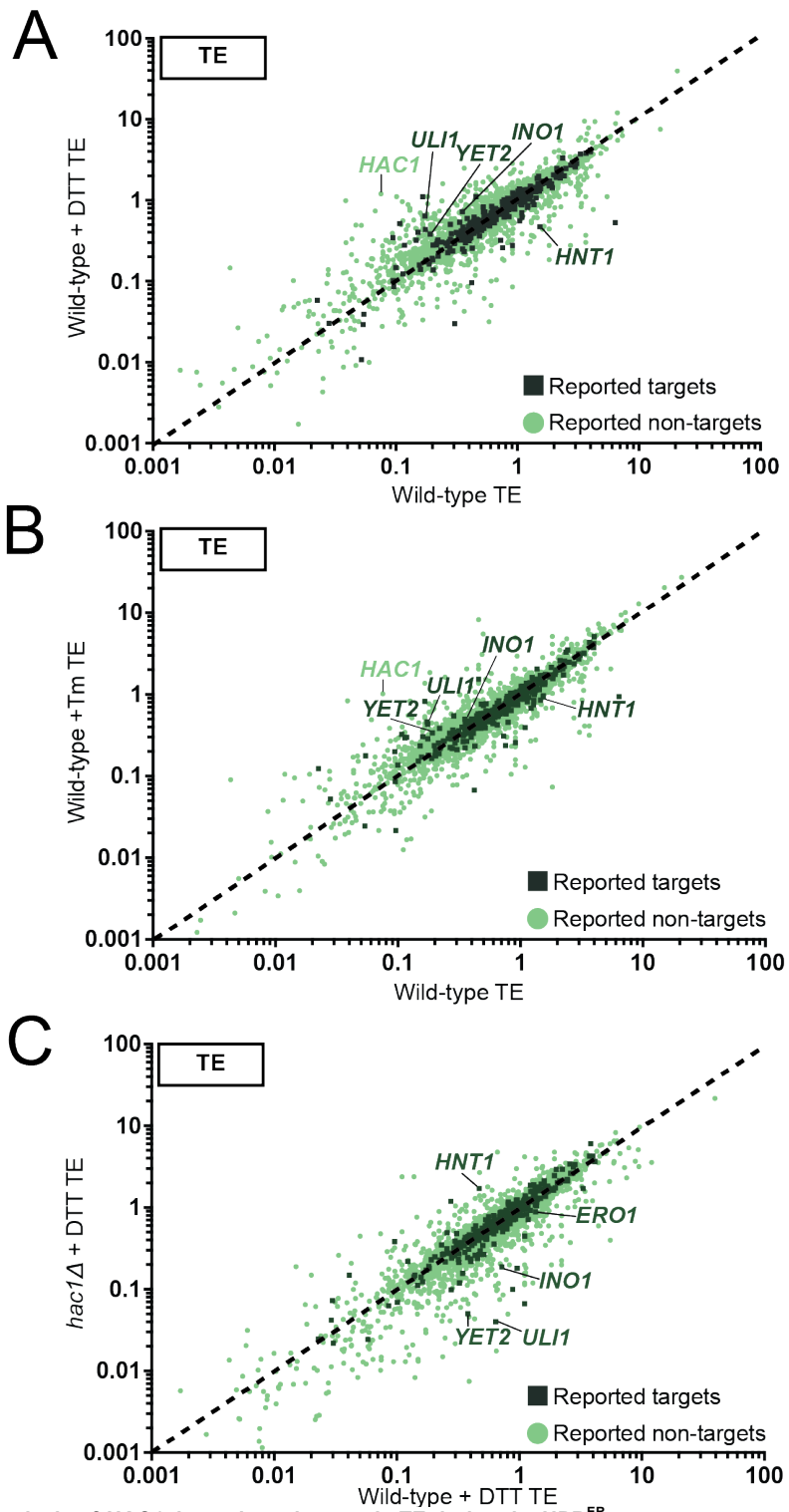

Figure 2.5. Global analysis of *HAC1*-dependent changes in TE during the UPR^{ER}.
A) Comparison of TEs for each gene between wild-type cells (BrÜn 1362) treated with 5mM DTT and wild-type cells (BrÜn 1362) grown in rich media only.
B) Comparison of TEs for each gene between wild-type cells (BrÜn 1362) treated with 2µg/mL Tm and wild-type cells (BrÜn 1362) grown in rich media only.
C) Comparison of TEs between *hac1Δ* (BrÜn 4431) and wild-type cells (BrÜn 1362) treated with 5 mM DTT.
Note that for panels A-C, collection is described in Figure 2.2. Previously reported Hac1 targets (Travers et al., 2000) are shown with dark squares while all other genes are shown with light circles.

HNT1 is a conserved member of the histidine triad superfamily (Séraphin, 1992). Its cellular function remains unclear, although a mammalian family member has recently been implicated in regulation of m^7G mRNA caps, suggesting that this gene family may be involved in translation (Kiss et al., 2017a, 2017b). Before investigating *HNT1* regulation, we first confirmed that our dataset reported the expected mRNA induction of canonical UPR^{ER} targets. As expected, a single *KAR2* mRNA isoform accumulated in a UPR^{ER}- and Hac1-dependent manner, as judged by northern blotting (Figure 2.6A). *KAR2* mRNA was well translated when present, with little change in TE seen upon UPR^{ER} activation (Figure 2.6B). In contrast, while UPR^{ER} activation resulted in increased overall *HNT1* mRNA levels (Figure 2.7A), it also resulted in a shift in the transcript isoforms present in cells. A longer *HNT1* mRNA species was observed by mRNA-seq and northern blotting following 1 hr of DTT or Tm treatment (Figure 2.7). The presence of the longer transcript was associated with lower TE values for the *HNT1* ORF and with translation of at least three uORFs in its extended 5' leader (Figure 2.7E, 2.7F). Despite exhibiting hallmarks of LUTI-based regulation, the canonical *HNT1* transcript persisted after 1 hr of UPR^{ER} induction (Figure 2.7B, 2.7C). Because the first LUTI case defined, $NDC80^{LUTI}$, resulted in complete disappearance of the canonical *NDC80* transcript when induced, we wondered if the apparently weaker LUTI induction observed for *HNT1* during the UPR^{ER} would be sufficient to have an effect on Hnt1 protein levels. We epitope-tagged endogenous Hnt1 and performed immunoblotting to detect protein levels following UPR^{ER} induction. Within 2 hr of DTT or Tm treatment, Hnt1 levels dropped to less than 50% of their levels prior to drug treatment (Figure 2.8). We confirmed that, like canonical UPR target *KAR2* (Figure 2.6C), production of the long *HNT1* transcript isoform was dependent on *IRE1,* and thus part of the canonical UPR^{ER} (Figure 2.7C).

We identified a strong type-2 unfolded protein responsive element (UPRE2), a DNA motif associated with Hac1 binding in the promoters of some UPR^{ER} targets (Patil et al., 2004), close to the distal *HNT1* TSS (Figure 2.7D). The location of the UPRE2, coupled with the observation that induction of the longer transcript was dependent on *HAC1*, led us to hypothesize that the long *HNT1* isoform was a direct Hac1 target. To test this hypothesis, we constructed reporters containing *GFP* under control of the extended promoter region of *HNT1,* either with an intact UPRE2 adjacent to the distal TSS or a mutated motif (Figure 2.9A). Following 90 min of DTT treatment, cells harboring *pHNT1-GFP* produced a high level of an extended *GFP* transcript isoform whose expression was severely reduced in the *pHNT1ΔUPRE2-GFP* mutant (Figure 2.9B, 2.9C). GFP protein levels in the wild-type reporter, but not the UPRE2 mutant, mirrored those of Hnt1 following UPR^{ER} induction (Figure 2.9D, 2.9E). We concluded that *HNT1* is a LUTI target of Hac1 and that the UPR^{ER} involves coordinated activation and repression of target gene expression through Hac1-regulated alternate TSS usage. We suspected that *HNT1* might be just one of a class of "negative" targets of Hac1 and thus performed a systematic analysis of our data, searching for the expected signatures of Hac1 LUTI targets, including Hac1-dependent decreases in TE and appearances of 5' extended transcripts (Cheng et al., 2018). We identified 18 additional potential LUTI targets (Table 2.3).

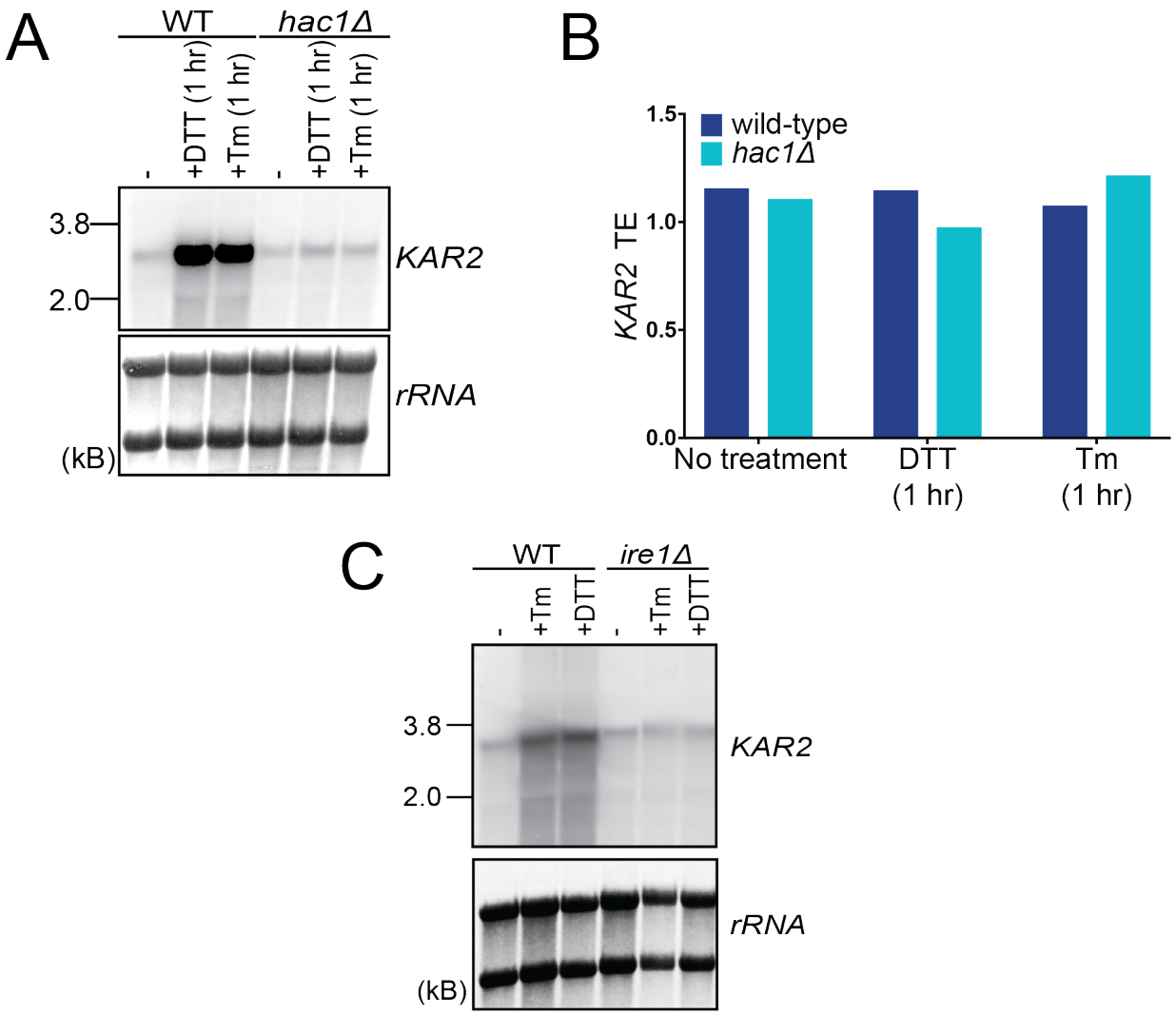

Figure 2.6. *HAC1*-dependent induction of *KAR2* during the UPR^{ER}.
A) Northern blotting for *KAR2* shows the abundance of a single transcript isoform increases upon 1 hr treatment with 5mM DTT or 2μg/mL Tm, in wild-type cells (BrÜn 1362) but not *hac1Δ* cells (BrÜn 4431). Total RNA from the collection described in Figure 2.2 was used for the blot shown.
B) Comparison of *KAR2* TEs in rich media alone, or with 5mM DTT or 2μg/mL Tm. TE values were calculated over the annotated ORF using mRNA-seq and ribosome profiling data obtained from the harvesting scheme described in Figure 2.2
C) Northern blotting for *KAR2* shows the abundance of a single transcript isoform increases upon 1 hr treatment with 5mM DTT or 2μg/mL Tm in wild-type cells (BrÜn 15) but not *ire1Δ* cells (BrÜn 15924).

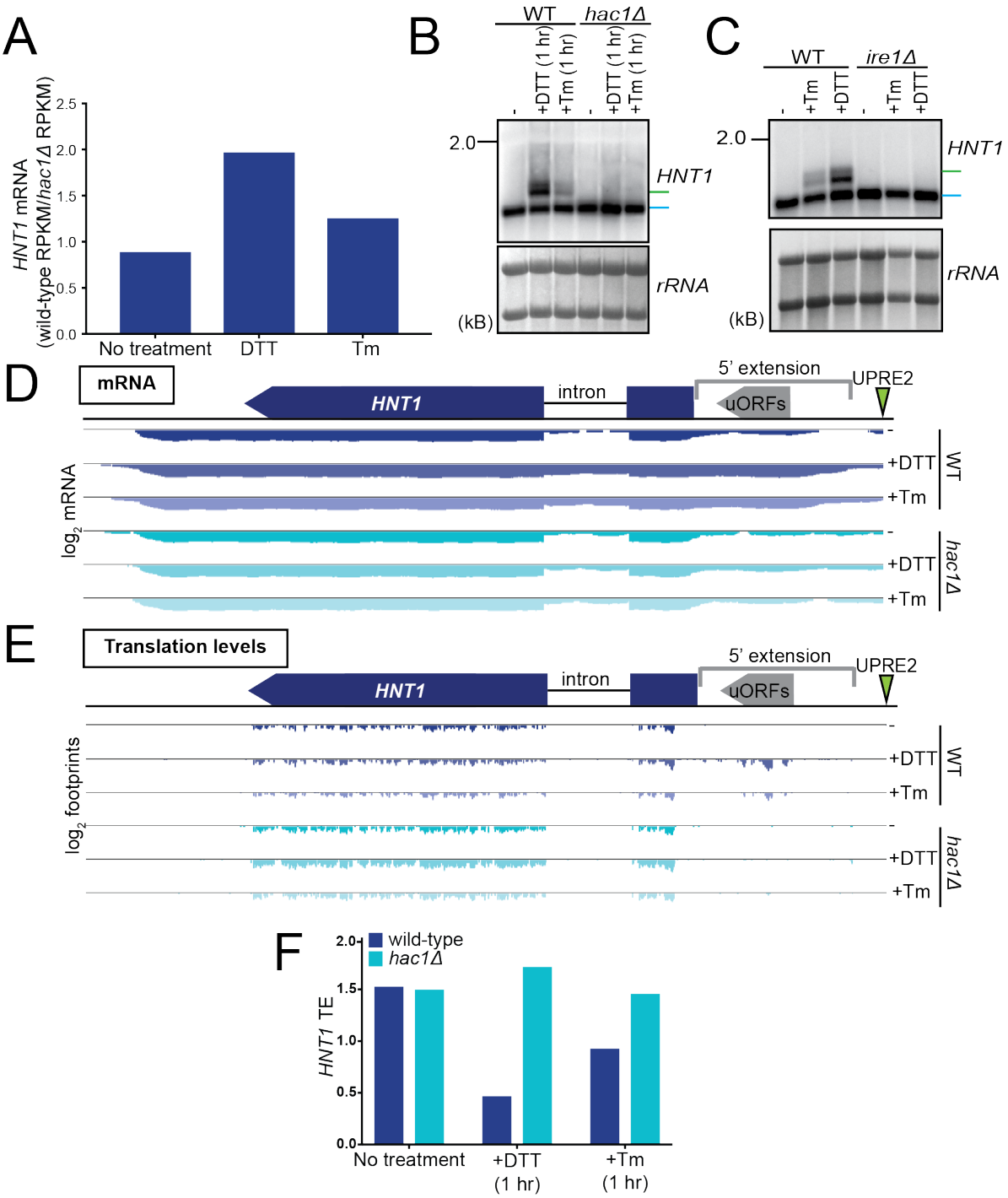

Figure 2.7. *HAC1*-dependent transcription of an alternate *HNT1* transcript isoform is correlated with decreased TE.
A) *HNT1* mRNA accumulates during UPR^{ER} induction by DTT or Tm (see Figure 2.2 for harvesting scheme).
B-C) Northern blotting for *HNT1* reveals an extended transcript isoform is produced upon 1 hr treatment with 5mM DTT or 2μg/mL Tm, dependent on *HAC1* and *IRE1*. Blue and green bars highlight canonical and extended transcripts, respectively.
D-E) Annotation of *HNT1* mRNA expression (D) and translation levels (E) during the UPR^{ER}, as determined by the experiment described in Figure 2.2. Above, gene model showing the *HNT1* ORF and intron, along with a 5' extension containing uORFs. The 5' extension begins just downstream of a UPRE2 motif. Below, $\log_2$ mRNA (D)/footprints(E) (RPKM) showing an extension in transcript length upon UPR^{ER} activation in wild-type cells and translation of uORFs in the extended leader.
F) Comparison of *HNT1* TEs in rich media alone, or with 5mM DTT or 2μg/mL Tm. TE values were calculated over the annotated ORF using mRNA-seq and ribosome profiling data obtained from the harvesting scheme described in Figure 2.2.

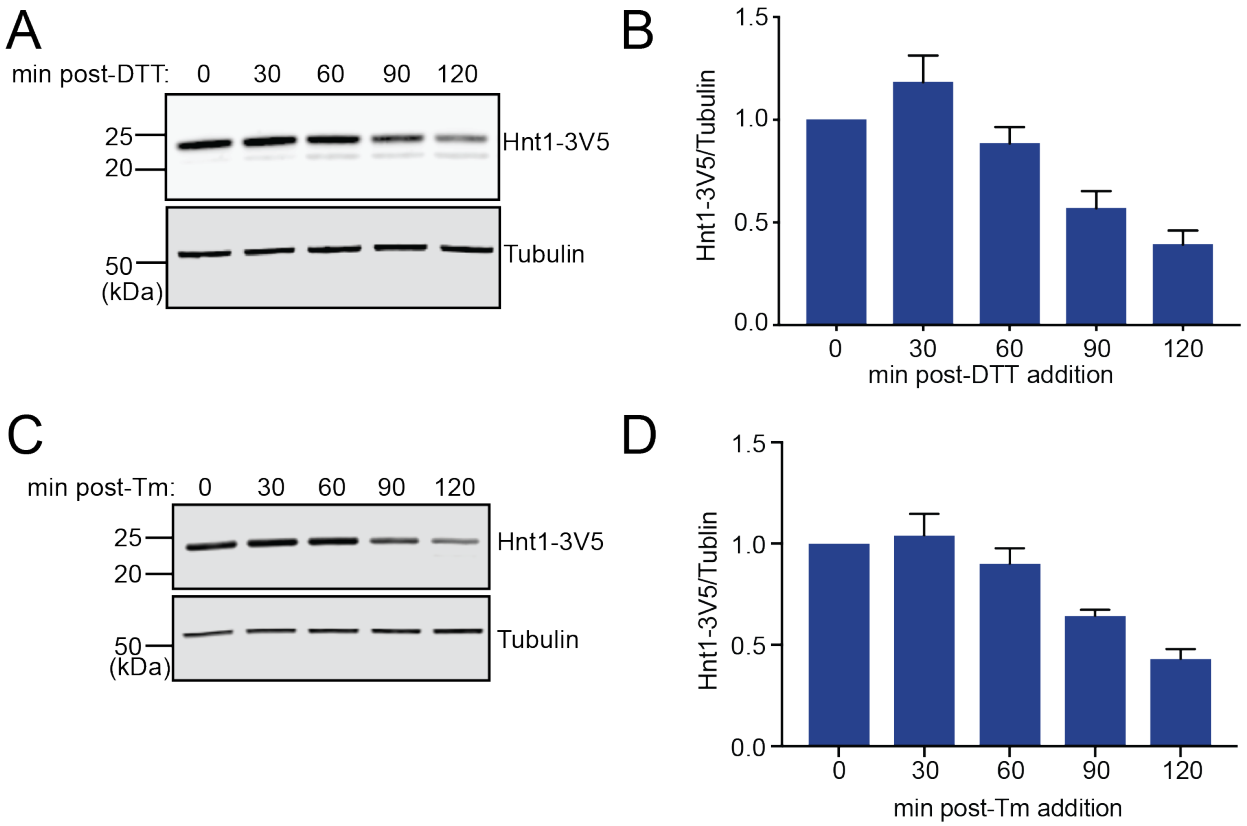

Figure 2.8. Expression of the *HNT1* alternate transcript isoform is correlated with decreased protein levels.
A) A time-dependent decrease in Hnt1-3V5 protein was observed by immunoblot upon treatment of BrÜn 10778 (*HNT1-3V5*) with 5mM DTT.
B) Quantification of Hnt1-3V5 protein levels during the DTT-induced UPR^{ER} in wild-type cells, as in panel A. The average of 3 biological replicates is shown with error bars representing SD.
C) A time-dependent decrease in Hnt1-3V5 protein was observed by immunoblot upon treatment of BrÜn 10778 (*HNT1-3V5*) with 2µg/mL Tm.
D) Quantification of Hnt1-3V5 protein levels during the Tm-induced UPR^{ER} in wild-type cells, as in panel C. The average of 3 biological replicates is shown with error bars representing SD.

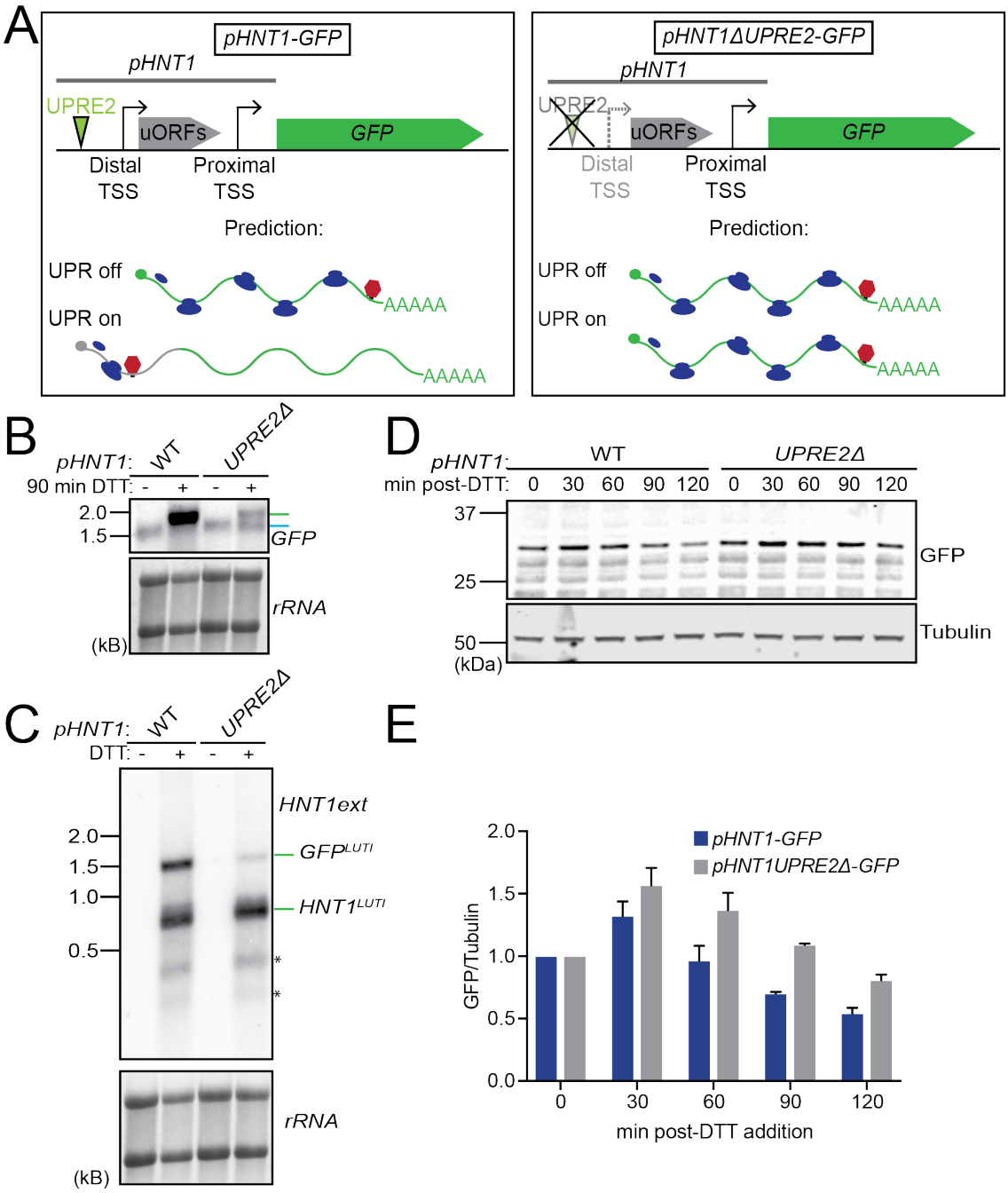

Figure 2.9. A UPRE2 motif in the distal *HNT1* promoter is required for robust expression of the alternate transcript and for decreased protein levels during the UPR^{ER}.

A) GFP reporters were constructed in order to assess the role of the UPRE2 in the *HNT1* distal promoter. For *pHNT1-GFP* (BrÜn 15968), *pHNT1* (-600 to +42) was cloned ahead of an unstable GFP construct (with the ubiquitin coding region fused upstream of the GFP coding region from pUB158). For *pHNT1ΔUPRE2-GFP* (BrÜn 16374), five of the six bp in the UPRE2 motif starting at -284 were deleted. Constructs were integrated at the *TRP1* locus.

B) Northern blotting for *GFP* (B) or the *HNT1* extended leader (C) shows a longer transcript isoform is produced upon UPR^{ER} induction (by 90 min 5 mM DTT treatment), but expression of the longer isoform is strongly reduced upon disruption of the UPRE2 motif. Blue and green bars highlight canonical and extended transcripts, respectively. Asterisks in (C) indicate bands likely to reflect low levels of premature termination of transcription from the distal TSS.

D) A time-dependent decrease in GFP protein levels upon treatment with 5mM DTT is observed in cells harboring *pHNT1-GFP* (BrÜn 15968), but is less efficient in cells harboring *pHNT1ΔUPRE2-GFP* (BrÜn 16374).

E) Quantification of GFP protein levels during the DTT-induced UPR^{ER}. The average of 3 biological replicates is shown with error bars representing SD.

		Wild-type/*hac1Δ* dataset		*AID-HAC1* dataset		
Gene	**Full name**	***HAC1*-dependent decrease in TE**	***HAC1*-dependent extended transcript**	**Hac1-dependent decrease in TE**	**Hac1-dependent extended transcript**	**Monosome shifted upon DTT addition[a]**
COX20	Cytochrome c OXidase	+	+	+	+	+
HNT1	Histidine triad NucleoTide-binding	+	+	+	+	+
MSK1	Mitochondrial aminoacyl-tRNA Synthetase, lysine (K)	+	+	+	+	-
SOM1	SOrting Mitochondrial	+	+	+	+	+
GTT1	GlutaThione Transferase	+	+	+	+	+
IRC4	Increased Recombination Centers	+	+	+	+	+
CRR1	CRH-Related	+	+	+	+	-
HEM1	HEMe biosynthesis	+	+	+	+	+
OXA1	cytochrome OXidase Activity	+	+	+[c]	+	+
NRG2	Negative Regulator of Glucose-controlled genes	+	+	+[c]	+	-
YPL067C	Histidine Triad with Channel	+	+	+	+	-
SRM1	Suppressor of Receptor Mutations	+	+	+	+	+
CTS1	ChiTinaSe	+	+	+[c]	+	-
PCM1	PhosphoaCetylglucosamine Mutase	+	+	+	+	+
YHB1	Yeast flavoHemogloBin	+	+	+	+	+
FLR1[d]	FLuconazole Resistance	+	+	-	+	-
PRY1[d]	Pathogen Related in Yeast	+	+[b]	+[c]	+[b]	-
SRL1[d]	Suppressor of Rad53 null Lethality	+	+	+[c]	+[b]	-
SET2[d]	SET domain-containing	+	+	-	+	-

[a]As reported in (Payne et al., 2008)
[b]Difficult to definitively call for reasons including locus complexity
[c]Hac1-dependence inconclusive
[d]Called as LUTI candidates in wild-type/*hac1Δ* but not *AID-HAC1*

Table 2.3. Hac1-dependent LUTI candidates. Systematic analysis of mRNA-seq and TE data from wild-type and *hac1Δ* cells (Figure 2.2) was used to predict LUTI candidates. Nineteen candidates were identified. Re-analysis of these same features using the *AID-HAC1* allele (Figure 2.13) confirmed 15 of these candidates, and many were previously reported to show decreased translation upon Tm addition (Labunskyy et al., 2014).

2.2.2 A degradable version of Hac1 enables high-confidence identification of its targets

Confidently identifying Hac1-dependent targets of the UPR^{ER}, whether canonical (positive) or non-canonical (LUTI-based negative), was done here and previously by using comparison of wild-type cells to those deleted for *HAC1* or other core UPR^{ER} genes (Travers et al., 2000). While this has been a valuable approach, the risk in comparing gene expression measurements from wild-type cells and constitutive mutants is that it is difficult to ensure that secondary effects—on gene expression and in the form of genetic suppressors—are not confounding, resulting in misinterpretation of results. Such suppressors have been reported in *hac1*Δ cells, including in our strain background (Lee et al., 2003). We were concerned that perhaps our identification of non-canonical Hac1 targets might be an unexpected artifact of such secondary effects. We therefore replaced Hac1 with a version that contained an auxin-inducible degron (AID) tag, which could be depleted on-demand by auxin addition. We found that *AID-HAC1* rescued the growth defect of *hac1*Δ cells grown with DTT, suggesting normal functionality (Figure 2.10A, 2.10B;[Nishimura et al., 2009]). AID-Hac1 was stable in the presence of auxin in strains lacking the exogenous plant *TIR1* F-box auxin receptor gene, but in strains carrying *TIR1*, AID-Hac1 that accumulated during DTT pre-treatment was rapidly depleted upon auxin addition (Figure 2.10C, 2.10D). Notably, AID-Hac1 protein was efficiently, but not fully, depleted in this background. As a result, we expected gene expression effects measured by comparing *AID-HAC1 TIR1* cells with and without auxin to be dampened relative to those from comparison of wild-type and *hac1*Δ cells.

We were concerned that a persisting nuclear pool of AID-Hac1 may be capable of robustly carrying out its TF function, spatially isolated from the location of degradation. To investigate this, we analyzed expression of *KAR2* in cells that were treated with auxin following 45 min DTT pre-treatment. *KAR2* levels were rapidly reduced under these conditions, suggesting that auxin-induced Hac1 degradation reduced its TF activity (Figure 2.11A). This result indicated that kinetic experiments using *AID-HAC1* cells might allow confident prediction of direct Hac1 transcriptional targets. The long isoform of *HNT1* (*$HNT1^{LUTI}$*) showed similar dynamics to the *KAR2* transcript, declining to undetectable levels within 20 min of auxin treatment following DTT pre-treatment (Figure 2.11B). This rapid timing provided additional evidence that the *$HNT1^{LUTI}$* is a direct target of Hac1.

Although robust changes to transcription were observed by this strategy, effects on protein level of the canonical target Kar2 were not readily reversible upon auxin addition (data not shown), perhaps because Kar2 protein is not rapidly turned over under these circumstances. Because we have found assaying protein level to be useful in determining whether a given transcriptional target is positive or negative (Cheng et al., 2018), we reasoned that pre-treating cells with auxin and subsequently inducing the UPR^{ER} would be a more fruitful strategy. To this end, we pre-treated cells with auxin for 15 min and then added DTT for up to 2 hr. In cells lacking *TIR1*, *KAR2* mRNA and protein levels revealed the expected induction upon DTT treatment regardless of auxin

addition (Figure 2.12). In contrast, in the *TIR1* background, DTT-dependent increases in *KAR2* transcript and protein levels were only observed if cells were pre-treated with vehicle. When pre-treated with auxin (depleting Hac1), efficient *KAR2* induction was largely prevented (Figure 2.12).

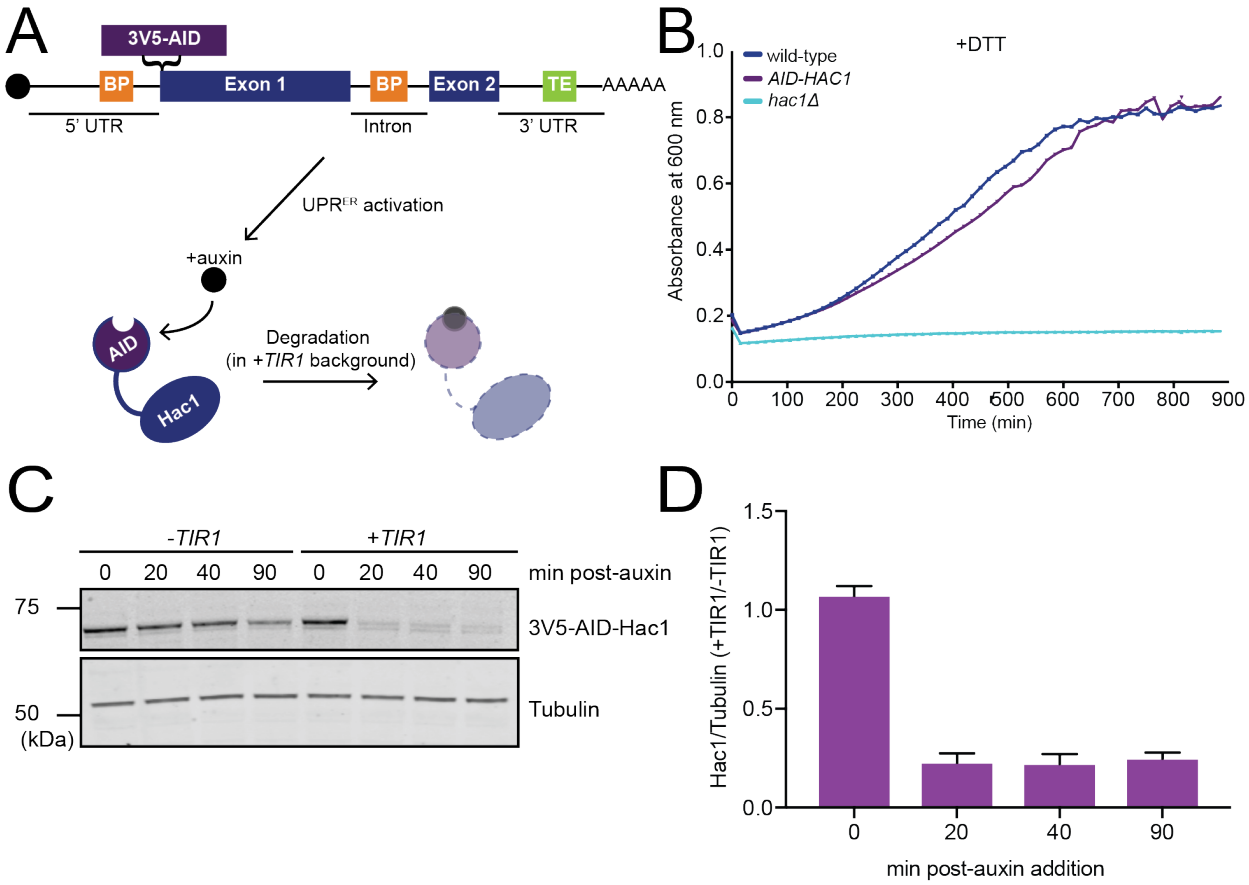

Figure 2.10. AID-Hac1 is functional and degradable upon auxin addition.
A) Schematic of the *AID-HAC1* allele. The *HAC1* promoter (507bp directly upstream of ATG) drives expression of *3V5-AID-HAC1*. The 3V5 tag and IAA7 degron (AID) were cloned in immediately after *HAC1*'s ATG start, and 844bp downstream of the *HAC1* ORF were also included in the construct. Note that regions of the 5' UTR and intron that participate in base-pairing (BP) to repress translation were unperturbed and are indicated in orange, and the 3' targeting element (TE) was also intact and is indicated in green. The entire construct was integrated at the *LEU2* locus in a strain lacking the endogenous copy of *HAC1*.
B) *AID-HAC1* (BrÜn 10353) rescues the growth defect of *hac1Δ* (BrÜn 4431) in 2.5mM DTT.
C) Immunoblotting for AID-Hac1 (anti-3V5) shows efficient degradation of the protein within 20 min of auxin addition following 45 min pre-treatment with 5mM DTT. As expected, this degradation occurred efficiently in the *+TIR1* strain (BrÜn 10744), but not the *–TIR1* strain (BrÜn 10532).
D) Quantification of AID-Hac1 protein levels upon auxin addition during the DTT-induced UPR^{ER}, as in panel C. The average of 3 biological replicates is shown with error bars representing SD.

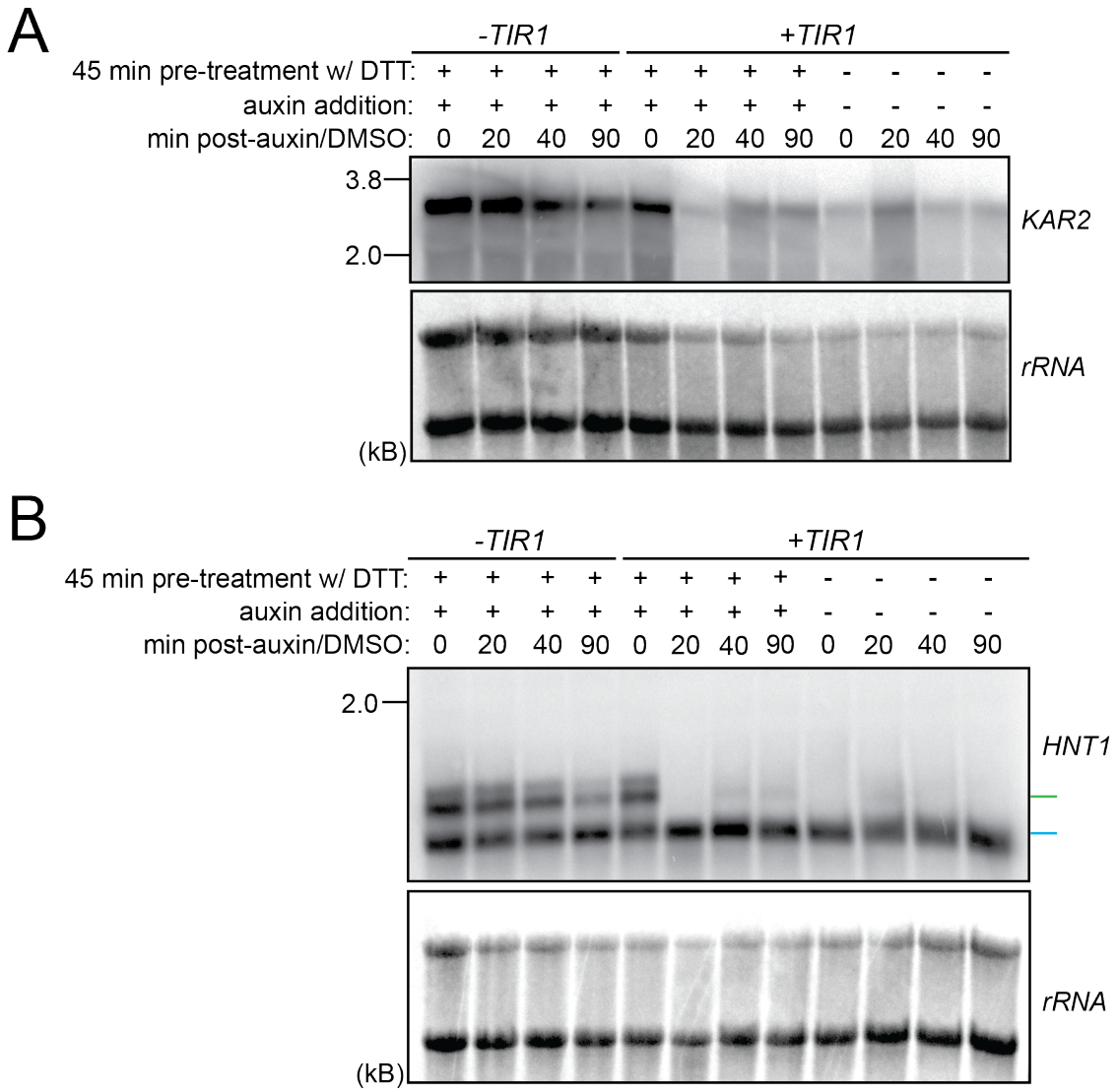

Figure 2.11. Degradation of AID-Hac1 results in observable changes in the levels of Hac1 targets.
A) Northern blotting for *KAR2* indicates that transcripts for canonical Hac1 targets decrease within 20 min of auxin addition following 45 min pre-treatment with 5 mM DTT. This decrease robustly occurs in the *+TIR1* strain background (BrÜn 10744), but not the *-TIR1* strain background (BrÜn 10532).
B) Northern blotting for *HNT1* reveals that *HNT1*^{LUTI} behaves in the same manner as *KAR2* (panel A) upon treatment with auxin following 45 min pre-treatment with 5mM DTT. Blue and green bars highlight canonical and extended transcripts, respectively.

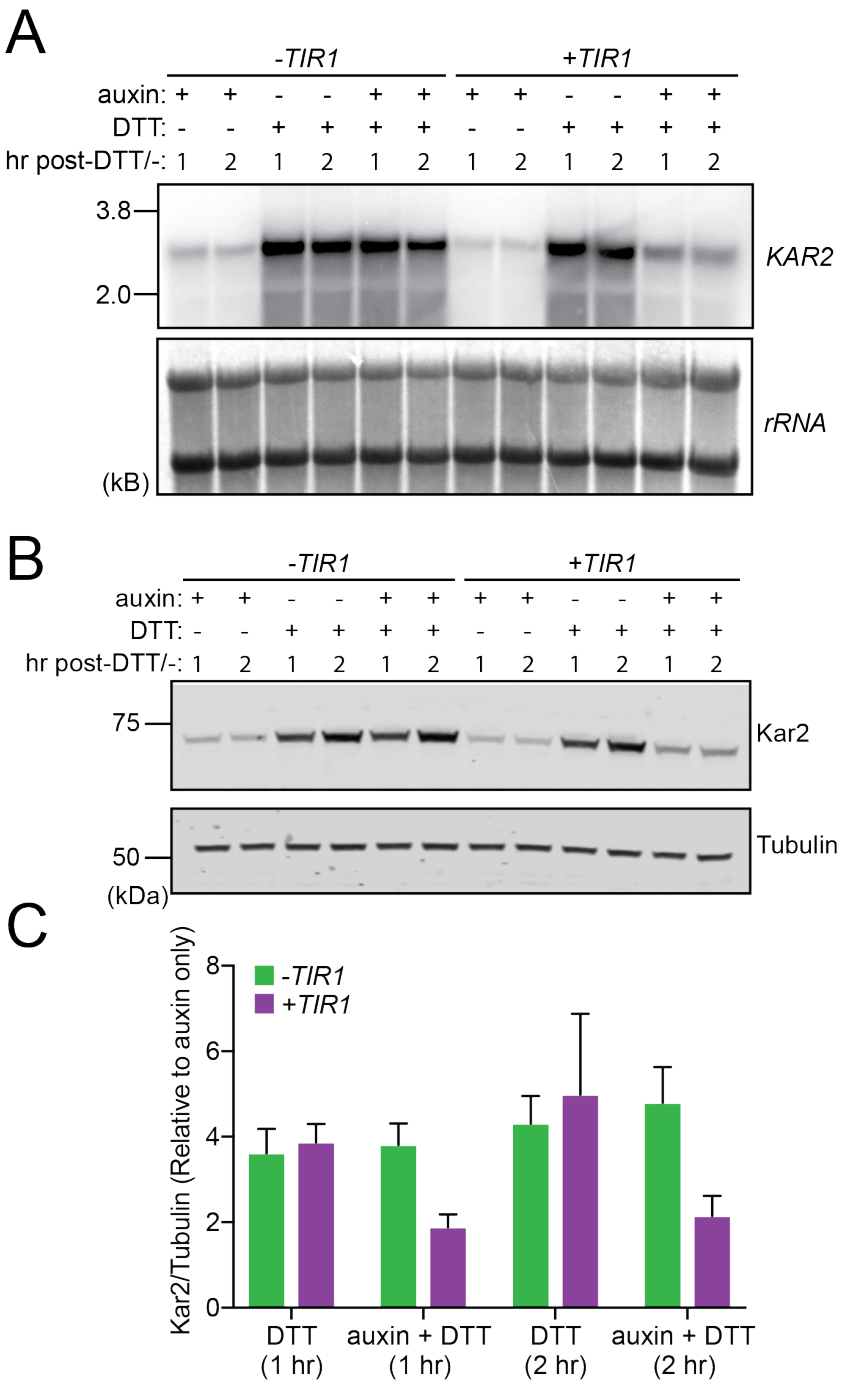

Figure 2.12. Pre-treating cells with auxin prevents expression of Hac1 targets upon subsequent UPR^{ER} activation.
A) Pre-treating cells with auxin for 15 min prevents increased *KAR2* expression upon subsequent treatment with 5mM DTT in the *+TIR1* background (BrÜn 10744), but not the *-TIR1* strain background (BrÜn 10532).
B) The effect of pre-treating cells with auxin for 15 min prior to 5 mM DTT treatment manifests in observable changes in Kar2 protein levels in the *+TIR1* background (BrÜn 10744), but not the *-TIR1* strain background (BrÜn 10532).
C) Quantification of Kar2 protein levels upon 5mM DTT treatment of auxin pre-treated cells, as in panel B. The average of 3 biological replicates is shown with error bars representing SD.

We next performed a new set of global gene expression measurements using the *AID-HAC1* strain background (Figure 2.13). We again measured mRNA and translation levels, and additionally collected matched extract for mass spectrometry in order to more completely evaluate Hac1-dependent effects on cellular physiology during the UPR^{ER}. Global effects on mRNA and translation were similar to those observed in our previous wild-type/*hac1*Δ experiment (Figure 2.14), but as expected, were milder than observed when comparing wild-type and *hac1*Δ cells. Nevertheless, we observed UPR^{ER}- and Hac1-dependent activation of known Hac1 targets, including *KAR2*, *ERO1*, and *PDI1* (2.14A). DTT-dependent induction of $HNT1^{LUTI}$ was observed by mRNA-seq, but not in cells depleted of Hac1 (Figure 2.15A). As before, translation of *HNT1* was decreased in a UPR^{ER}- and Hac1-dependent manner and was associated with translation of uORFs in the extended 5' leader, unless cells were depleted of Hac1 (Figure 2.15B, 2.15C). We confirmed the DTT and Hac1-dependent induction of $HNT1^{LUTI}$, as well as the correlated decrease in Hnt1 protein level, by northern and immunoblotting (Figure 2.16). We concluded that expression of $HNT1^{LUTI}$ results in decreased Hnt1 protein levels, dependent on Hac1, suggesting that our original results were not an artifact of constitutive *HAC1* deletion.

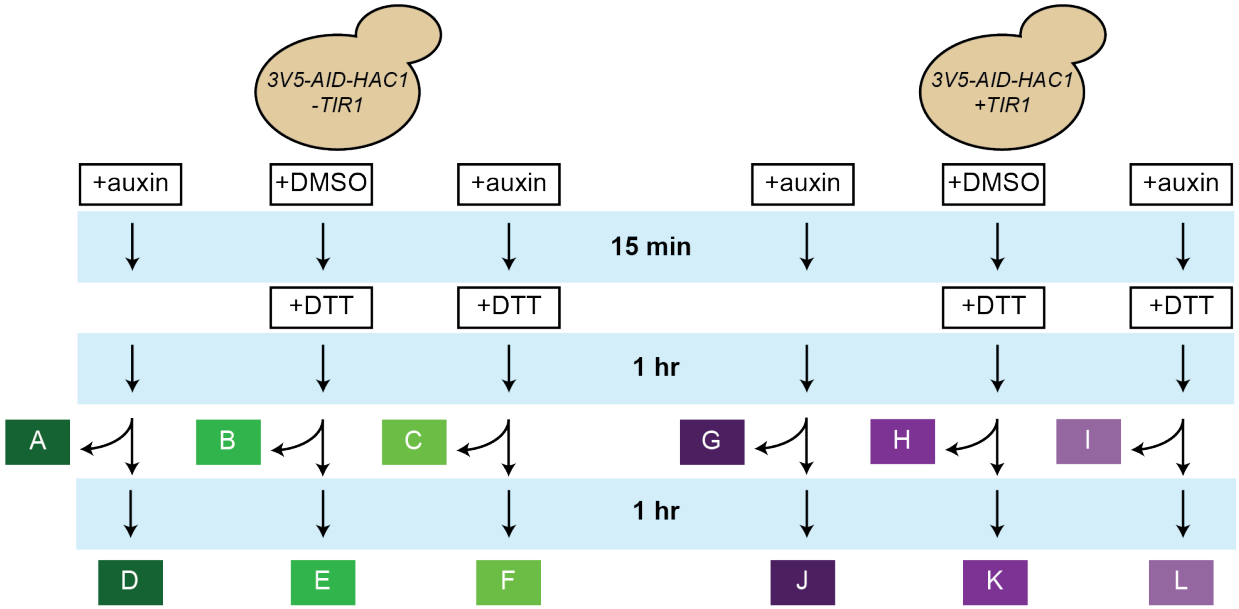

Figure 2.13. Schematic of harvesting scheme for *AID-HAC1* experiment. Parallel cultures of *AID-HAC1* containing strains, with (BrÜn 10744) and without (BrÜn 10532) *TIR1* in the background, were pre-treated with auxin (or vehicle) for 15 min. 5mM DTT was added to cultures as indicated, and samples A-C and G-I were collected following 1 hr of DTT treatment. After 1 additional hr, samples D-F and J-L were collected. Matched extract from each sample was used for mRNA-seq, ribosome profiling, and mass spectrometry.

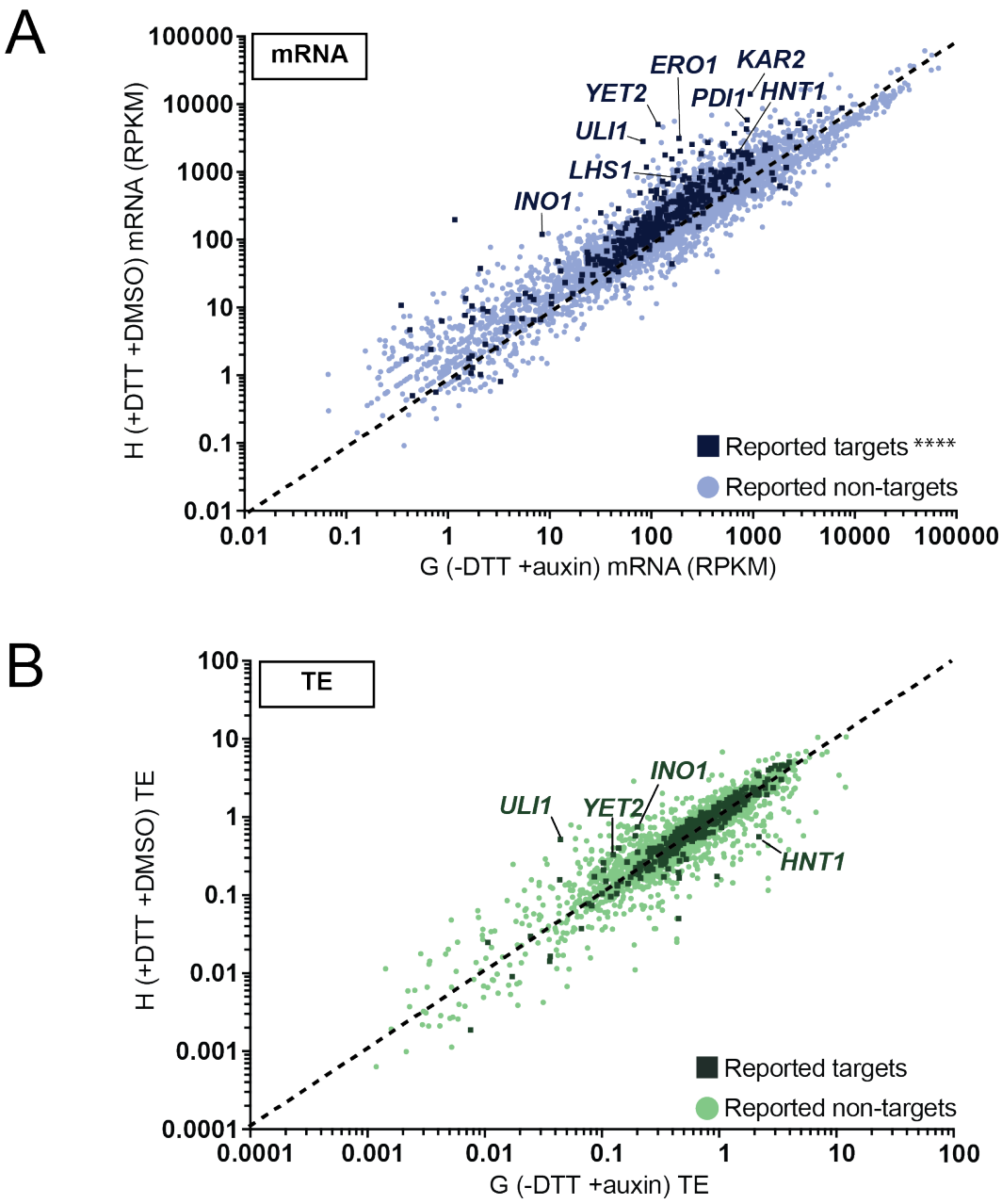

Figure 2.14. Global analysis of UPR^{ER}-dependent changes in gene expression in the *AID-HAC1* background.
A) mRNA levels from sample H (+*TIR1*, treated with vehicle and DTT) compared to from sample G (+*TIR1*, treated only with auxin). Reported Hac1 targets were significantly (****p<0.0001) more likely to be upregulated upon UPR^{ER} induction than the full gene set. B) TEs from sample H (+*TIR1*, treated with vehicle and DTT) compared to from sample G (+*TIR1*, treated only with auxin). Note that for panels A-B, collection is described in Figure 2.13. Previously reported Hac1 targets (Travers et al., 2000) are shown with dark squares while all other genes are shown with light circles.

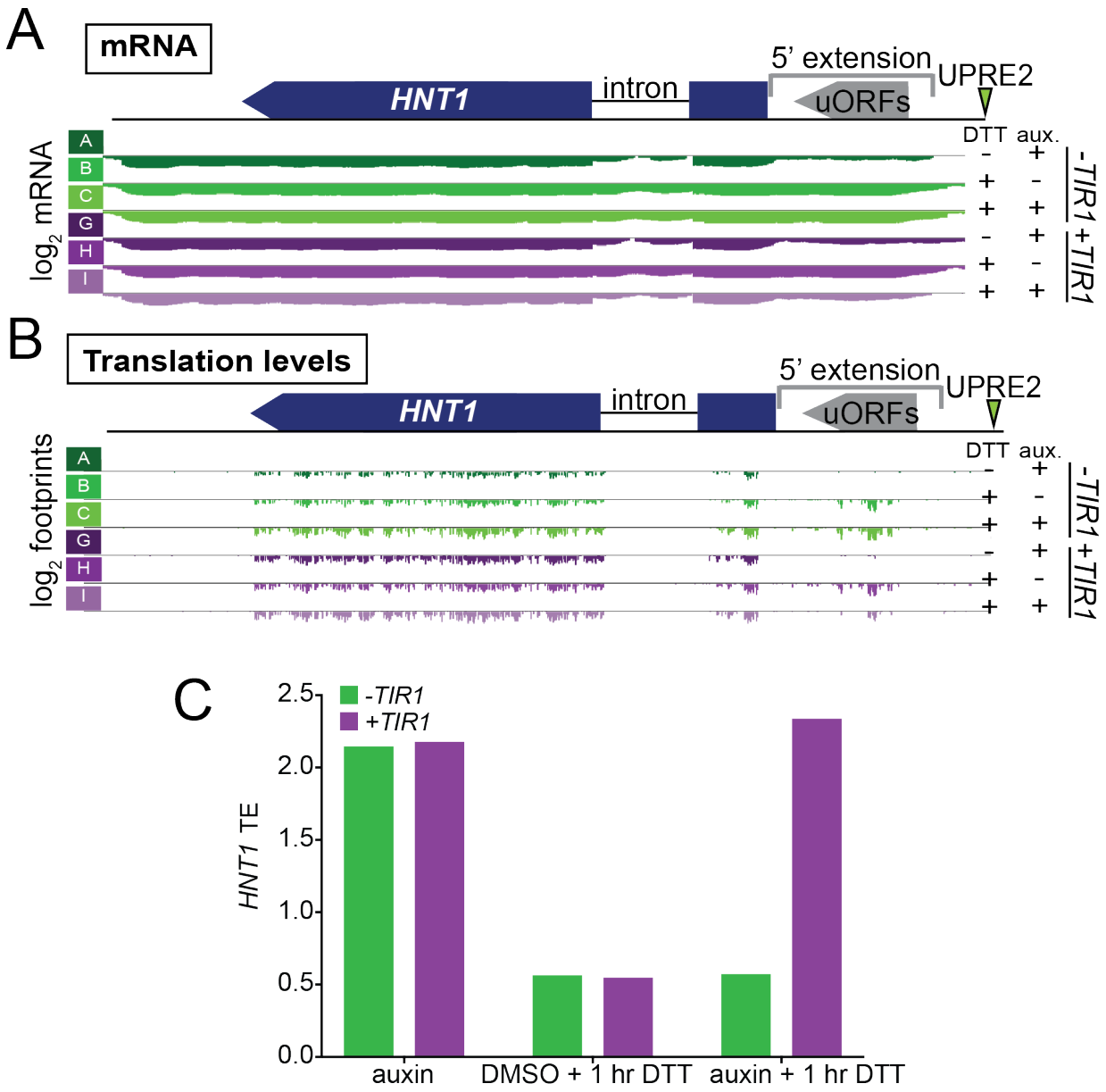

Figure 2.15. AID-Hac1 dependent transcription of an alternate *HNT1* transcript isoform is correlated with decreased TE. A-B) Annotation of *HNT1* mRNA expression (A) and translation levels (B) in the *AID-HAC1* background during the UPR^{ER}, as determined by the experiment described in Figure 2.13. Above, gene model. Below, log_2 mRNA (RPKM) (A)/footprints (RPKM) (B) showing an AID-Hac1 dependent *HNT1* transcript extension and translation of uORFs within the extension upon UPR^{ER} induction. C) Comparison of *HNT1* TE across samples A-C and G-I, showing a dramatic increase in TE when AID-Hac1 is degraded relative to TE during the UPR^{ER} without AID-Hac1 degradation.

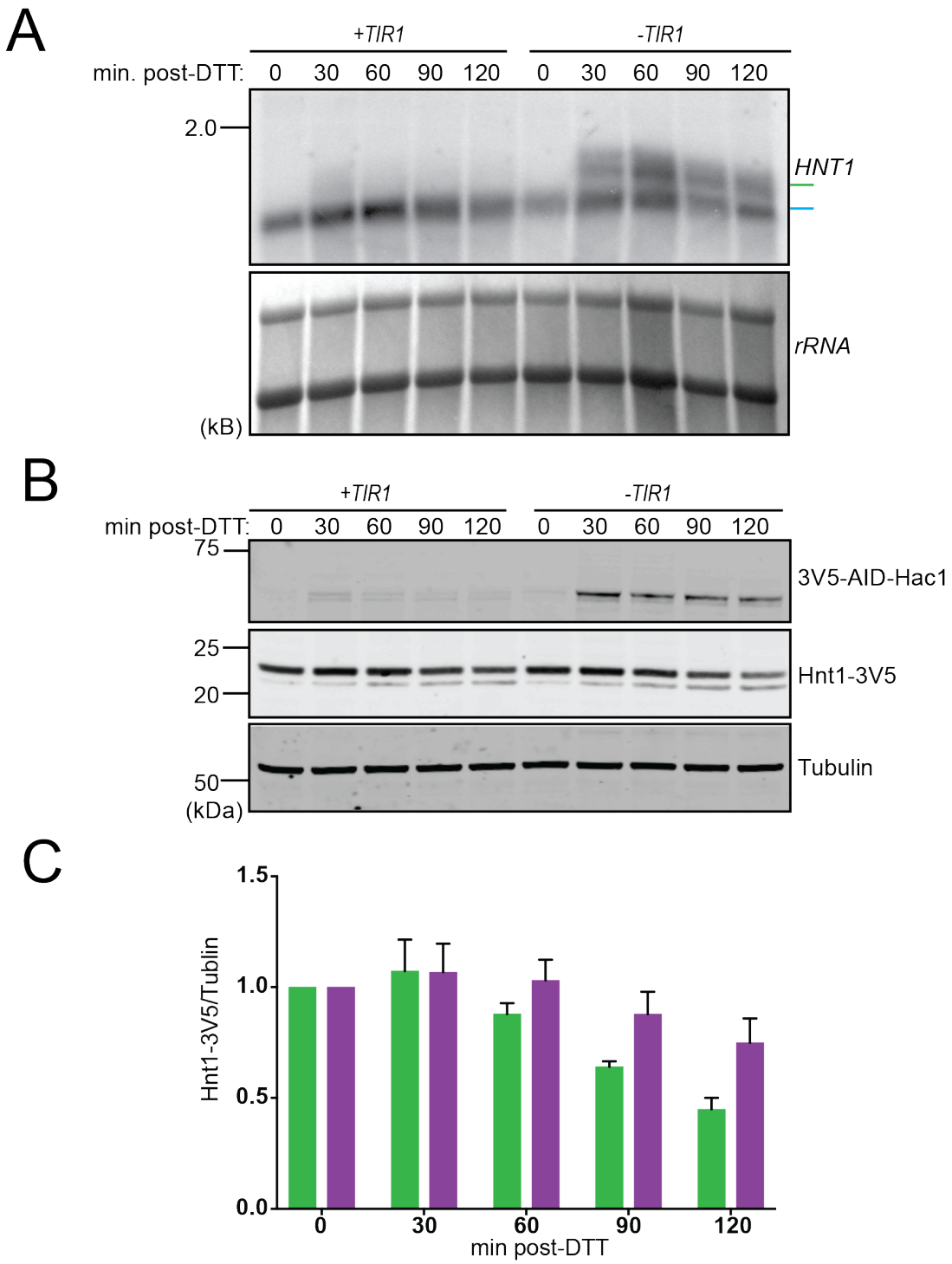

Figure 2.16. Hnt1 protein levels decrease during UPR^{ER} activation, dependent on AID-Hac1.
A) Northern blot analysis of *HNT1*^{LUTI} mRNA expression with (BrÜn 10924) and without (BrÜn 10925) AID-Hac1 degradation. Blue and green bars highlight canonical and extended transcripts, respectively.
B) Immunoblot showing AID-Hac1 dependent reduction in Hnt1-3V5 protein levels upon treatment with 5mM DTT (following 15 min auxin pre-treatment) in the *+TIR1* background (BrÜn 10924), but not the *-TIR1* background (BrÜn 10925).
C) Quantification of Hnt1-3V5 protein levels in *+TIR1* (BrÜn 10924) and *–TIR1* (BrÜn 10925) strains, showing Hnt1-3V5 levels remain higher when AID-Hac1 is degraded (*+TIR1* [BrÜn 10924]), as in panel B. The average of 3 biological replicates is shown with error bars representing SD.

2.2.3 Hac1 "negative" targets include genes involved in ETC function

We found that 15 of the original 19 annotated long transcript isoforms could be confirmed as UPR^{ER}- and Hac1-dependent in the *AID-HAC1* background (Table 2.3). Of the four that could not, two did not show the expected TE decrease and two showed the decrease independent of Hac1. These cases may be a result of yet undefined secondary effects in the delete background. We concluded that a set of LUTI targets is induced by Hac1 as part of the UPR^{ER}.

Several of the 15 Hac1-dependent LUTI-regulated genes were involved in electron transport chain (ETC) function, specifically in assembly of Complex IV (cytochrome c oxidase), which LUTI targets *COX20, OXA1,* and *SOM1* all contribute to. We thus investigated the possibility that downregulation of ETC components might be linked to UPR^{ER} activation and partly controlled by LUTI-based regulation. We first examined the regulation of *COX20,* a gene responsible for Cox2 processing and subsequent assembly of Complex IV (Hell et al., 2000). We confirmed the Hac1-dependent appearance of a dramatically 5' extended transcript isoform upon UPR^{ER} activation by mRNA-seq (Figure 2.17A) and translation of a uORF near the 5' end of this extended transcript, which was adjacent to a high-scoring UPRE2 (Figure 2.17B). Northern blotting for *COX20* revealed Hac1-dependent induction of a longer transcript upon DTT or Tm treatment, confirming that the mRNA-seq data did not simply reflect a partially overlapping transcript that excluded the *COX20* ORF (Figure 2.18). This longer *COX20* transcript isoform was also dependent on *IRE1* (Figure 2.18D).

We were initially concerned that the bands representing the two *COX20* transcript isoforms did not show the stoichiometry expected based on our mRNA-seq data from either large-scale experiment, with the longer transcript reproducibly resulting in a much fainter band than the canonical transcript. We attribute this effect to the large size difference between the transcripts (0.8 Kb versus approximately 2.6 Kb; Figure 2.18), as we observe that longer transcripts transfer less efficiently than shorter transcripts using our northern blotting protocol. Nevertheless, like the canonical UPR^{ER} target *KAR2*, production of $COX20^{LUTI}$ was abrogated with Hac1 depletion after 45 min UPR^{ER} pre-activation, suggesting direct dependency on Hac1 (Figure 2.18A). Upon UPR^{ER} activation, we observed a decrease in *COX20* TE and Cox20-3V5 protein that was alleviated when Hac1 was depleted (Figure 2.17C, 2.18A, 2.18B). This Cox20 protein decline was even more apparent in DTT-treated wild-type cells (Figure 2.19C, 2.19D), and was similar in extent but delayed in timing upon Tm treatment, consistent with the slower appearance of $COX20^{LUTI}$ upon Tm treatment (Figure 2.19E, 2.19F). Importantly, levels of canonical target protein Kar2 continued to increase with Tm treatment over this timescale (Figure 2.19E). Also consistently, the *COX20* TE decreased more dramatically with DTT treatment than with Tm treatment (Figure 2.17D). We concluded that *COX20* is a LUTI target of Hac1, with protein levels that are downregulated as part of the UPR^{ER}.

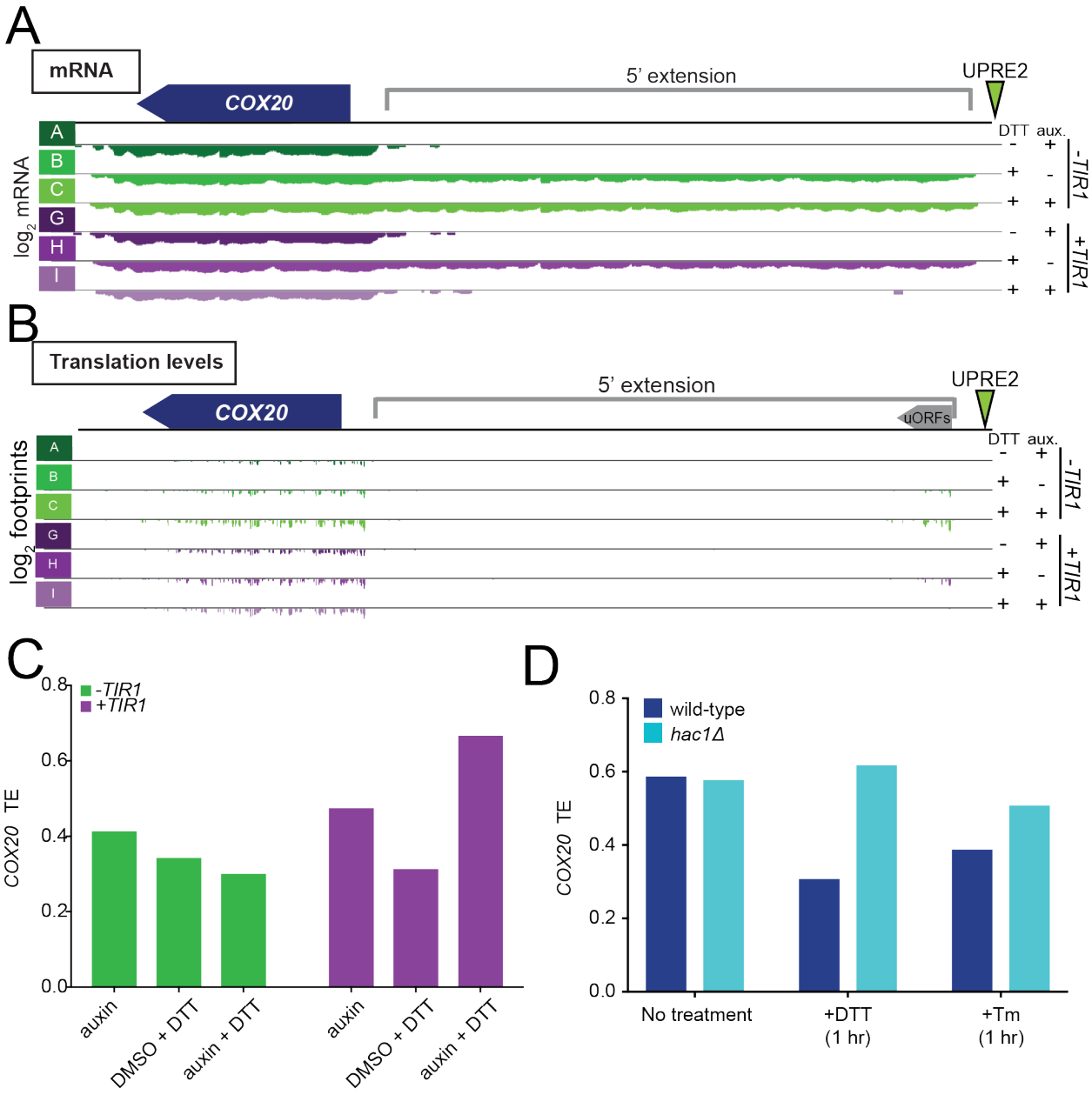

Figure 2.17. An alternate *COX20* isoform is expressed during the UPR^{ER} and is correlated with decreased TE values.
A-B) Annotation of *COX20* mRNA expression (A) and translation levels (B) during the UPR^{ER}, as determined by the experiment described in Figure 2.13. Above, gene model showing the *COX20* ORF and indicating the location of a ~1.8kb 5' extension. A UPRE2 motif is just upstream of the extension (beginning at –2015 relative to the *COX20* ATG). Below, $\log_2$ mRNA (RPKM) (A) or footprints (RPKM) (B) showing an extension in *COX20* transcript length and translation from uORFs in the extension upon UPR^{ER} activation in cells not depleted of AID-Hac1.
C) Comparison of *COX20* TEs in cells with and without AID-Hac1 degradation reveals a UPR^{ER} dependent decrease in TE that is abrogated upon AID-Hac1 degradation. Sample collection is described in Figure 2.13.
D) Comparison of *COX20* TEs in rich media alone, or with 5mM DTT or 2µg/mL Tm. TE values were calculated over the annotated ORF using mRNA-seq and ribosome profiling data obtained from the harvesting scheme described in Figure 2.2.

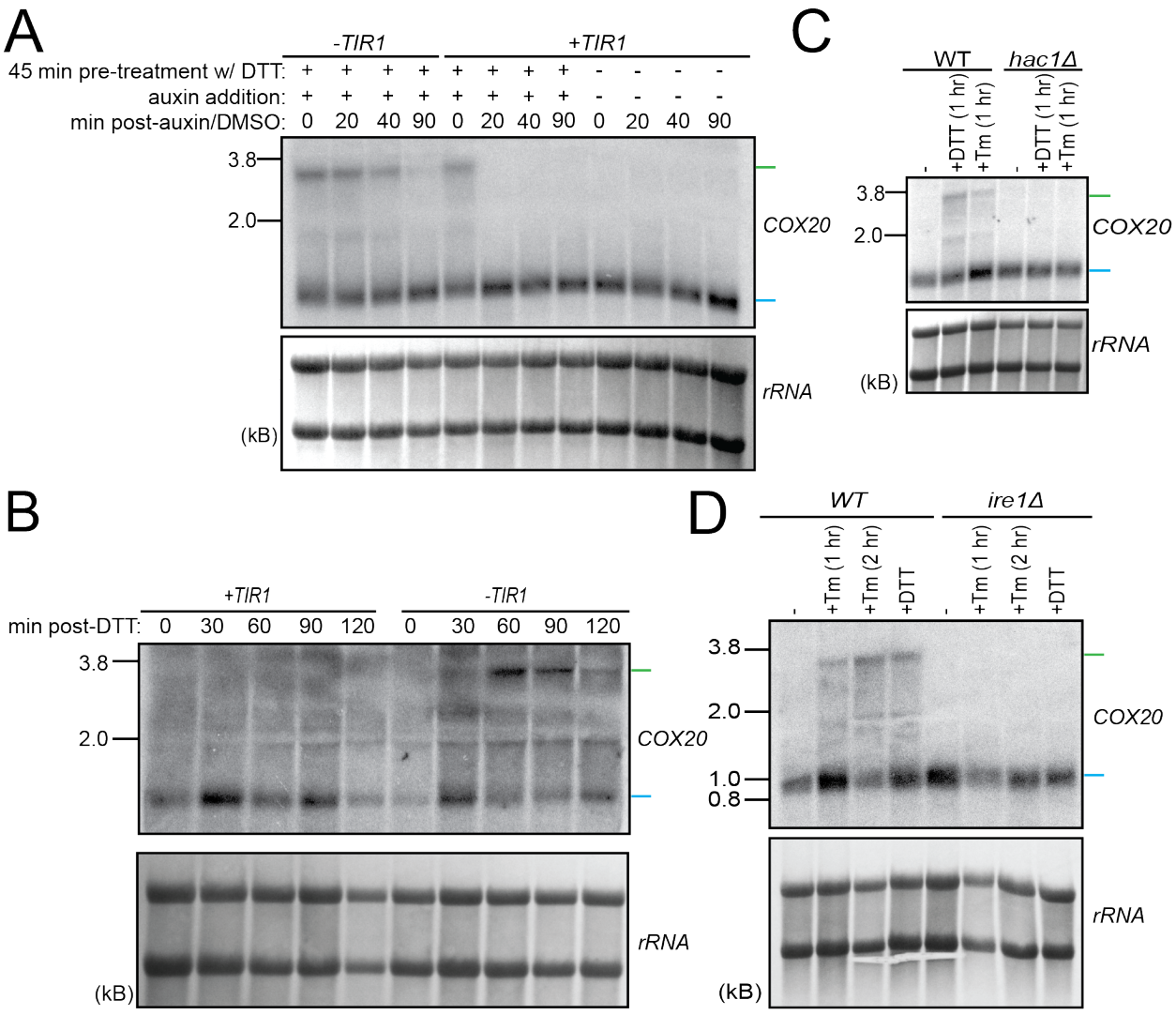

Figure 2.18. *COX20*^{LUTI} expression during the response to ER stress depends on an intact UPR^{ER}.
A) Northern blotting for *COX20* confirms expression of an extended transcript isoform, which decreases within 20 min of auxin addition following 45 min pre-treatment with 5mM DTT. This decrease occurs robustly in the *+TIR1* strain background (BrÜn 10744), but not the *-TIR1* strain background (BrÜn 10532).
B) Northern blot analysis of *COX20* expression with (BrÜn 10929) and without (BrÜn 11133) AID-Hac1 degradation. Expression of COX20^{LUTI} upon 5mM DTT treatment is abrogated when cells are pre-treated with auxin in the *–TIR1* background (BrÜn 11133), but not the *+TIR1* background (BrÜn 10929). Note that all cells were pre-treated with auxin for 15 min prior to DTT addition.
C-D) The extended *COX20*^{LUTI} transcript was also observed in wild-type cells (BrÜn 1362, 15) upon treatment with DTT or Tm, but not *hac1Δ* (BrÜn 4431) (C) or *ire1Δ* (BrÜn 15924) (D) cells.
Note that for A-D, blue and green bars highlight canonical and extended transcripts, respectively.

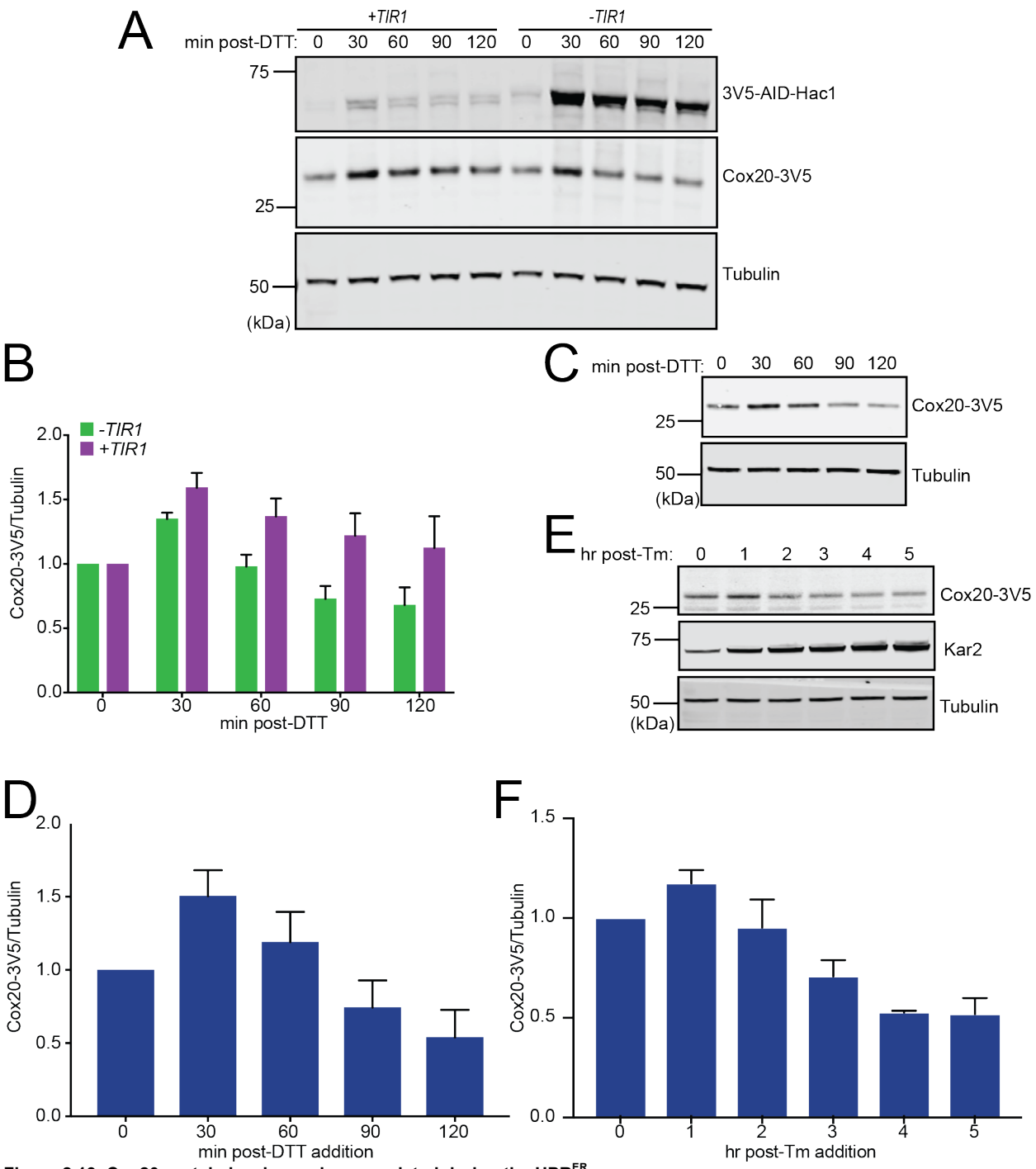

Figure 2.19. Cox20 protein levels are downregulated during the UPR^{ER}.

A) Immunoblot analysis of Cox20-3V5 levels with (BrÜn 10929) and without (BrÜn 11133) AID-Hac1 degradation during UPR^{ER} activation. A modest AID-Hac1-dependent reduction in Cox20-3V5 protein levels is observed upon treatment with 5mM DTT (following 15 min auxin pre-treatment), specifically in the *+TIR1* background (BrÜn 10929).

B) Quantification of Cox20-3V5 protein levels during the UPR^{ER} in the *AID-HAC1* background, as in panel A. The average of 3 biological replicates is shown with error bars representing SD.

C) A time-dependent decrease in Cox20-3V5 protein level was observed by immunoblot upon treatment of wild-type cells (BrÜn 10781) with 5mM DTT.

D) Quantification of Cox20-3V5 protein levels during the DTT-induced UPR^{ER} in wild-type cells, as in panel C. The average of 3 biological replicates is shown with error bars representing SD.

E) A time-dependent decrease in Cox20-3V5 protein level was observed by immunoblot upon treatment of wild-type cells (BrÜn 10781) with 2µg/mL Tm. Kar2 levels continued to increase over this time scale.

F) Quantification of Cox20-3V5 protein levels during the Tm-induced UPR^{ER} in wild-type cells, as in panel E. The average of 3 biological replicates is shown with error bars representing SD.

2.3.4 UPR^{ER} activation drives a global proteomic and metabolic shift

Why do UPR^{ER}-activated cells couple upregulation of canonical targets, like *KAR2,* with downregulation of non-canonical ones, like *COX20*? In the case of *COX20*, the downregulation of its protein level was intriguing, given its role in ETC function. The UPR^{ER} in flies has been associated with the induction of glycolytic enzymes and a cell-type specific metabolic shift to increased glycolytic flux (Lee et al., 2015). A similar shift from aerobic respiration to glycolysis is commonly observed in cancer cells and termed the "Warburg effect" in that context (Warburg, 1956). We sought to determine whether such an effect might be a core part of the Hac1-dependent UPR^{ER} by using additional global measurements in our *AID-HAC1* system. First, we performed metabolomic profiling, comparing cells with and without UPR^{ER} activation by Tm, and with and without Hac1 depletion. Of all glycolysis and TCA intermediates measured, most did not change in a statistically significant manner in our experiment. Several did, however, and we noted that the two TCA intermediates (citrate and malate) that changed significantly between Hac1-containing and –depleted cells were lower in Tm-treated cells containing Hac1 than with its levels depleted, potentially suggesting reduced respiration in Hac1-containing UPR^{ER}-activated cells (Figure 2.20A). Glycolysis-associated metabolites tended to either remain roughly constant or to be higher in UPR^{ER}-activated cells containing Hac1 (Figure 2.20A). These results were subtle and, while consistent with a shift from respiration in Hac1-containing UPR^{ER}-activated cells, did not provide definitive proof due to our inability to detect statistically significant shifts in many relevant intermediates with and without *TIR1*. We hypothesized that this may have resulted from the dampened range of effects that we note above in Hac1-depletion experiments compared to those using wild-type versus *hac1*Δ cells. Indeed, similar analyses in cells carrying *HAC1* showed consistent, significant dis-enrichment of TCA intermediates and enrichment of glycolytic intermediates with Tm treatment (Figure 2.20B).

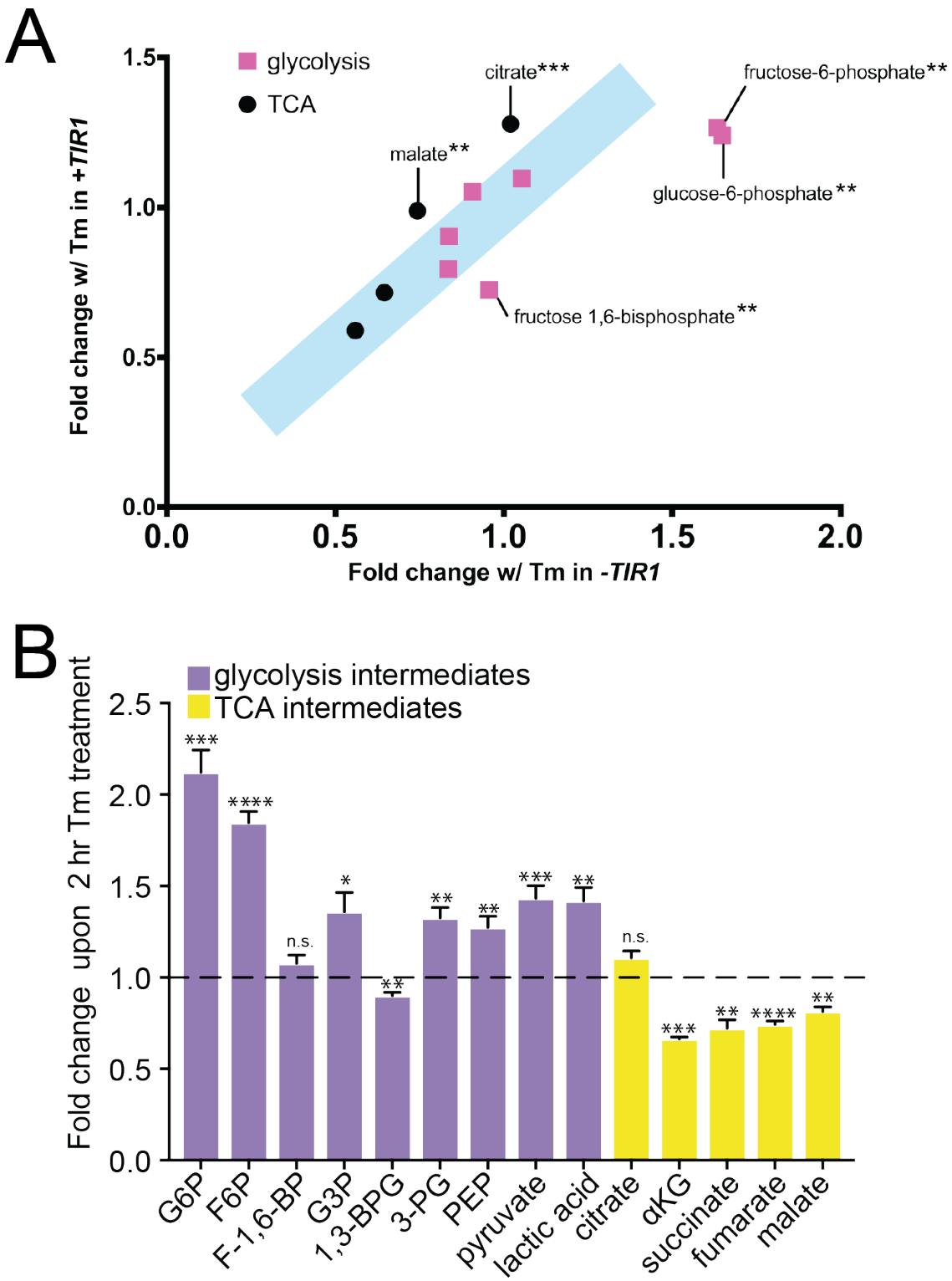

Figure 2.20. Induction of the UPR^{ER} appears to promote metabolic reprogramming.
A) Metabolomic analysis revealed modest increases in three glycolysis intermediates following 2 hr Tm treatment of AID-Hac1 containing cells (-*TIR1* background, BrÜn 10532) relative to AID-Hac1 depleted cells (+*TIR1* background, BrÜn 10744). Conversely, TCA intermediates are higher in AID-Hac1 depleted cells. Asterisks indicate metabolites exhibiting significantly different levels between 2µg/mL Tm treated cells with and without AID-Hac1 degradation. **p<0.01, ***p<0.001.
B) Metabolite levels following 2 hr 2µg/mL Tm treatment of wild-type cells (BrÜn 15). Average fold change of 6 technical replicates is shown, with error bars representing SEM. A t-test was used to evaluate significance. *p<0.05, **p<0.01, ***p<0.001, ****p<0.0001.

To more comprehensively determine the degree to which UPR^{ER} activation may couple downregulation of specific physiological cellular processes—such as aerobic respiration—to upregulation of classic UPR^{ER} targets like ER chaperones, we performed proteomic measurements in samples identical to those measured for mRNA and translation (Figure 2.13). We used TMT-based isobaric labeling to compare shifts in proteome composition with and without Hac1 depletion, and with and without UPR^{ER} activation. This experiment yielded a deep dataset, allowing comparison of the levels of 2577 proteins with and without DTT and Hac1 (Figure 2.21A). The data were of high quality, revealing the expected patterns for Hnt1, Cox20, and canonical UPR^{ER} targets (Figure 2.21B). A broad view of the data revealed dramatic overall shifts in proteome composition with DTT addition, with a subset of these changes dependent on Hac1. A discrete cluster of 72 proteins, which included canonical targets Kar2, Ero1, Pdi1, and Lhs1, emerged as increased in a UPR^{ER}- and Hac1-dependent manner. GO analysis of the genes encoding these proteins (Figure 2.21A; Table 2.4) showed that they were strongly enriched for roles in protein transport and ER function. A second cluster of 197 proteins showed increased protein expression following UPR^{ER} activation that was delayed following Hac1 depletion. GO analysis of the genes encoding them revealed strong enrichment for proteolysis functions and the ER-associated degradation (ERAD) pathway [Figure 2.21A, Table 2.5; consistent with (Travers et al., 2000)]. A third cluster of 282 proteins showed decreased protein levels with UPR^{ER} activation, with at least partial dependence on Hac1. The associated genes were heavily enriched for roles in translation and ribosome assembly (Figure 2.21A, Table 2.6). This observation is intriguing, as the downregulation of translation is a well-defined aspect of the UPR^{ER} in other eukaryotes (Walter and Ron, 2011). This effect has thus far been less clear in budding yeast studies, and our results suggest that it warrants revisiting. Most interestingly, given the Hac1-dependent LUTI regulation seen for Cox20 and our hypothesis that metabolism shifts away from respiration in UPR^{ER}-activated cells, the genes encoding the group of UPR^{ER}-dependent downregulated proteins was also enriched for roles in ATP synthesis coupled electron transport, oxidative phosphorylation, the ETC, cytochrome complexes, and the mitochondrial respiratory chain (Table 2.7). KEGG pathway analysis also revealed enrichment for components of the ETC and aerobic respiration ($p=0.0027$) among these downregulated genes, further supporting a metabolic shift away from aerobic respiration as part of the UPR^{ER}. Finally, isolation of data for glycolytic enzymes revealed a complementary upregulation of protein levels that was dependent on UPR^{ER} activation, although only some of these increases were dependent on Hac1 (Figure 2.21C).

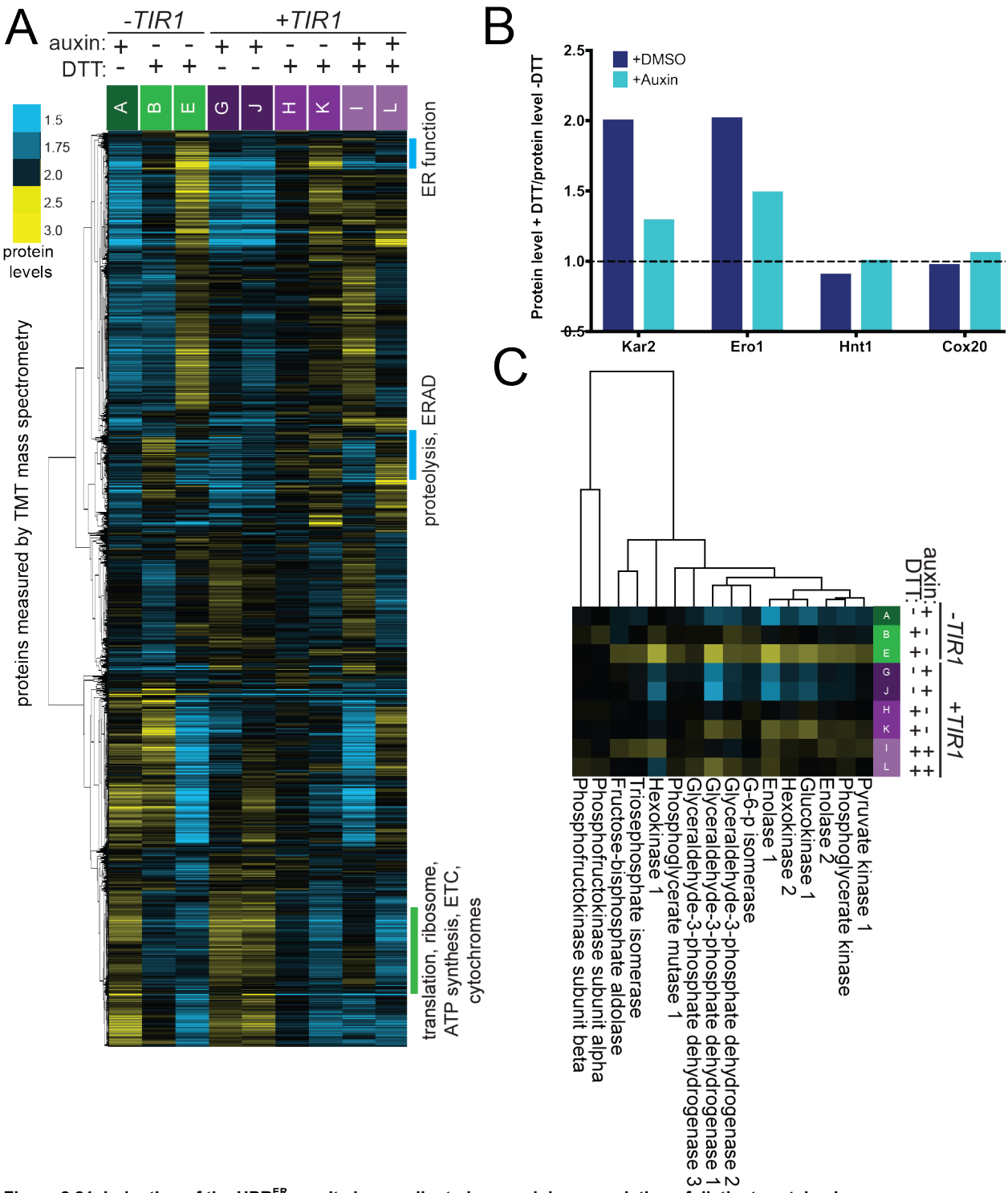

Figure 2.21. Induction of the UPR^{ER} results in coordinated up- and downregulation of distinct protein classes.
A) The set of proteins that we could quantify via TMT-based mass spectrometry are clustered by protein abundance patterns, with each normalized to the same total protein level across the row to enable comparison of trends. Proteins involved in ER function, proteolysis, and ERAD appear to be upregulated in an AID-Hac1 dependent manner (blue bars). Proteins involved in translation, ribosome biogenesis, ATP synthesis, the ETC, and cytochromes appear to be downregulated in an AID-Hac1 dependent manner (green bar).
B) Protein levels for canonical Hac1 targets and the newly identified LUTI-based Hac1 targets were determined by TMT-based mass spectrometry and compared between cells treated with and without 5mM DTT. Sample G was used to determine protein levels without DTT treatment, and samples H (dark blue, +vehicle) and I (light blue, +auxin) were used to determine the AID-Hac1 dependence of observed changes.

C) TMT-mass spectrometry revealed a cluster of glycolysis-related genes upregulated at the protein level during the UPR^{ER}. Some of those increases are AID-Hac1-dependent.
Note that cell collection for panels A-C is described in Figure 2.13.

Biological process	p-value
protein localization to endoplasmic reticulum	0.001078519
cellular macromolecule localization	0.016096783
protein transport	0.022904199
cellular protein localization	0.029913224
glycoprotein metabolic process	0.033854463
establishment of protein localization	0.039605617
ERAD pathway	0.042848239
protein exit from endoplasmic reticulum	0.047666463
Cellular component	**p-value**
endoplasmic reticulum	7.88E-11
endomembrane system	1.46E-09
endoplasmic reticulum part	3.42E-09
nuclear outer membrane-endoplasmic reticulum membrane network	7.07E-07
endoplasmic reticulum membrane	2.61796E-06
endoplasmic reticulum lumen	0.000606019
cytoplasm	0.004872508
cytoplasmic part	0.006571157

Table 2.4. Gene ontology (GO) analysis for the cluster of 72 proteins.

Biological process	p-value
proteolysis involved in cellular protein catabolic process	7.02E-07
modification-dependent macromolecule catabolic process	7.76E-07
cellular protein catabolic process	1.0335E-06
proteasome-mediated ubiquitin-dependent protein catabolic process	1.40951E-06
ubiquitin-dependent protein catabolic process	2.01929E-06
modification-dependent protein catabolic process	2.01929E-06
proteasomal protein catabolic process	2.10149E-06
protein catabolic process	6.2987E-06
vesicle-mediated transport	8.91442E-06
response to endoplasmic reticulum stress	0.000103722
ER-associated ubiquitin-dependent protein catabolic process	0.001108943
ERAD pathway	0.001969105
cellular macromolecule catabolic process	0.002282859
vesicle organization	0.006564231
single-organism cellular process	0.006688525
membrane organization	0.020670296
macromolecule catabolic process	0.021450232

protein localization	0.028020208
single-organism process	0.03160032
proteolysis	0.032359078
response to chemical	0.03318573
cellular localization	0.043477087
Cellular component	**p-value**
endomembrane system	2.66E-08
cell cortex part	2.82469E-05
actin cortical patch	0.000132823
cortical actin cytoskeleton	0.000151137
endocytic patch	0.000161989
cell cortex	0.000162155
cytoplasmic region	0.000162155
cortical cytoskeleton	0.000252358
actin cytoskeleton	0.001022665
cellular bud	0.002126584
cytosolic proteasome complex	0.003006641
cytoplasmic vesicle	0.005369055
intracellular vesicle	0.005369055
cell projection part	0.006174305
vesicle	0.006469936
site of polarized growth	0.009352794
proteasome storage granule	0.00941004
cell periphery	0.010939651
cell projection	0.011999127
plasma membrane	0.018933941
bounding membrane of organelle	0.020099789

Table 2.5. Gene ontology (GO) analysis for the cluster of 197 proteins.

Biological process	**p-value**
cytoplasmic translation	9.17E-40
organonitrogen compound metabolic process	1.77E-39
organonitrogen compound biosynthetic process	3.53E-38
ribosome biogenesis	4.50E-25
nitrogen compound metabolic process	3.23E-23
ribonucleoprotein complex biogenesis	4.78E-22
cellular amino acid metabolic process	1.04E-19
ribosomal small subunit biogenesis	1.39E-19
amide biosynthetic process	6.62E-18
translation	2.79E-17
cellular amino acid biosynthetic process	3.05E-17
peptide biosynthetic process	4.12E-17

cellular amide metabolic process	1.10E-16
rRNA processing	5.97E-16
peptide metabolic process	1.01E-15
rRNA metabolic process	6.88E-15
organic acid biosynthetic process	9.57E-15
carboxylic acid biosynthetic process	9.57E-15
alpha-amino acid biosynthetic process	1.97E-14
ribosome assembly	3.29E-14
alpha-amino acid metabolic process	4.22E-14
carboxylic acid metabolic process	4.65E-14
ncRNA metabolic process	5.03E-14
cellular biosynthetic process	1.29E-13
oxoacid metabolic process	3.54E-13
organic acid metabolic process	3.98E-13
maturation of SSU-rRNA from tricistronic rRNA transcript (SSU-rRNA, 5.8S rRNA, LSU-rRNA)	5.18E-13
biosynthetic process	6.25E-13
ncRNA processing	7.59E-13
ribosomal large subunit biogenesis	2.25E-12
organic substance biosynthetic process	2.78E-12
small molecule metabolic process	3.03E-12
maturation of SSU-rRNA	1.06E-11
cellular nitrogen compound metabolic process	4.64E-10
cellular metabolic process	8.28E-10
primary metabolic process	4.16E-09
organic substance metabolic process	1.37E-08
ribonucleoprotein complex assembly	4.83E-08
metabolic process	9.03E-08
glutamine family amino acid metabolic process	2.20E-07
ribonucleoprotein complex subunit organization	2.86E-07
small molecule biosynthetic process	6.62E-07
ribosomal small subunit assembly	9.49E-07
single-organism biosynthetic process	1.35715E-06
ribosomal large subunit assembly	1.78013E-06
RNA processing	2.00633E-06
glutamine family amino acid biosynthetic process	2.64149E-06
purine nucleoside monophosphate metabolic process	6.44817E-06
purine ribonucleoside monophosphate metabolic process	6.44817E-06
nucleoside monophosphate metabolic process	7.64213E-06
gene expression	9.02789E-06
cellular component biogenesis	9.53032E-06
cellular nitrogen compound biosynthetic process	2.15842E-05

ribonucleoside monophosphate metabolic process	2.31329E-05
ATP synthesis coupled electron transport	3.51183E-05
mitochondrial ATP synthesis coupled electron transport	3.51183E-05
branched-chain amino acid biosynthetic process	5.20392E-05
organelle assembly	5.86835E-05
oxidative phosphorylation	7.3364E-05
ribonucleoside metabolic process	7.36683E-05
purine-containing compound metabolic process	0.000112682
purine ribonucleoside metabolic process	0.000114132
purine nucleoside metabolic process	0.000132255
purine nucleotide metabolic process	0.000186158
ribonucleotide metabolic process	0.000189572
nucleoside triphosphate metabolic process	0.000225663
isoleucine biosynthetic process	0.000297119
arginine biosynthetic process	0.000305887
ribonucleoside triphosphate metabolic process	0.000311647
nucleoside metabolic process	0.000359252
purine ribonucleotide metabolic process	0.000466753
respiratory electron transport chain	0.000507179
glycosyl compound metabolic process	0.000662584
purine nucleoside monophosphate biosynthetic process	0.000895855
purine ribonucleoside monophosphate biosynthetic process	0.000895855
purine nucleoside triphosphate metabolic process	0.001108264
electron transport chain	0.001175853
ATP metabolic process	0.001797499
isoleucine metabolic process	0.001799838
ribose phosphate metabolic process	0.002088765
nucleoside monophosphate biosynthetic process	0.002566277
hydrogen ion transmembrane transport	0.003825371
purine ribonucleoside triphosphate metabolic process	0.003838969
arginine metabolic process	0.006215676
maturation of LSU-rRNA	0.00652271
nucleobase-containing small molecule metabolic process	0.007621193
nucleotide metabolic process	0.007752619
ribonucleoside monophosphate biosynthetic process	0.008454926
ribonucleoside biosynthetic process	0.008454926
ribonucleoside triphosphate biosynthetic process	0.00977133
nucleoside biosynthetic process	0.010270001
nucleoside phosphate metabolic process	0.010915935
purine nucleoside biosynthetic process	0.011244931
purine ribonucleoside biosynthetic process	0.011244931

ribonucleotide biosynthetic process	0.016320673
branched-chain amino acid metabolic process	0.01871702
glycosyl compound biosynthetic process	0.021532068
cellular respiration	0.022247361
energy coupled proton transport, down electrochemical gradient	0.023109172
ATP synthesis coupled proton transport	0.023109172
nucleoside triphosphate biosynthetic process	0.023554566
chorismate biosynthetic process	0.026650898
aspartate family amino acid metabolic process	0.030495455
single-organism metabolic process	0.031151471
purine ribonucleotide biosynthetic process	0.033164541
purine-containing compound biosynthetic process	0.036111009
tRNA aminoacylation for protein translation	0.040173584
ribose phosphate biosynthetic process	0.042544225
glutamine metabolic process	0.048768087
ATP biosynthetic process	0.048768087
Cellular component	**p-value**
cytosolic ribosome	2.55E-42
ribosome	2.73E-37
intracellular ribonucleoprotein complex	4.89E-37
ribonucleoprotein complex	4.89E-37
ribosomal subunit	8.04E-37
cytosolic part	7.87E-34
preribosome	5.18E-25
cytosolic large ribosomal subunit	1.73E-24
large ribosomal subunit	4.28E-21
non-membrane-bounded organelle	1.32E-18
intracellular non-membrane-bounded organelle	1.32E-18
macromolecular complex	1.49E-14
cytosolic small ribosomal subunit	2.54E-14
90S preribosome	6.71E-13
small ribosomal subunit	1.01E-12
small-subunit processome	3.75E-11
preribosome, large subunit precursor	4.65E-09
mitochondrial protein complex	1.85E-08
nucleolus	2.64E-08
intracellular part	1.55E-07
intracellular	2.98E-07
inner mitochondrial membrane protein complex	1.12419E-06
cell part	1.37214E-06
cell	1.51136E-06

intracellular organelle part	5.5401E-06
organelle part	6.485E-06
cytosol	1.47236E-05
intracellular organelle	1.95288E-05
organelle	2.01694E-05
mitochondrial part	2.72293E-05
cytoplasmic part	6.01497E-05
respiratory chain	6.17299E-05
organelle inner membrane	7.01167E-05
mitochondrial inner membrane	7.91326E-05
mitochondrial respiratory chain	0.000174055
respiratory chain complex	0.000174055
mitochondrion	0.000256099
oxidoreductase complex	0.000444223
cytoplasm	0.000458802
mitochondrial membrane part	0.001172898
cytochrome complex	0.001915375
transporter complex	0.001915375
membrane-enclosed lumen	0.002366705
organelle lumen	0.002366705
intracellular organelle lumen	0.002366705
mitochondrial intermembrane space protein transporter complex	0.003763896
mitochondrial envelope	0.018350679
mitochondrial membrane	0.030088516
cytoplasmic stress granule	0.031017323
Molecular function	**p-value**
structural constituent of ribosome	1.41E-31
structural molecule activity	9.86E-20
ligase activity	0.0041653
snoRNA binding	0.011129754
rRNA binding	0.034867531
aminoacyl-tRNA ligase activity	0.039680562
ligase activity, forming carbon-oxygen bonds	0.039680562
ligase activity, forming aminoacyl-tRNA and related compounds	0.039680562

Table 2.6. Gene ontology (GO) analysis for the cluster of 282 proteins.

Pathway	p-value
arginine biosynthesis	0.00201461
aerobic respiration, electron transport chain	0.002655529
superpathway of leucine, isoleucine, and valine biosynthesis	0.014781469
chorismate biosynthesis	0.041433172

Table 2.7. Kyoto encyclopedia of genes and genome (KEGG) pathway analysis for the cluster of 282 proteins.

Because TMT-based measurements often yield values that appear dampened in range relative to other methods (Wenger et al., 2011), we also used label free quantification (LFQ), an orthogonal approach, on the same samples. This allowed for better determination of the degree of specific protein level changes following UPR^{ER} activation. LFQ analysis revealed trends that mirrored those seen with TMT-based quantification, but that were less muted in degree (Figure 2.21B, 2.22A). As expected, UPR^{ER} induction still showed increased levels of canonical UPR^{ER} target proteins, such as Kar2 (Figure 2.22B). Untagged Hnt1 protein levels were dramatically reduced in a Hac1-dependent manner, to an even greater degree than observed for the epitope-tagged protein. The degree of Hnt1 decrease in Hac1-containing cells relative to cells depleted for Hac1 was roughly equivalent to the degree of Kar2 increase (Figure 2.22A), suggesting potential for a strong cellular effect from the Hac1-dependent induction of $HNT1^{LUTI}$. Cox20 showed a 2.4-fold decrease in UPR^{ER}-activated cells containing Hac1 compared to those depleted for it (Figure 2.22A), which was similar to the decrease observed for the epitope-tagged protein (Figure 2.19) and which suggests potential for a strong physiological effect.

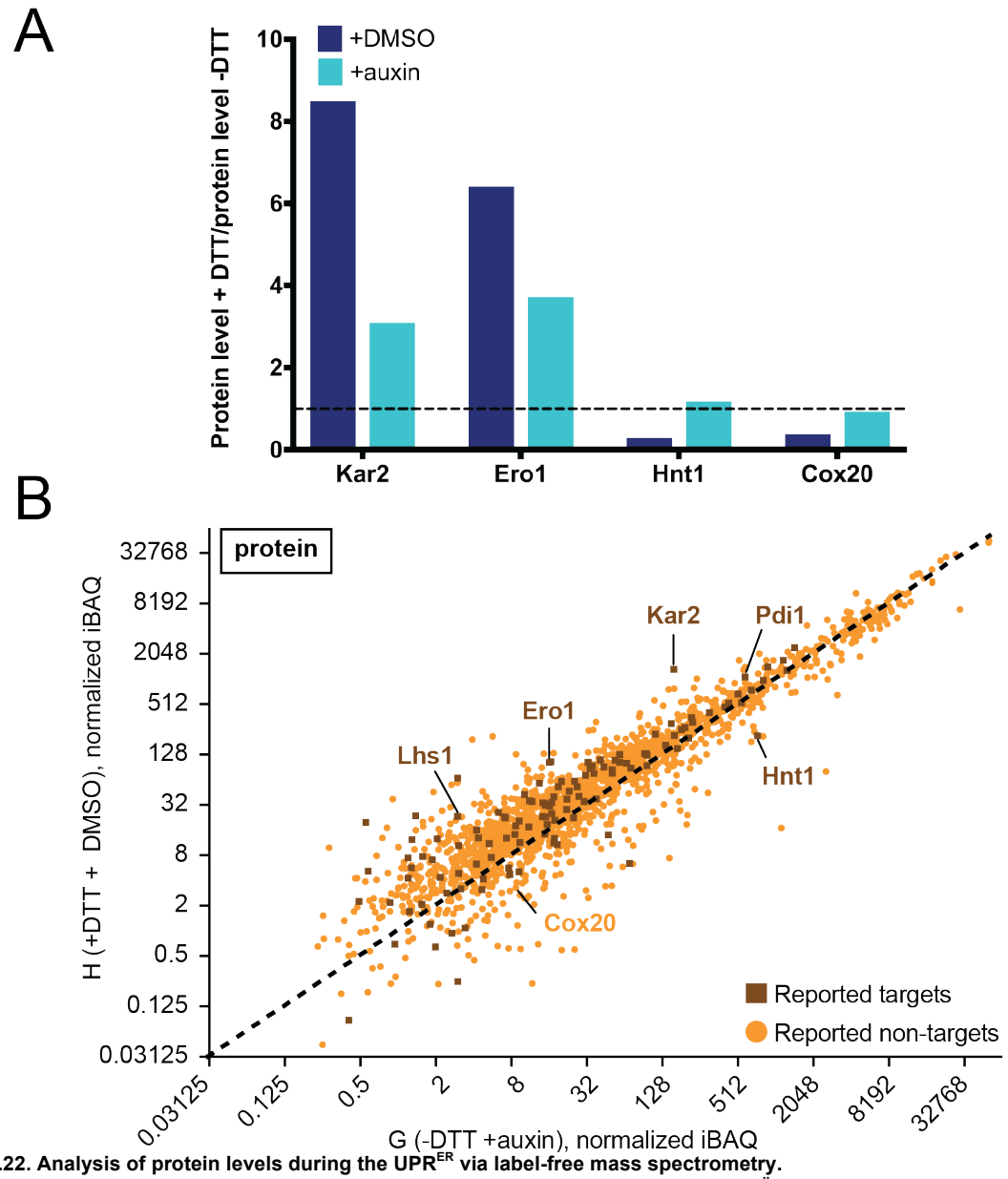

Figure 2.22. Analysis of protein levels during the UPR^{ER} via label-free mass spectrometry.
A) Protein levels obtained via label-free mass spectrometry analysis of sample H (+*TIR1* (BrÜn 10744), + DTT +DMSO) compared to sample G (+*TIR1* (BrÜn 10744), -DTT +auxin) are plotted with previously reported Hac1 transcriptional targets shown in dark squares.
B) Equivalent label free mass spectrometry data to that shown in Figure 2.21A.
Note that for panels A-B, sample collection is described in Figure 2.13.

2.2.5 Preventing aerobic respiration ameliorates cellular growth defects due to UPR^{ER} activation

Oxygen consumption assays revealed a time-dependent, significant decrease in oxygen consumption rates (OCR) of cells treated with Tm (Figure 2.23A), consistent with a decrease in aerobic respiration in UPR^{ER}-activated cells. To investigate a potential functional role for downregulated aerobic respiration in the UPR^{ER}, we leveraged the fact that budding yeast cells can grow well in rich media in the absence of aerobic respiration resulting from mutation in ETC-related genes. We examined cells deleted for

PET100, a gene that is required for assembly of ETC complex IV (Church et al., 1996). We compared cell doubling of untreated wild-type and *pet100*Δ cells in rich media, observing the expected moderate growth defect in the latter background (Figure 2.23B). We then repeated the experiment in the presence of DTT and observed that, while both wild-type and *pet100*Δ cells doubled more slowly than in untreated conditions, the previously observed growth defect in *pet100*Δ cells relative to wild-type was strongly suppressed (Figure 2.23C). In fact, under these conditions, *pet100*Δ cells robustly surpassed wild-type cells in their growth rate. Because of possible confounding effects of using a strong reducing agent like DTT for these experiments, we performed a similar analysis instead activating the UPR^{ER} by Tm addition, which is stable enough for use in plate-based growth assays, in contrast to DTT. Cell growth following dilution on plates containing 0 to 0.75µg/mL Tm produced results similar to the DTT growth rate data (Figure 2.23D). wild-type cells formed larger colonies than *pet100*Δ cells without Tm, but with increasing Tm concentration, *pet100*Δ cells were able to surpass wild-type in growth ability. Based on these experiments, we concluded that downregulation of factors responsible for aerobic respiration, which accompanies UPR^{ER} activation and is partially modulated by Hac1 activity, is likely to be a functionally important component of the UPR^{ER} in yeast.

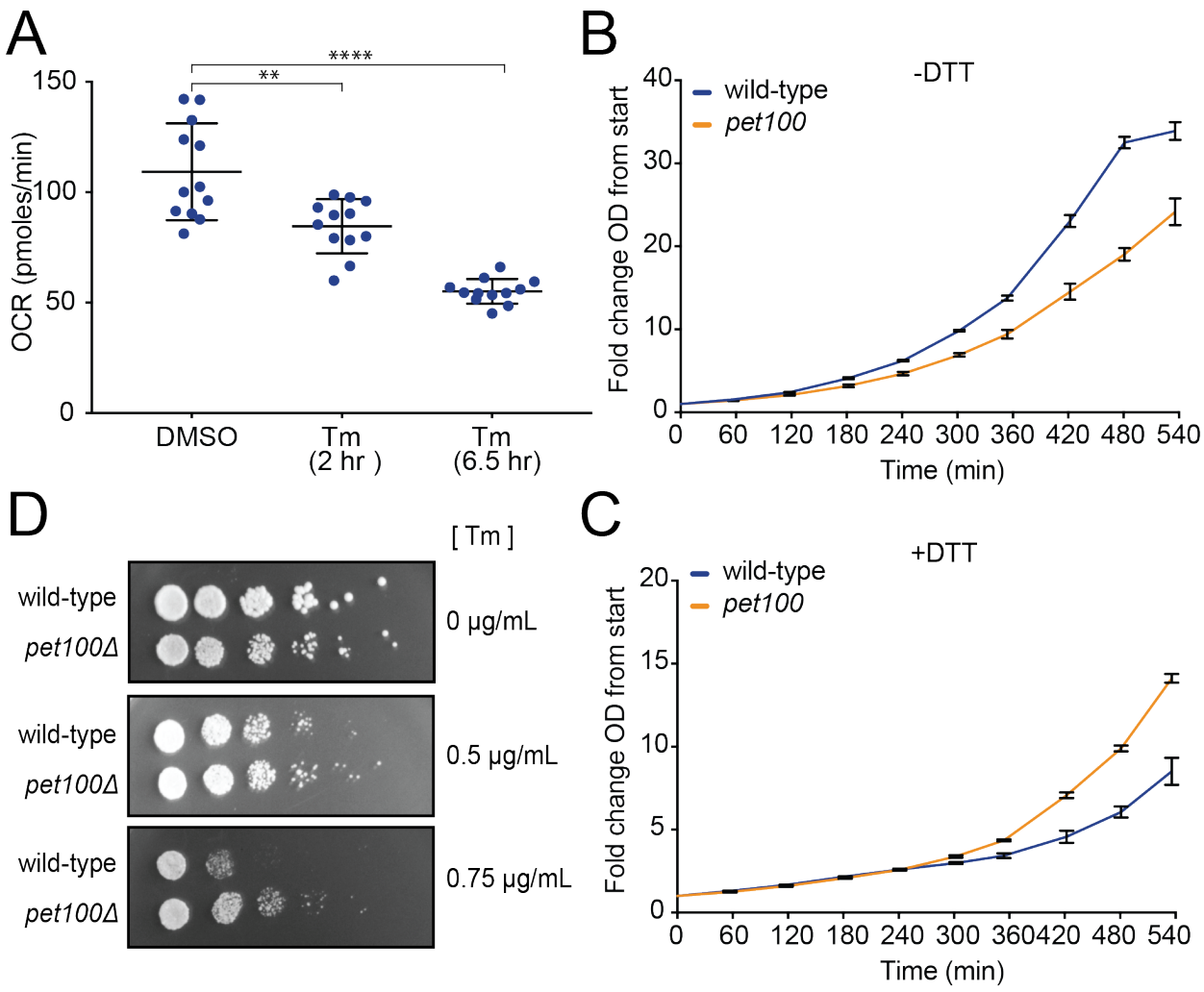

Figure 2.23. Crippled respiration confers a growth advantage to UPR^{ER}-activated cells.
A) Basal oxygen consumption rates were measured following treatment of wild-type (BrÜn 15) cells with 2µg/mL Tm for 2 and 6.5 hr. Rates determined from 12 replicate wells for each condition are plotted, with overlaid bars representing average and standard deviation. Note that all rates are adjusted to normalize for OD differences. A Mann-Whitney test was used to statistically compare OCR. **p<0.01, ****p<0.0001.
B) Growth of wild-type (BrÜn 15) versus *pet100Δ* (BrÜn 2781) cells in rich media. Fold change in OD relative to the starting OD is plotted against time. The average of 3 biological replicates is shown, with error bars representing SD.
C) Growth of wild-type (BrÜn 15) versus *pet100Δ* (BrÜn 2781) cells treated with 5mM DTT in rich media. Fold change in OD relative to the OD at the time of DTT treatment is plotted against time. The average of 3 biological replicates is shown, with error bars representing SD.
D) Serial dilution-based growth assay of wild-type (BrÜn 15) versus *pet100Δ* (BrÜn 2781) cells on plates containing rich media alone and plates containing either 0.5 or 0.75µg/mL Tm. All dilutions were 5-fold, starting with cultures back-diluted to OD_{600}0.1.

2.3 Discussion

Here we report that, in addition to its characterized role in the induction of ER-related target genes during the UPR^{ER}, Hac1 also down-regulates a set of genes by driving production of mRNAs that ultimately result in reduced protein levels. Hac1 thus coordinates up- and downregulation of distinct targets, contributing to a shift in the proteome and metabolism of UPR^{ER}-activated cells (Figure 2.24). We report that Hac1-dependent transcription results in downregulation of at least 15 genes during the UPR^{ER}

(Table 2.3). More broadly, our study provides a set of new examples of LUTI-based regulation, a recently defined mode of gene regulatory control that pervasively shapes the proteome of budding yeast cells during the meiotic program (Cheng et al., 2018; and Ünal, 2018). The fact that this regulation can be mediated by the conserved transcription factor Hac1 as part of a conserved stress response suggests that it may be broadly used in transcriptional regulatory responses.

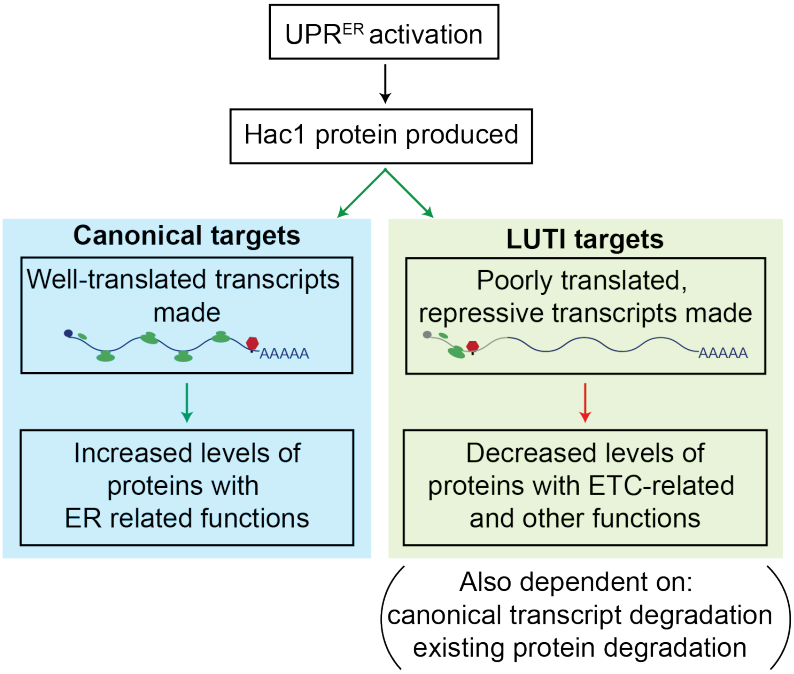

Figure 2.24. A model for Hac1-coordinated up- and downregulation of distinct protein sets during the UPR^{ER}. By inducing both canonical and LUTI targets, this single transcription factor can promote increased synthesis of ER proteins and decreased synthesis of proteins involved in a variety of functions, including the ETC.

A key component of LUTI-based regulation is cis-silencing of the proximal TSS (Chia et al., 2017). While transcriptional interference is well established (for example [Cullen et al., 1984; Martens et al., 2004]), LUTI-based regulation involves production of an interfering transcript containing a coding region that is translationally repressed. The ultimate effect of this regulation is counterintuitive from a classical gene regulatory perspective, as it involves mRNA-inducing TFs acting effectively as repressors of gene expression and results in an uncoupling of overall mRNA and protein synthesis levels due to a greater importance of the isoform *type* than overall transcript levels in directing protein synthesis (Chen et al., 2017; Cheng et al., 2018). This can be seen in the Hac1 LUTI cases defined here, including *HNT1*, which was previously reported to be an upregulated UPR^{ER} target based on Hac1-dependent mRNA accumulation in response to UPR^{ER} activation (Travers et al., 2000). Consistently, we find that the total mRNA abundance for *HNT1* is increased during the UPR^{ER}, dependent on Hac1. However, expression of the Hac1-dependent LUTI transcript that accounts for this mRNA increase results in *decreased* protein production. Due to their relative ease of measurement, mRNA abundance values have been widely used as a proxy for gene expression

output. While these measurements are undoubtedly useful and may accurately predict protein level changes in many instances, they can also be misleading. *HNT1* is a prime example of this in the simple and well-defined cellular response explored here. It is likely that many other existing gene expression datasets hold such examples, which may lead to misinterpretation of the cellular consequences of transcriptional responses.

While cases like *HNT1* are particularly striking, an overall mRNA increase is not necessarily seen in cases of LUTI production. Most of the new cases identified here instead exhibit a shift in type of mRNA made without dramatically altering total mRNA quantity for a given gene. In these cases, mRNA levels are uninformative unless this information is integrated with translation data, and ideally measurements of protein, the ultimate gene expression output. Our use of integrated measurements from matched extract enabled a view of the UPR^{ER} gene expression program that would have been impossible to gain from analysis of existing gene expression datasets. For example, matched protein measurements in our study were key to showing that this unconventional mechanism has a cellular effect. Our protein data, which shows decreases in levels of LUTI-regulated proteins within 1-2 hr of UPR^{ER} activation, argue that active degradation of existing protein pools is likely also occurring under our experimental conditions, although we do not yet know the mechanism for the proteins explored here. Similarly, for this mechanism to be effective, transcript half-lives must be relatively short. While transcript destabilization is actively achieved during periods of UPR^{ER} activation for a subset of ER-localized mRNAs by regulated Ire1-dependent decay (RIDD) in some organisms [(Hollien et al., 2009); reviewed in (Maurel et al., 2014)], this mechanism has not been observed in budding yeast. A recent study, however, reports mRNA half-lives in budding yeast to be much shorter than previously thought (Chan et al., 2017), suggesting that an additional mechanism for degradation of canonical transcripts of LUTI-regulated genes may not be required for this regulation to be rapid and effective.

Our study is not the first to suggest that the UPR^{ER} may directly or indirectly result in translational downregulation of a set of genes. Several studies have investigated this possibility and reanalysis of their data, in light of our LUTI model and complementary measurements, reveals results consistent with our findings. For example, microarray analyses of polysome fractions with and without DTT treatment showed that ribosome biogenesis genes were translationally repressed in a DTT-dependent manner, while canonical targets, like *ERO1*, were well-translated under these conditions (Payne et al., 2008). Interestingly, 10 of the 15 Hac1 LUTI targets that we annotate here—including *HNT1* and *COX20*—were among the genes detected in that study to show a DTT-dependent shift from polysomes to a sub-polysome fraction, indicating translational repression (Table 2.3). More recently, mRNA-seq and ribosome profiling were reported from cells with and without Tm treatment (Labunskyy et al., 2014). This study concluded that genes that were upregulated in response to Tm-driven UPR^{ER} activation tended to be transcriptional targets of Hac1 and that downregulated targets tended to be regulated at the level of TE (Labunskyy et al., 2014). This is consistent with our finding that Hac1 acts as a transcriptional activator for canonical targets and indirectly acts as a translational repressor for LUTI targets. Intriguingly, the Tm-dependent translationally

downregulated genes in this previous ribosome profiling study were enriched for roles in ATP metabolic processes (p=0.026) and mitochondria (p=0.030), and several ETC-related genes were in this set, including two that are required for Complex IV assembly (Table 2.8; [Labunskyy et al., 2014]). Although their results are consistent with our data, neither of these previous studies included strains deleted or depleted for *HAC1*, so the degree to which these effects were dependent on Hac1 was unclear, and the lack of transcript isoform data available precludes reanalysis for other features of LUTI-based regulation.

Biological process	**p-value**
ATP metabolic process	0.025774795
purine ribonucleoside triphosphate metabolic process	0.036653814
purine nucleoside triphosphate metabolic process	0.041976504
ribonucleoside triphosphate metabolic process	0.04793892
Cellular component	**p-value**
mitochondrion	0.029763264
mitochondrial part	0.031916478

Table 2.8. Gene ontology (GO) analysis for the translationally downregulated genes upon Tm treatment reported in (Labunskyy et al., 2014)

Our study reveals two separate but linked key findings: the existence of Hac1-dependent LUTI-based regulation and coordinated up- and downshifting of levels of distinct protein groups during the UPR^{ER}. We propose, based on examples like *COX20*, that the downregulation of genes involved in aerobic respiration observed during the UPR^{ER} is at least partially mediated by Hac1-based induction of repressive mRNA isoforms. However, we do not find evidence that all respiratory protein downregulation is dependent on this mechanism. For most of the ETC proteins that we measured to be reduced during UPR^{ER} activation, no associated alternate transcript isoforms were observed. This could be a result of the challenges in predicting alternate transcript isoforms based on mRNA-seq data alone, as we did in this study as a necessity, but it seems unlikely that LUTI-based regulation can directly explain the downregulation of all proteins observed here to decrease during the UPR^{ER}. It is more likely that either a few LUTI-regulated genes act as linchpin components that cause remaining complex members to become unstable or that there are parallel, potentially synergistic mechanisms to decrease levels of respiratory proteins during the UPR^{ER}. The cellular consequence of our newly identified cases of Hac1-dependent, LUTI-based gene repression is another outstanding question. We note an apparent enrichment for ETC function among the group, but we have not identified enough cases to confidently assay statistical significance for LUTI-based regulation for this or other processes. It is likely, however, that ETC regulation is not the function of all newly proposed Hac1 LUTI mRNAs. Although several of the 15 genes encode mitochondrial proteins, most do not. Additionally, some of these genes, including *HNT1*, have such poorly defined cellular roles that determining the possible importance of their downregulation during the UPR^{ER} is difficult at this time.

Our proteomic data suggest a reallocation of cellular resources in UPR^{ER}-activated cells from ribosome biogenesis to ER function, and away from respiration. It is not surprising that a stress response would require a shift in proteome content, but in this case, it is unclear why the Warburg-like shift in ATP-generation mode would bolster cellular fitness during the UPR^{ER} (Figure 2.21, 2.22, 2.23; [Lee et al., 2015]). Nonetheless, our results show that such a shift occurs and is advantageous, as cells without the ability to respire show a growth advantage relative to wild-type cells when grown in UPR^{ER}-activating conditions. While this result suggests that this shift is a relevant functional component of the UPR^{ER}, it does not explain *why* this is the case. It has been proposed that reduction of TCA cycle activity associated with the Warburg effect seen in cancer cells allows acetyl-CoA to be shunted towards the robust new lipid synthesis required for membrane expansion that accompanies rapid cell division (Vander Heiden et al., 2009). A similar explanation is enticing in this case, as one of the hallmarks of UPR^{ER} activation is an increase in ER membrane volume, which requires new lipid synthesis and membrane expansion. It is alternatively possible that it is important to down-regulate an alternate ETC function for the UPR^{ER}. For example, it has recently been shown that the redox function of the ETC through NAD^+ recycling is responsible for the growth defect seen in ETC-deficient mammalian cells (Titov et al., 2016).

Why do UPR^{ER} -activated cells employ the LUTI mechanism for downregulation of a subset of targets? In principle, a transcriptional repressor that is linked to UPR^{ER} activation should allow a similar overall effect, although no such regulator has been identified, to our knowledge. We argue, however, that LUTI-based regulation is as effective as this alternative classical mode of regulation. We note that several Hac1-dependent LUTI target proteins, including Cox20 and Som1, show robust *upregulation* in response to DTT in the absence of Hac1. Hac1-dependent induction of the LUTI transcript in these cases appears effective at preventing and even reversing these protein level increases. Further, this modular mechanism of regulation allows cells to use pre-existing trans-factors for both up- and downregulation of targets, precluding the need for an additional protein to act as a dedicated transcriptional repressor (Chen et al., 2017; Cheng et al., 2018). Perhaps most importantly, a major advantage of this mechanism is that the use of a single TF—Hac1 in this case—allows for direct coordination of upregulation of some genes with downregulation of others (Cheng et al., 2018). This type of coordination is an attractive strategy for mediating rapid cellular responses to acute stress. Whether or not the LUTI mechanism also plays a role in the gene expression programs of metazoans, which notably can also achieve gene repression through the RIDD and PERK pathways, remains to be determined.

The fact that a well-studied, conserved stress response program employs this unconventional mode of gene regulation suggests that LUTI-based regulation may be broadly used to modulate gene expression in contexts of cellular state change. Construction of new, integrated datasets aimed at identifying such regulation, along with revisiting traditional conceptual models of gene expression, will be required to ultimately determine whether this is the case.

2.4 Materials and methods

Strain	Relevant genotype	Source
BrÜn 13	*MATa,* wild-type	Brar-Ünal lab
BrÜn 15	*MATa/α,* wild-type	Brar-Ünal lab
BrÜn 1362	*MATa/α,* wild-type	Brar-Ünal lab
BrÜn 2781	*MATa/α, pet100::KanMX*	This study
BrÜn 4431	*MATa/α, hac1::NatMX/hac1::KanMX*	This study
BrÜn 10353	*MATα, hac1::NatMX, leu2::pHAC1-3V5-IAA7-HAC1::LEU2*	This study
BrÜn 10532	*MATa/α, hac1::NatMX, leu2::pHAC1-3V5-IAA7-HAC1::LEU2*	This study
BrÜn 10744	*MATa/α, hac1::NatMX, leu2::pHAC1-3V5-IAA7-HAC1::LEU2, his3::pCUP1-osTIR1::HIS3*	This study
BrÜn 10778	*MATa, hnt1::HNT1-3V5::KanMX*	This study
BrÜn 10781	*MATa, cox20::COX20-3V5::KanMX*	This study
BrÜn 10924	*MATa, hac1::NatMX, leu2::pHAC1-3V5-IAA7-HAC1::LEU2, his3::pCUP1-osTIR1::HIS3, hnt1::HNT1-3V5::KanMX*	This study
BrÜn 10925	*MATa, hac1::NatMX, leu2::pHAC1-3V5-IAA7-HAC1::LEU2, hnt1::HNT1-3V5::KanMX*	This study
BrÜn 10929	*MATa, hac1::NatMX, leu2::pHAC1-3V5-IAA7-HAC1::LEU2, his3::pCUP1-osTIR1::HIS3, cox20::COX20-3V5::KanMX*	This study
BrÜn 11133	*MATa, hac1::NatMX, leu2::pHAC1-3V5-IAA7-HAC1::LEU2, cox20::COX20-3V5::KanMX*	This study
BrÜn 15924	*MATa/α, ire1::NatMX/ire1::KanMX*	This study
BrÜn 15968	*MATa, trp1::pHNT1-GFP::TRP1*	This study
BrÜn 16374	*MATa, trp1::pHNT1ΔUPRE2-GFP::TRP1*	This study

Table 2.9. Yeast strains used in Chapter 2.

Plasmid	Backbone	Description
pÜB1073	pRS305	*pHAC1-3V5-IAA7-HAC1 LEU2*
pÜB1397	pNH604	*pHNT1-GFP TRP1*
pÜB1406	pNH604	*pHNT1ΔUPRE2-GFP TRP1*

Table 2.10. Plasmids used in Chapter 2.

Name	Sequence (5'-3')	Modifications
oCJ200-oligoDT	GATCGTCGGACTGTAGAACTCTGAACCTGTCG/iSp18/CAAGCAGAAGACGGCATACGAGATTTTTTTTTTTTTTTTTTTTTVN	5' phosphorylated, internal hexa-ethyleneglycol spacer (iSp18)
asDNA-1b	GATCGGTCGATTGTGCACC	5' biotin
asDNA-2b	CCGCTTCATTGAATAAGT	5' biotin
asDNA-3b	GACGCCTTATTCGTATCCATCTATA	5' biotin
oNTI231	CAAGCAGAAGACGGCATACGA	N/A
Index primers	AATGATACGGCGACCACCGAGATCGGAAGAGCACACGTCTGAACTCCAGTCAC-barcode-CGACAGGTTCAGAGTTC (6 base barcodes)	N/A
KAR2 forward	CACCGATGATGAAAGATTGATTG	N/A
KAR2 reverse	TAATACGACTCACTATAGGCTCCTTTGACACTTACTTCTACAG	N/A
HNT1 forward	CATGGTGCGAAGTTGCATG	N/A
HNT1 reverse	TAATACGACTCACTATAGGCCACCCTACAATCAAACCAC	N/A
GFP forward	ACAATGTATACATCATGGCAGAC	N/A
GFP reverse	TAATACGACTCACTATAGG TCAAGAAGGACCATGTGGTCTCTC	N/A
HNT1 5' extension forward	TATGGTGCGAATCGTTACAG	N/A

HNT1 5' extension reverse	TAATACGACTCACTATAGGCGTGCTGATTGCCCTTTTAC	N/A
COX20 forward	CGTGGTCAAATCAGACAGAAG	N/A
COX20 reverse	TAATACGACTCACTATAGGCATCTAATCGAGTCCCAAGC	N/A

Table 2.11. Oligonucleotides used in Chapter 2.

2.4.1 Yeast strain construction

All experiments were performed using *Saccharomyces cerevisiae* strains of the SK1 background.

Gene deletion strains:
Deletions were created by one-step gene deletion, as described in (Longtine et al., 1998).

AID-HAC1 strain:
Construction of this strain required deleting endogenous *HAC1* and replacing it ectopically with an auxin-inducible degron (AID)-tagged version. We ensured that the promoter, intron, and UTRs, which are all required for proper regulation of *HAC1*, were not disrupted in this construct (Figure 2.10A; [Aragón et al., 2009; Bowring and Llewellyn, 2001; Ogawa and Mori, 2004; Sathe et al., 2015]). To build the allele, we cloned 507bp upstream of the *HAC1* ORF in front of a 3V5 tag, followed by the IAA7 degron, the *HAC1* ORF, and 844bp downstream of the *HAC1* stop codon. The entire construct was cloned into a *LEU2* integrating vector (resulting in plasmid pÜB1073) and the AflII (NEB) digestion product was subsequently transformed into a strain heterozygous for *hac1Δ*. Following sporulation, haploids were chosen that carried the *AID-HAC1* allele as their sole source of Hac1.

HNT1-3V5 and COX20-3V5 strains:
A c-terminal *3V5* tag, marked by a G418 resistance cassette, was integrated into the endogenous locus, replacing the stop codon.

GFP reporter strains:
For *pHNT1-GFP*, *pHNT1* (-600 to +42) was cloned ahead of a ubiquitin-GFP fusion, followed by the *Candida albicans ADH1* terminator, resulting in pÜB1397. For *pHNT1ΔUPRE2-GFP*, the first five of the six bp in the UPRE2 motif starting at -284 were deleted from pÜB1397 via Q5 mutagenesis, resulting in pÜB1406. Constructs were integrated at the *TRP1* locus via transformation with the PmeI (NEB) digestion product of the relevant plasmid.

2.4.2 Yeast growth conditions

Strains were grown in YEPD(2%) at 30C, with shaking. Plate-based growth assays were carried out on YEPD(4%) plates at 30C.

2.4.3 Sample collection for sequencing experiments

wild-type/ *hac1Δ*:
BrÜn 1362 (wild-type) and 4431(*hac1Δ*) were inoculated into YEPD and grown at 30C overnight, then diluted to OD_{600}0.05 in YEPD. After approximately 2 doublings, cultures were split into 3 subcultures. Per strain, a first subculture received no treatment, a second was treated with 5mM DTT, and a third was treated with 2µg/mL Tm (Calbiochem). After 1 hr, 500 mL samples were collected as in (Brar et al., 2012), using 30 sec cycloheximide treatment, filtration, and flash freezing (in 2 portions - ~90% for ribosome profiling and ~10% for mRNA-sequencing). 2mL flash frozen buffer (20mM TRIS pH8, 140mM KCl, 1.5mM $MgCl_2$, 100µg/mL cycloheximide, 1% Triton X-100) was added to each ribosome profiling aliquot. Samples were lysed via Retsch mixermilling (6X 3 min, 15 Hz). Resulting powder was thawed and spun at 4C for 5 min, 3,000 x g. Supernatant was removed and cleared at 4C for 10 min, 20,000 x g.

AID-HAC1:
BrÜn 10532 (*AID-HAC1 -TIR1*) and 10744(*AID-HAC1 +TIR1*) were inoculated into YEPD and grown at 30C overnight, then diluted to OD_{600}0.05 in YEPD. After approximately 2 doublings, cultures were split into 2 subcultures. Per strain, one subculture was treated with 500µM auxin (Sigma) and 4µM IP_6 (Sigma) and the other with equivalent volumes of DMSO and water. After 15 min, the subcultures treated with auxin and IP6 were further split into 2 subcultures. Per strain, 1 auxin-pre-treated culture was not treated further (+auxin), and 1 was treated with 5mM DTT (+auxin +DTT). For each strain, the DMSO pre-treated subculture was treated with 5mM DTT (+DTT +vehicle). After 1 hr, 500 mL per culture was harvested identically as in the wild-type/*hac1Δ* experiment, except the buffer was supplemented with 2µg/mL Aprotinin (Sigma), 10µg/mL Leupeptin (Sigma), 1 mM PMSF (Sigma), 1:100 PIC2 (Sigma), and 1:100 PIC3 (Sigma). After 1 additional hr, a second 500 mL sample was harvested from each culture. Extract was prepared as in the wild-type/*hac1Δ* experiment, and identical extract was used for ribosome profiling and mass spectrometry.

2.4.4 Additional sample collection for protein/RNA analyses

wild-type*/hac1Δ* transcript comparisons:
One biological replicate was derived from total RNA prepared for the sequencing experiment described above. An additional replicate was collected similarly, except was harvested by filtration without the addition of cycloheximide.

wild-type/ *ire1Δ* transcript comparisons:
Two biological replicates were collected as follows. BrÜn 15 (wild-type) and 15924 (*ire1Δ*) were inoculated into YEPD and grown at 30C overnight, then diluted to OD_{600}0.05 in YEPD. After approximately 2 doublings, cultures were split into 3 subcultures. Per strain, a first subculture received no treatment, a second was treated with 5mM DTT, and a third was treated with 2µg/mL Tm (Calbiochem). Samples were harvested at the indicated times by filtration.
Additional AID-HAC1 transcript comparisons:

For cases where cells were pre-treated with auxin and subsequently treated with DTT, one biological replicate was derived from total RNA prepared for the sequencing experiment above. An additional replicate was collected similarly, except was directly harvested by filtration without the addition of cycloheximide. For analysis of AID-Hac1 protein levels in these experiments, 3 biological replicates were collected similarly except 2.5 OD units were harvested at each time point and treated with 5% trichloroacetic acid (TCA).

For cases where cells were pre-treated with DTT and subsequently treated with auxin, 2 biological replicates were collected as follows. BrÜn 10532 (*AID-HAC1 -TIR1*) and 10744(*AID-HAC1 +TIR1*) were inoculated into YEPD and grown at 30C overnight, then diluted to OD_{600}0.05 in YEPD. After approximately 2 doublings, the BrÜn 10744 culture was split into 2 subcultures. BrÜn 10532 and one of the BrÜn 10744 subcultures were treated with 5 mM DTT, while the other BrÜn 10744 subculture remained untreated. After 45 min, samples from each culture were collected by filtration. Both DTT-treated cultures were then treated with 500μM auxin (Sigma) and 4μM IP_6 (Sigma/Santa Cruz Biotechnology), while the untreated culture was treated with DMSO. Additional samples were collected by filtration at the indicated times. For analysis of Kar2 protein levels in these experiments, 3 biological replicates were collected similarly except 2.5 OD units were harvested at each time point and treated with 5% TCA.

Evaluation of *HNT1* and *COX20* expression:
For evaluation of Hnt1 and Cox20 protein levels upon DTT or Tm treatment (Figure 2.8, 2.19C-2.19F), BrÜn 10778 (*HNT1-3V5*) and 10781 (*COX20-3V5*) were harvested as follows. The appropriate strain was inoculated into YEPD and grown at 30C overnight, then diluted to OD_{600}0.05 in YEPD. After ~2 doublings, 2.5 OD units were collected and treated with 5% TCA, and cultures were subsequently treated with either DTT or Tm. Additional samples (2.5 OD units each time) were taken at the indicated times. Three full biological replicates were harvested for each condition. For similar experiments in the *AID-HAC1* background, BrÜn 10924 and 10925 were used for Hnt1 analysis, and BrÜn 10929 and 11133 were used for Cox20 analysis. Collection was the same, except that cultures were pre-treated for 15 min with 500μM auxin (Sigma) and 4μM IP_6 (Sigma) prior to initial sample collection and 5mM DTT treatment. Additionally, approximately 20mL per culture was collected at each time point and used for downstream RNA applications.

Evaluation of *GFP* reporter expression:
For evaluation of *GFP* transcript levels, BrÜn 15968 (*pHNT1-GFP*) and 16374 (*pHNT1ΔUPRE2-GFP*) were inoculated into YEPD and grown at 30C overnight, then diluted to OD_{600}0.05 in YEPD. After ~2 doublings, cultures were treated with 5mM DTT. Following 90 min treatment, samples were harvested by filtration and flash-frozen for total RNA isolation. Two biological replicates were harvested for each condition.

For evaluation of GFP protein levels (Figure 2.9D, 2.9E), BrÜn 15968 (*pHNT1-GFP*) and 16374 (*pHNT1ΔUPRE2-GFP*) were inoculated into YEPD and grown at 30C overnight, then diluted to OD_{600}0.05 in YEPD. After ~2 doublings, 2.5 OD units were

collected and treated with 5% TCA, and cultures were subsequently treated with 5mM DTT. Additional samples (2.5 OD units each time) were taken at the indicated times. Three biological replicates were harvested for each condition.

2.4.5 Growth curves

For Figure 2.10B, growth curve was performed as follows: BrÜn 13 (wild-type), BrÜn 4431 (*hac1Δ*), and BrÜn 10353 (*AID-HAC1*) were inoculated into YEPD and grown at 30C overnight, then diluted to OD_{600}0.05 in YEPD. After 7 hr, cultures were back-diluted to OD_{600}0.15 in YEPD. In a 96-well plate, 150µL cells were treated in triplicate with 2.5mM DTT. Cultures were grown overnight in a 30C, shaking plate reader (Tecan Infinite M1000), with absorbance at 600nm measurements taken every 15 min. Absorbance readings in Figure 3B represent averaged values across triplicate wells.

For Figures 2.23B, 2.23C, growth curves were performed as follows: BrÜn 15 (wild-type) and BrÜn 2781 (*pet100Δ*) were inoculated into YEPD and grown at 30C overnight, then diluted to OD_{600}0.05. After ~2 doublings, cultures were split into 2 subcultures, one of which remained untreated and one of which was treated with 5mM DTT. OD_{600} readings were taken every hr. OD_{600} values in Figure 2.23B, 2.23C are normalized to the exact OD_{600} reading just before treatment and represent average fold change from starting OD_{600} across 3 biological replicates.

2.4.6 Plate-based growth assays

BrÜn 15 (wild-type) and BrÜn 2781(*pet100Δ*) were inoculated into YEPD and grown at 30C overnight, then diluted to OD_{600}0.2 in YEPD. Approximately 4.5 hr later, cultures were diluted to OD_{600}0.1 in water. Samples were briefly sonicated to prevent clumping, and 5-fold dilutions were prepared in water. 3 µL of each dilution were plated on YEPD (4%) containing 0µg, 0.5µg or 0.75µg/mL Tm (Calbiochem). Plates were imaged after 2 nights at 30C.

2.4.7 Northern blotting

All RNA was isolated using the hot acid phenol method. 8-10µg of total RNA was denatured in glyoxal mix [1M glyoxal (Sigma), 50% DMSO, 10mM $NaPO_4$ pH 6.8] for 10 min at 70C. Denatured samples were loaded onto a 1.1% agarose gel, separated at 116V for 3 hr, and transferred overnight to a nylon membrane (Hybond-N+ [GE]). Following UV crosslinking and methylene blue staining, the membrane was blocked at 68C for at least 45 min with Ultrahyb buffer (Invitrogen) supplemented with boiled sonicated salmon sperm DNA (Agilent). All probe templates were generated by PCR (primers in Table 2.11) of wild-type yeast genomic DNA, except the *GFP* probe template, which was generated by amplification from a *GFP*-containing plasmid. The probe was in vitro transcribed (MaxiScript T7 Kit [Invitrogen]) using all kit components, except cold UTP was replaced with alpha-P32 labeled UTP (PerkinElmer). The blot was incubated with the hot probe at 68C overnight, and subsequently washed for 2X 5 min at RT with low stringency wash buffer (2X SSC, 0.1% SDS) and 2X 15 min at 68C with

high stringency wash buffer (0.1X SSC, 0.1% SDS). Typhoon phosphor imaging was used for visualization. For each transcript probed, at least 2 biological replicates were performed and sizing was confirmed on a sample blot with ladders and, more routinely, by comparison to rRNA bands. In our experience, likely due to their highly stable structural features, rRNA (2.0 kB and 3.8 kB) species tend to migrate slightly faster than would be expected for mRNAs, making all of our size comparisons approximate.

2.4.8 Immunoblotting

Immunoblotting was performed using a TCA protocol, similar to that described by (Chen et al., 2017). Briefly, 2.5 OD units of culture were treated with 5% TCA at 4C for at least 10 min. Samples were then washed with 1mL acetone. Acetone was aspirated and pellets were dried overnight at RT. Lysates were made by adding 100µl protein lysis buffer (50mM TE, 3mM DTT, 1.1mM PMSF (Sigma), 1µM pepstatin A, 1X protease inhibitor cocktail [Roche]) and 1 volume acid-washed glass beads (Sigma), and bead-beating for 5 min at RT. 3X SDS loading buffer was added and samples were boiled for 5 min. Beads were pelleted by centrifugation and 5µL supernatant was loaded onto 4-12% Bis-Tris polyacrylamide gels. Following electrophoresis, proteins were transferred using a semi-dry transfer apparatus (Trans-Blot Turbo, BioRad). The following antibodies were used: mouse anti-V5 (Invitrogen, 1:2,000), rat anti-tubulin (Serotec, 1:10,000), rabbit anti-Kar2 (gift of Mark Rose, 1:100,000), mouse anti-GFP (Clontech, 1:500), goat anti-rat680 (LI-COR, 1:15,000), goat anti-mouse800 (LI-COR, 1:15,000), goat anti-rabbit 800 (LI-COR, 1:15,000).

2.4.9 Ribosome profiling library generation

Ribosome profiling libraries were prepared as described as in (Cheng et al., 2018). Briefly, footprints were prepared by treating extract with 15U RNase I (Ambion) per A_{260} unit for 1 hr at RT. Monosomes were isolated by sucrose gradient (10-50%). RNA was isolated by the hot acid phenol method. Samples were size-selected (by PAGE), dephosphorylated (PNK [NEB]), polyA-tailed (PolyA polymerase [NEB] with oCJ200-oligodT), subtracted of rRNA (MyOne Streptavidin C1 dynabeads [Invitrogen] with asDNA1b-3b), and reverse transcribed (Superscript III [Invitrogen]). RT products were size-selected (by PAGE), circularized (Circ ligase [Epicenter]), and PCR amplified [Phusion polymerase (NEB) with oNTI231and index primers]. Following gel purification, libraries were sequenced using standard Illumina oligos. Oligonucleotide sequences are included in Table 2.11.

2.4.10 mRNA-sequencing library generation

mRNA-sequencing libraries were prepared as described in (Cheng et al., 2018). Briefly, RNA was extracted by the hot acid phenol method and was polyA-selected (oligodT Dynabeads [Ambion]). Samples were alkaline fragmented, then size-selected (by PAGE) and subsequently dephosphorylated, polyA-tailed, and reverse transcribed as for the ribosome profiling libraries. RT products were similarly size-selected,

circularized, and PCR amplified. Following gel purification, libraries were sequenced using standard Illumina oligos.

2.4.11 Sequencing

All sequencing was done at the UC-Berkeley Vincent J. Coates QB3 Sequencing Facility. Libraries were sequenced on an Illumina HiSeq 2500, 50SRR, with multiplexing.

2.4.12 Metabolic profiling

Samples were harvested as follows: For Figure 2.20A, BrÜn 10532 (*AID-HAC1 –TIR1*) and 10744 (*AID-HAC1 +TIR1*) were inoculated into YEPD and grown at 30C overnight, then diluted to OD_{600}0.05 in YEPD. After approximately 2.5 doublings, cultures were treated with 500μM auxin (Sigma) and 4μM IP_6 (Sigma). After 15 min, cultures were split into subcultures. Per strain, one subculture was not treated further (+auxin), and one was treated with 2μg/mL Tm (Calbiochem) (+auxin +Tm). After 2 hr, cultures were harvested by centrifugation (4C, 2,000 x g, 1 min), washed in cold water (4C, 15,000 x g, 30 sec), and flash frozen in ~30mg aliquots. Five technical replicates were collected per condition. For Figure 2.20B, BrÜn 15 (wild-type) was used, except without the addition of auxin/IP6 and 6 technical replicates were collected per condition.

For both experiments, metabolomic analyses were performed as reported previously (Louie et al., 2016). Briefly, frozen cell pellets were resuspended with 150mL 40:40:20 acetonitrile/methanol/water containing 10nmoles D_3N^{15} serine internal standard (Cambridge isotopes). Samples were vortexed thoroughly for 30 sec and bath sonicated for 15 sec before centrifugation at 21,000 x g for 10 min. Supernatant was collected and frozen at -80^{o} C until analysis. 20 mL of supernatant was analyzed by single-reaction monitoring (SRM)-based targeted LC-MS/MS. Separation of metabolites was performed by normal-phase chromatography using a Luna-5 mm NH2 column (50 mm x 4.60 mm, Phenomenex). Mobile phases were run as follows: Buffer A, acetonitrile; Buffer B, 95:5 water/ acetonitrile with 0.1% formic acid or 0.2% ammonium hydroxide with 50 mM ammonium acetate for positive and negative ionization modes, respectively. Flow rate began at 0.2 mL/min for 2 min, followed by a gradient starting at 0% B and increasing linearly to 100% B over the course of 13 min with a flow rate of 0.7 mL/min, followed by an isocratic gradient of 100% B for 10 min with a flow rate of 0.7mL/min before equilibrating for 5 min at 0% B with a flow rate of 0.7 mL/min. MS analysis was performed using an electrospray ionization (ESI) source on an Agilent 6430 QQQ LC-MS/MS. Capillary voltage was 3.0 kV, fragmentor voltage was 100 V, drying gas temperature 350^{o} C, drying gas flow rate was 10 L/min, and the nebulizer pressure was 35 psi. Representative metabolites were quantified by SRM of the transitions from precursor to product ions at associated collision energies. Data was analyzed by calculating area under the curve using Agilent Qualitative Analysis software.

2.4.13 Oxygen consumption assay

Except for materials needed for yeast cultures, all steps were carried out using components from a Seahorse Extracellular FluxPak (Agilent).

Preparation of cartridge:
A Seahorse Extracellular Flux cartridge was hydrated with 200µl water per well overnight at 30C. Approximately 90 min prior to taking basal OCR measurements, water was removed and replaced with 200µl pre-warmed XF Calibrant solution.

Preparation of cell culture plate:
Wells were coated with 20µl 0.1mg/mL poly-L-lysine (Sigma) for 10 min at RT. Poly-L-lysine was then removed and the plate allowed to dry before adding cells. Cells were grown and plated as follows. BrÜn 15 (wild-type) was inoculated into YEPD and grown at 30C overnight, then diluted to OD_{600}0.05 in YEPD. After ~2 doublings, cells were treated with 2µg/mL Tm (Calbiochem). This culture was used for the 6.5 hr Tm treatment samples. After 4.5 hr, an additional OD_{600}0.05 culture was started from the overnight inoculation, and after ~2 doublings, cells were treated with 2µg/mL Tm (Calbiochem) or vehicle. These cultures were used for the 2 hr Tm treatment samples and the control samples, respectively. After 6 hr and 1.5 hr, respectively, 0.3 OD units centrifuged at 1,500 x g, 2 min, RT. Cells were resuspended in 2 mL and then diluted 1:6 in fresh media (supplemented with Tm as appropriate). 180ul was added to each of 12 wells per condition. The plate was spun at 500 x g for 3 min at RT and then placed at 30C for 30 min. Immediately before OCR measurements, the plate was spun again as before.

OCR measurements:
Following initial calibration, basal OCR was measured using a 2 min mix, 2 min measure protocol. Measurements, corrected for OD_{600} differences at the end of the assay, are reported in Figure 2.23A.

2.4.14 Mass spectrometry

TMT-labeling and sample fractionation:
Proteins were precipitated by adding -20°C cold acetone to the lysate (acetone to eluate ratio 10:1) and overnight incubation at -20°C. The proteins were pelleted by centrifugation at 20000xg for 15 min at 4°C. The supernatant was discarded and the pellet was left to dry by evaporation. The protein pellet was reconstituted in 100µl urea buffer (8M Urea, 75mM NaCl, 50mM Tris/HCl pH 8.0, 1mM EDTA), and protein concentrations were determined by BCA assay (Pierce). Fifteen µg of total protein per sample were processed further. Disulfide bonds were reduced with 5mM DTT and cysteines were subsequently alkylated with 10mM iodoacetamide. Samples were diluted 1:4 with 50mM Tris/HCl (pH 8.0) and sequencing grade modified trypsin (Promega) was added in an enzyme-to-substrate ratio of 1:50. After 16hr of digestion, samples were acidified with 1% formic acid (final concentration). Tryptic peptides were desalted on C18 StageTips according to (Rappsilber et al., 2007) and evaporated to

dryness in a vacuum concentrator. Desalted peptides were labeled with the TMT11plex mass tag labeling reagent according to the manufacturer's instructions (Thermo Scientific) with small modifications. Briefly, 0.2units of TMT10plex reagent was used per 15µg of sample. Peptides were dissolved in 30µl of 50mM Hepes pH 8.5 solution and the TMT10plex reagent was added in 12.3µl of MeCN. After 1hr incubation, the reaction was stopped with 2.5µl 5% Hydroxylamine for 15min at 25°C. Differentially labeled peptides were mixed for each replicate (A-L were labeled with 126C, 127N, 127C, 128N, 128C, 129N, 129C, 130N, 130C, 131N, 131C, respectively) and subsequently desalted on C18 StageTips (Rappsilber et al., 2007) and evaporated to dryness in a vacuum concentrator.

The peptide mixtures were fractionated by Strong Cation Exchange (SCX) using StageTips as previously described (Rappsilber et al., 2007) with slight modifications. Briefly, one StageTip was prepared per sample by three SCX discs (3M, #2251) topped with two C18 discs (3M, #2215). The packed StageTips were first washed with 100µl methanol and then with 100µl 80% acetonitrile and 0.2% formic acid. Afterwards, they were equilibrated by 100µl 0.2% formic acid and the sample was loaded onto the discs. The sample was transeluted from the C18 discs to the SCX discs by applying 100µl 80% acetonitrile; 0.2% formic acid, which was followed by 3 stepwise elutions and collections of the peptide mix from the SCX discs. The first fraction was eluted with 50µl 50mM NH_4AcO; 20% MeCN (pH ~7.2), the second with 50µl 50mM NH_4HCO_3; 20% MeCN (pH ~8.5) and the sixth with 50µl 0.1% NH_4OH; 20% MeCN (pH ~9.5). 200µl of 0.2% acetic acid was added to each of the three fractions, and they were subsequently desalted on C18 StageTips as previously described (Rappsilber et al., 2007) and evaporated to dryness in a vacuum concentrator. Peptides were reconstituted in 10µl 0.2% formic acid. Both the unfractionated samples plus the fractionated, less complex samples were then analyzed by LC-MS/MS on a Q-Exactive HF was performed as previously described (Keshishian et al., 2015).

Approximately 1µg of total peptides was analyzed on an Eksigent nanoLC-415 HPLC system (Sciex) coupled via a 25cm C18 column (inner diameter of 100µm, packed in-house with 2.4µm ReproSil-Pur C18-AQ medium, Dr. Maisch GmbH) to a benchtop Orbitrap Q Exactive HF mass spectrometer (Thermo Fisher Scientific). Peptides were separated at a flow rate of 200nL/min with a linear 106min gradient from 2% to 25% solvent B (100% acetonitrile, 0.1% formic acid), followed by a linear 5min gradient from 25 to 85% solvent B. Each sample was run for 170min, including sample loading and column equilibration times. Data was acquired in data dependent mode using Xcalibur 2.8 software. MS1 Spectra were measured with a resolution of 60,000, an AGC target of 3E6 and a mass range from 375 to 2000m/z. Up to 15 MS2 spectra per duty cycle were triggered at a resolution of 60,000, an AGC target of 2E5, an isolation window of 1.6 m/z and a normalized collision energy of 36.

Label Free Quantification:
In order to validate the TMT-based quantification results, we performed proteomics based on LFQ, which does the quantification on the MS1 level, instead of the MS2 level, and does not allow multiplexing as does TMT labeling. Therefore, different systematic biases are introduced by LFQ based proteomics than by TMT based proteomics, and it

serves as a quite stringent test to our deep proteome quantification results obtained by our TMT based approach. We quantified all 11 matched samples.
Proteins were precipitated by adding -20°C cold acetone to the lysate (acetone to eluate ratio 10:1) and overnight incubation at -20°C. The proteins were pelleted by centrifugation at 20000xg for 15min at 4°C. The supernatant was discarded and the pellet was left to dry by evaporation. The protein pellet was reconstituted in 100µl urea buffer (8M Urea, 75mM NaCl, 50mM Tris/HCl pH 8.0, 1mM EDTA) and protein concentrations were determined by BCA assay (Pierce). 20µg of total protein per sample were processed further. Disulfide bonds were reduced with 5mM DTT and cysteines were subsequently alkylated with 10mM iodoacetamide. Samples were diluted 1:4 with 50mM Tris/HCl (pH 8.0) and sequencing grade modified trypsin (Promega) was added in an enzyme-to-substrate ratio of 1:50. After 16h of digestion, samples were acidified with 1% formic acid (final concentration). Tryptic peptides were desalted on C18 StageTips according to (Rappsilber et al., 2007) and evaporated to dryness in a vacuum concentrator. Desalted peptides were reconstituted in Buffer A (0.2% Formic acid).

LC-MS/MS analysis was performed on a Q-Exactive HF. Approximately 1µg of total peptides were analyzed on an Eksigent nanoLC-415 HPLC system (Sciex) coupled via a 25cm C18 column (inner diameter 100µm packed in-house with 2.4µm ReproSil-Pur C18-AQ medium, Dr. Maisch GmbH) to a benchtop Orbitrap Q Exactive HF mass spectrometer (Thermo Fisher Scientific). Peptides were separated at a flow rate of 200nL/min with a linear 106min gradient from 2% to 25% solvent B (100% acetonitrile, 0.1% formic acid), followed by a linear 5min gradient from 25 to 85% solvent B. Each sample was run for 170min, including sample loading and column equilibration times. Data was acquired in data dependent mode using Xcalibur 2.8 software. MS1 Spectra were measured with a resolution of 60,000, an AGC target of 3E6 and a mass range from 375 to 2000m/z. Up to 15 MS2 spectra per duty cycle were triggered at a resolution of 15,000, an AGC target of 2E5, an isolation window of 1.6 m/z and a normalized collision energy of 27.

2.4.15 quantification and statistical analyses

Sequence alignments and analysis:
Performed as described in (Cheng et al., 2018), we observed the high technical and biological reproducibility that our lab typically observes using ribosome profiling and mRNA-sequencing. Alignments were done using bowtie2 (Langmead and Salzberg, 2012). Genome browser analysis was done using Mochiview (Homann and Johnson, 2010). Cluster analysis and visualization were done using Cluster 3.0 and Java Treeview, respectively (de Hoon et al., 2004; Saldanha, 2004).

LUTI identification:
mRNA-seq and ribosome profiling data for wild-type and *hac1Δ* cells, with either no treatment or treatment with DTT or Tm, as described above, were analyzed by genome browser (Mochiview). All annotated yeast genes were inspected visually for evidence of an alternate, 5' extended transcript with translated uORFs that was Hac1- and UPR^{ER}-

dependent. This approach was enabled by the simple transcript structures of most budding yeast genes. Of the ~30 candidates found by this approach, 19 showed an associated Hac1-dependent decrease in TE and were defined as candidate LUTIs. This set of 19 was reevaluated one-by-one in the AID-Hac1 experiment to determine if these hallmarks remained strong. In 15 cases, this was true, and these genes are presented in Table 2.3. Note that a major caveat of this approach is that it is biased towards analysis of highly expressed mRNAs, as it is much more straightforward in these cases to detect the robust presence of alternate transcripts.

Translation efficiency calculations:
TE values were obtained as described in (Ingolia et al., 2009). We calculated TE by dividing unfiltered footprint RPKMs by unfiltered mRNA RPKMs, summing reads over each annotated canonical ORF.

Hac1 target gene expression:
We analyzed our sequencing and mass spectrometry data to determine if reported Hac1 targets (Travers et al., 2000) displayed the expected trends. In cases where we show changes in transcript or translation levels upon DTT or Tm treatment (Figure 2.3A, 2.3B, 2.4A, 2.4B, 2.14A), we calculated the number of reported Hac1 targets upregulated upon DTT or Tm treatment (fold-change Y/X > 1). We performed a resampling test (10,000 iterations) by taking subsamples from the overall gene set of size equal to the target gene set and calculating the number of upregulated genes. P-values were determined from the frequency distribution of the number of upregulated genes compared to the Hac1 target gene set. In cases where we show differences in transcript or translation levels between cells with and without Hac1 (Figure 2.3C, 2.4C), we performed identical analyses using the inverse of the fold change (X/Y).

Metabolomics data:
Reported p-values were generated by t-tests.

Oxygen consumption data:
Reported p-values were generated by a two-tailed Mann-Whitney test.

Immunoblot quantification:
Quantification of triplicate biological replicates was performed on raw images in Image Studio Lite (LI-COR). Signal intensity was normalized to that of a tubulin loading control.

Analysis of TMT mass spectrometry:
All raw data were analyzed with MaxQuant software version 1.6.0.16 (Cox and Mann, 2008) using a UniProt yeast database (release 2014_09, strain ATCC 204508 / S288c), and MS/MS searches were performed with the following parameters: The five mass spec runs were grouped together. TMT11plex labeling on the MS2 level, oxidation of methionine and protein N-terminal acetylation as variable modifications; carbamidomethylation as fixed modification; Trypsin/P as the digestion enzyme; precursor ion mass tolerances of 20 p.p.m. for the first search (used for nonlinear mass re-calibration) and 4.5 p.p.m. for the main search, and a fragment ion mass tolerance of

20 p.p.m. For identification, we applied a maximum FDR of 1% separately on protein and peptide level. We required 1 or more unique/razor peptides for protein identification and a ratio count for each of the 11 TMT channels. This gave us a total of 2577 quantified protein groups.

Finally, we normalized the MaxQuant generated corrected TMT intensities such that at each condition/time point the corrected TMT intensity values added up to exactly 1,000,000; therefore each protein group value can be regarded as a normalized microshare (we did this separately for each TMT channel for all proteins that made our filter cutoff in all the TMT channels).

Note: In order to compare protein group specific intensity values between the TMT quantified samples and our control label free quantified (LFQ) samples, we adjusted the normalization for the TMT data in order to incorporate the MS1 information as well. Each protein group of a TMT labeled sample got its proportional fraction of the MS1 based iBAQ intensities based on its labeling channel specific TMT MS2 intensity relative to the sum of TMT MS2 intensities of all labeled channels for the corresponding protein group. Afterwards we normalized these fractional MS1 iBAQ intensities such that at each condition/time point these intensity values added up to exactly 1,000,000, therefore each protein group value can be regarded as a normalized microshare. These microshare values are then comparable to the normalized microshare iBAQ based intensities from our label free samples (see below).

Analysis of LFQ mass spectrometry:
All raw data were analyzed with MaxQuant software version 1.6.0.1 (Cox and Mann, 2008) using a UniProt yeast database (release 2014_09, strain ATCC 204508 / S288c), and MS/MS searches were performed with the following parameters: Oxidation of methionine and protein N-terminal acetylation as variable modifications; carbamidomethylation as fixed modification; Trypsin/P as the digestion enzyme; precursor ion mass tolerances of 20 p.p.m. for the first search (used for nonlinear mass re-calibration) and 4.5 p.p.m. for the main search, and a fragment ion mass tolerance of 20 p.p.m. For identification, we applied a maximum FDR of 1% separately on protein and peptide level. “Match between the runs” was activated, as well as the “iBAQ” field. A total of 2475 protein groups was identified by at least 1 or more unique/razor peptides in any of the 11 samples. For any comparison between different samples only protein groups that had been assigned iBAQ values in each of the samples that were used.

Finally, we normalized the MaxQuant generated iBAQ intensities such that at each condition/time point the iBAQ intensity values added up to exactly 1,000,000; therefore each protein group value can be regarded as a normalized microshare (we did this separately for each sample for all proteins that were present in that sample).

2.4.16 Data availability

All sequencing data can be accessed at NCBI GEO with accession number GSE115366. Mass spectrometry data are available on the MassIVE platform with accession number MSV000082454.

Chapter 3: Investigation of physiological UPR^{ER} activation in budding yeast meiosis

3.1 Introduction

Studies of the UPR^{ER} in yeast have traditionally relied on induction of the pathway with drugs such as DTT or tunicamycin, as in (Travers et al., 2000; Chapter 2). Treatment with such drugs results in a global unfolding of ER clients and a burden of misfolded proteins unlikely to recapitulate natural cellular conditions, therefore limiting our understanding of UPR^{ER} signaling in a physiologically relevant context. Recently, induction of the UPR^{ER} was observed in budding yeast meiosis, in the absence of an external perturbation (Brar et al., 2012). Two waves of meiotic *HAC1* splicing and translation were observed – one following transfer to sporulation medium, and a second, stronger wave approximately six hours after transfer to sporulation medium, corresponding roughly to the end of meiosis I. In the latter wave, approximately 50% of the *HAC1* message is spliced, compared to ~80% spliced with DTT treatment and ~10% spliced during the first wave of meiotic induction (Brar et al., 2012; Rüegsegger et al., 2001). We propose that meiosis is a useful context for studying the UPR^{ER} under physiologically relevant conditions, more closely mirroring that of developmentally regulated induction of this pathway, for example, during B-cell differentiation (Reimold et al., 2001; Gass et al., 2002). The fact that this type of internally programmed induction could be seen in yeast offered us the advantages of studying natural UPR^{ER} induction using a tractable model organism that contains only the conserved Hac1/XBP1 UPR^{ER} signaling branch.

In addition to providing a useful context in which to study physiological UPR^{ER} activation, meiotic UPR^{ER} induction also raises questions about meiotic differentiation itself. Traditionally, study of the meiotic program has centered on chromosome segregation, largely ignoring the complex cellular remodeling and organellar dynamics required to form healthy gametes (spores in yeast). Understanding whether or not the UPR^{ER} plays an important role in this developmental program, and the nature of such a role, may shed light on the conserved process of gamete formation. Interestingly, there is evidence of spliced XBP1 (the metazoan ortholog of *HAC1*) in late stages of *Xenopus* oogenesis, suggesting conservation of meiotic UPR^{ER} activation (Cao et al., 2006).

We decided to take a two-pronged approach to studying the UPR^{ER}, undertaking lines of investigation both to understand what role the UPR^{ER} might play in meiosis and to use the meiotic induction context to study physiological activation and transcriptional targets of the UPR^{ER}. By analyzing sporulation efficiency in a variety of UPR^{ER} mutants, we showed that having an intact UPR^{ER} prior to and/or during entry promotes meiotic success, suggesting a previously unrecognized physiological role for this conserved pathway in budding yeast. To begin to investigate what might activate the UPR^{ER} in meiosis, we evaluated Hac1 expression in variety of meiotic mutants to see what aspects of meiotic differentiation are required for UPR^{ER} induction. We found that the second wave of UPR^{ER} induction is independent of meiosis II and sporulation-related

events, as cells carrying mutated alleles of genes important for these events still showed robust Hac1 expression. However, we showed that the second wave of UPR^{ER} activation does depend on expression of *NDT80*, which encodes a transcription factor important for exit from meiotic prophase. We observed dynamic ER remodeling in meiotic cells (also observed by [Suda et al., 2007]), which, when combined with work by others in the lab (George Otto, unpublished data), suggests that meiotic ER remodeling might be related to UPR^{ER} activation. Additionally, we developed strategies for determining transcriptional targets of Hac1 in meiosis, generating two complementary global gene expression datasets that will likely be informative in establishing what gene targets Hac1 turns on in a physiologically relevant context.

3.2 Results

3.2.1 Stable Hac1 protein is produced during two waves of meiotic UPR^{ER} induction

To determine whether the previously observed *HAC1* splicing and translation results in stable, detectable Hac1 protein during meiosis, we performed a meiotic time course in the *AID-HAC1* background (described in Chapter 2) and took advantage of this epitope-tagged allele to test for stable Hac1 protein presence by immunoblot (Figure 3.1A). As was expected based on the timing of *HAC1* splicing and translation, we observed Hac1 protein both early (~5 min post-transfer to sporulation medium) and late in meiosis, with a robust wave of expression beginning approximately ~6 hours after meiotic induction. Interestingly, the predominant protein species during the second wave of Hac1 expression appeared to migrate more slowly than that of the first wave, raising the possibility that perhaps the Hac1 protein is modified during late meiosis. Concurrent work by others in the lab employed analysis of matched samples subjected to mRNA-seq, ribosome profiling, and mass spectrometry, and showed stable expression of the untagged, endogenous Hac1 protein by mass spectrometry at the expected time, bolstering our finding that the Hac1 protein is stably produced during meiosis (Cheng et al., 2018).

While the only reported function of the Hac1 protein is in transcriptional regulation, we wondered if the localization of Hac1 during meiosis is consistent with its transcription factor function or if it might suggest an alternate, previously unreported function of the protein. We evaluated Hac1 localization by immunofluorescence, again taking advantage of the epitope-tagged allele (Figure 3.1B). We noted that the localization of the protein during meiosis was very similar to that during DTT treatment of vegetative cells, suggesting that Hac1's predominant function during meiosis is nuclear, consistent with a role in transcriptional regulation.

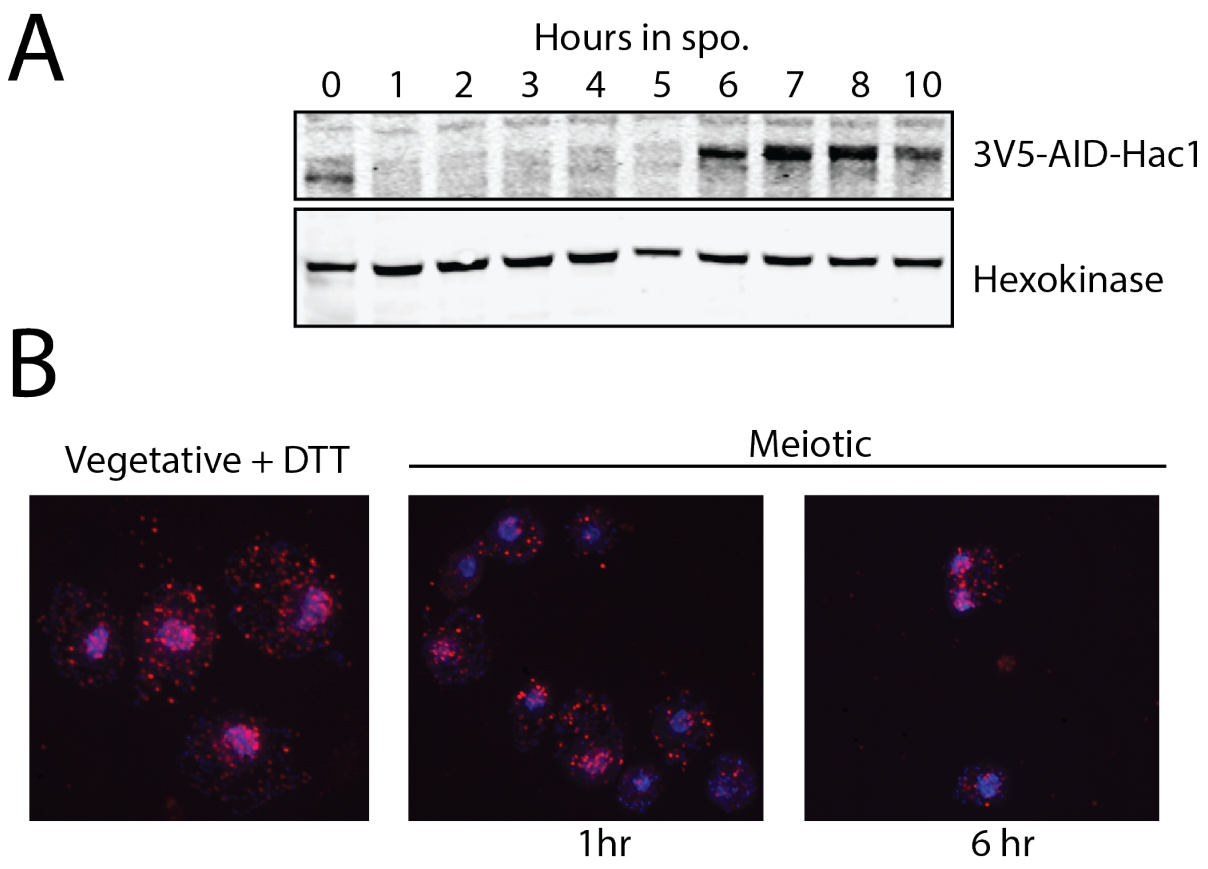

Figure 3.1 Hac1 protein is expressed during meiosis and shows a similar localization pattern as it has in DTT-treated cells.

A) Immunoblotting for Hac1 (3V5-AID-Hac1) reveals that the Hac1 protein is stable expressed in two waves as BrÜn 13403 progresses through meiosis.

B) The localization of Hac1 (3V5-AID-Hac1, red) in meiosis is similar to the localization pattern in cells treated with 5mM DTT for 1 hr. In both cases, there is a nuclear pool (as judged by overlap with DAPI stain). BrÜn 8669 was used for both experiments. Representative images early (1hr) and late (6hr) in meiosis are shown.

3.2.2 Constitutive UPR^{ER} mutants show decreased sporulation efficiency

Because it appeared that *HAC1* splicing and translation in meiosis results in detectable, nuclear Hac1 protein, we wondered if UPR^{ER} activation is an important part of the meiotic program. To determine whether or not an intact UPR^{ER} is required for meiotic success, we sought to construct a constitutive *hac1* deletion strain. In the SK1 strain background, it has been previously reported that constitutive deletion of UPR^{ER} components in haploid cells results in an autodiploidization event, making such a strain hard to generate (Lee et al., 2003). We decided to attempt sequential deletion of both *HAC1* alleles in diploid cells, reasoning that because the reported ploidy defect seemed restricted to increasing ploidy to 2N, starting with a diploid may circumvent this issue. Prior to performing meiotic analyses with the resulting *hac1Δ* strain (described in Chapter 2), we wanted to verify that this mutant maintained diploidy. To this end, we performed a flow-cytometry based analysis of DNA content, comparing *hac1Δ* cells to wild-type cells (Figure 3.2A). We observed that the ploidy of putative *hac1Δ* diploids matched that of known wild-type diploids, verifying that meiotic analyses with this strain would not be complicated by ploidy maintenance issues and suggesting that this

strategy of sequential deletion in diploids would be fruitful in making strains mutated for other UPR^{ER} components.

We then asked whether *hac1Δ* cells successfully complete the meiotic program. We performed a meiotic time course and compared the sporulation efficiency of *hac1Δ* cells to that of wild-type cells (Figure 3.2B). Fewer *hac1Δ* cells packaged spores than did wild-type cells, suggesting *HAC1* is required for meiotic success. To determine whether *hac1Δ* cells robustly enter meiosis, we used protein samples collected during a meiotic time course to determine the timing of induction of the meiotic cohesion protein, Rec8 (Klein et al., 1998). We observed a marked delay in the timing of Rec8 expression in *hac1Δ* cells compared to in wild-type cells (Figure 3.2C). We concluded that *hac1Δ* cells exhibit a meiotic entry and/or prophase defect, though it should be noted that this result does not rule out the possibility of an additional, later meiotic defect.

Because analyses of constitutive deletion mutants can be complicated by suppressor mutations, we repeated these experiments in cells deleted for another UPR^{ER} regulator, the transmembrane kinase/endonuclease *IRE1*. Cells deleted for *IRE1* exhibited a similar defect in sporulation efficiency as that of *hac1Δ* cells (Figure 3.2D). We assayed the expression of another early meiotic protein, Zip1 (a component of the synaptonemal complex, a structure assembled between homologous chromosomes during meiotic prophase [Sym et al., 1993]), and again observed a 2-3 hr delay in prophase induction (Figure 3.2E). We concluded that cells constitutively deleted for UPR^{ER} components show decreased meiotic success, at least in part stemming from a defect in entry and/or prophase.

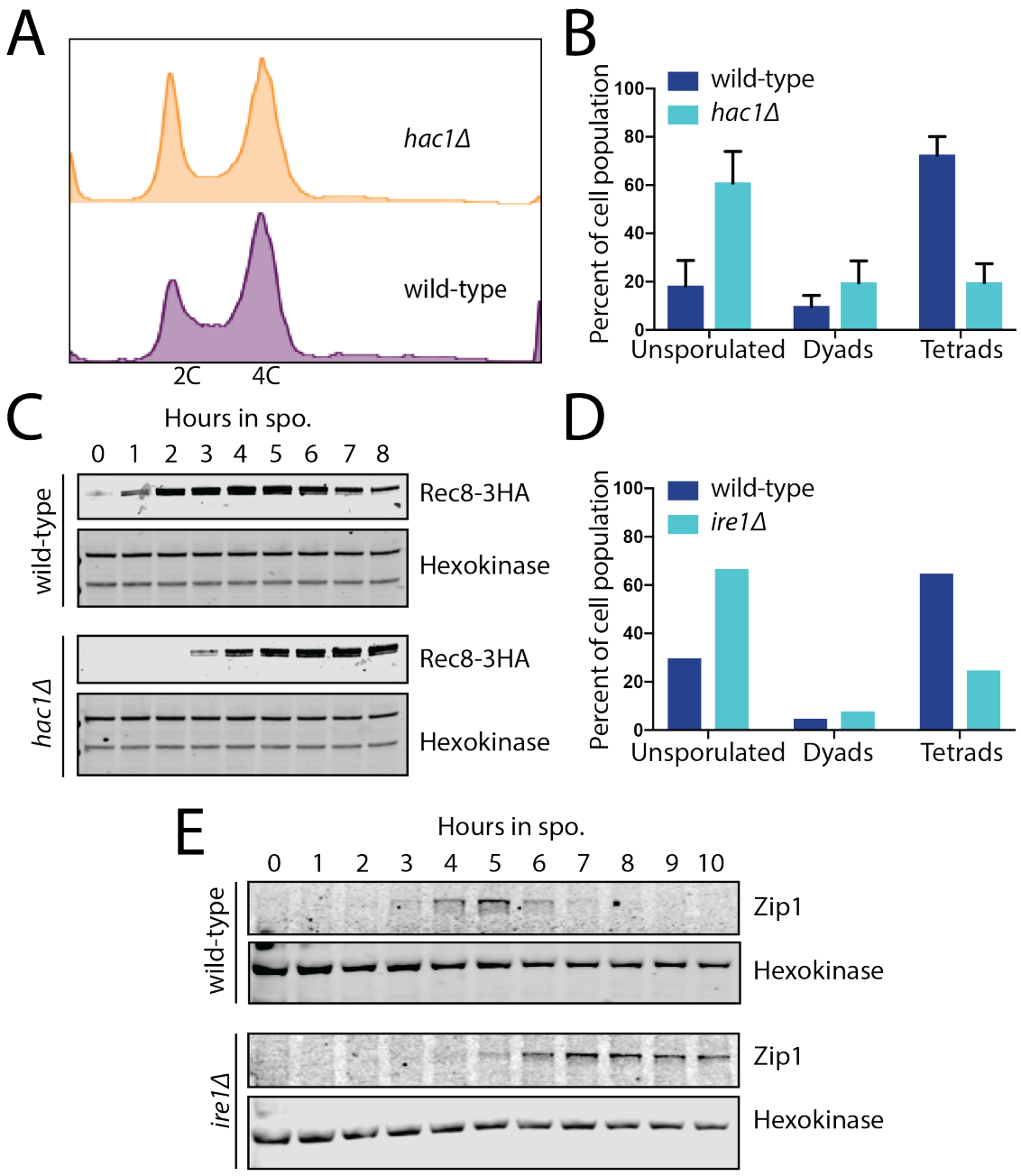

Figure 3.2. Constitutive UPR^{ER} mutants display a meiotic defect.

A) *hac1Δ* cells are maintained as diploids as judged by flow cytometry. DNA content of vegetative *hac1Δ* cells (BrÜn 4431, orange) is compared to that of a wild-type, known diploid (BrÜn 1362, purple).

B) 24 hr sporulation efficiency of wild-type cells (BrÜn 1362) compared to *hac1Δ* cells (BrÜn 4431). Average sporulation efficiencies of 3 biological replicates are shown, with error bars representing SD. At least 200 cells were counted per strain for each replicate.

C) Rec8 immunoblots (anti-HA) reveal an entry-related defect in *hac1Δ* cells (BrÜn 4431) compared to wild-type cells (BrÜn 1362).

D) 24 hr sporulation efficiency of wild-type cells (BrÜn 15) compared to *ire1Δ* cells (BrÜn 15924). 200 cells were counted per strain.

E) Zip1 immunoblots reveal an entry-related defect in *ire1Δ* cells (BrÜn 15924) compared to wild-type cells (BrÜn 15).

3.2.3 Inositol addition does not rescue the meiotic defect of UPR^{ER} mutants

We wondered if the observed entry-related defect in UPR^{ER} mutant cells might be related to the nutritional conditions used to promote entry. Meiosis in yeast is induced by nutritional deprivation (reviewed in [van Werven and Amon, 2011]), and the media used to promote sporulation lacks inositol, a sugar that when absent in normal yeast media promotes UPR^{ER} activation (Cox et al., 1997). We therefore decided to test whether or not addition of inositol to the sporulation medium would suppress the meiotic defect of *hac1Δ* cells. We supplemented sporulation medium with increasing concentrations of inositol, and found no effect on sporulation efficiency even at the highest inositol concentration (Figure 3.3A). Similarly, the timing of Rec8 induction was not impacted by addition of inositol (Figure 3.3B). We concluded that the meiotic defect of UPR^{ER} mutants is not simply due to an inability to tolerate inositol deprivation.

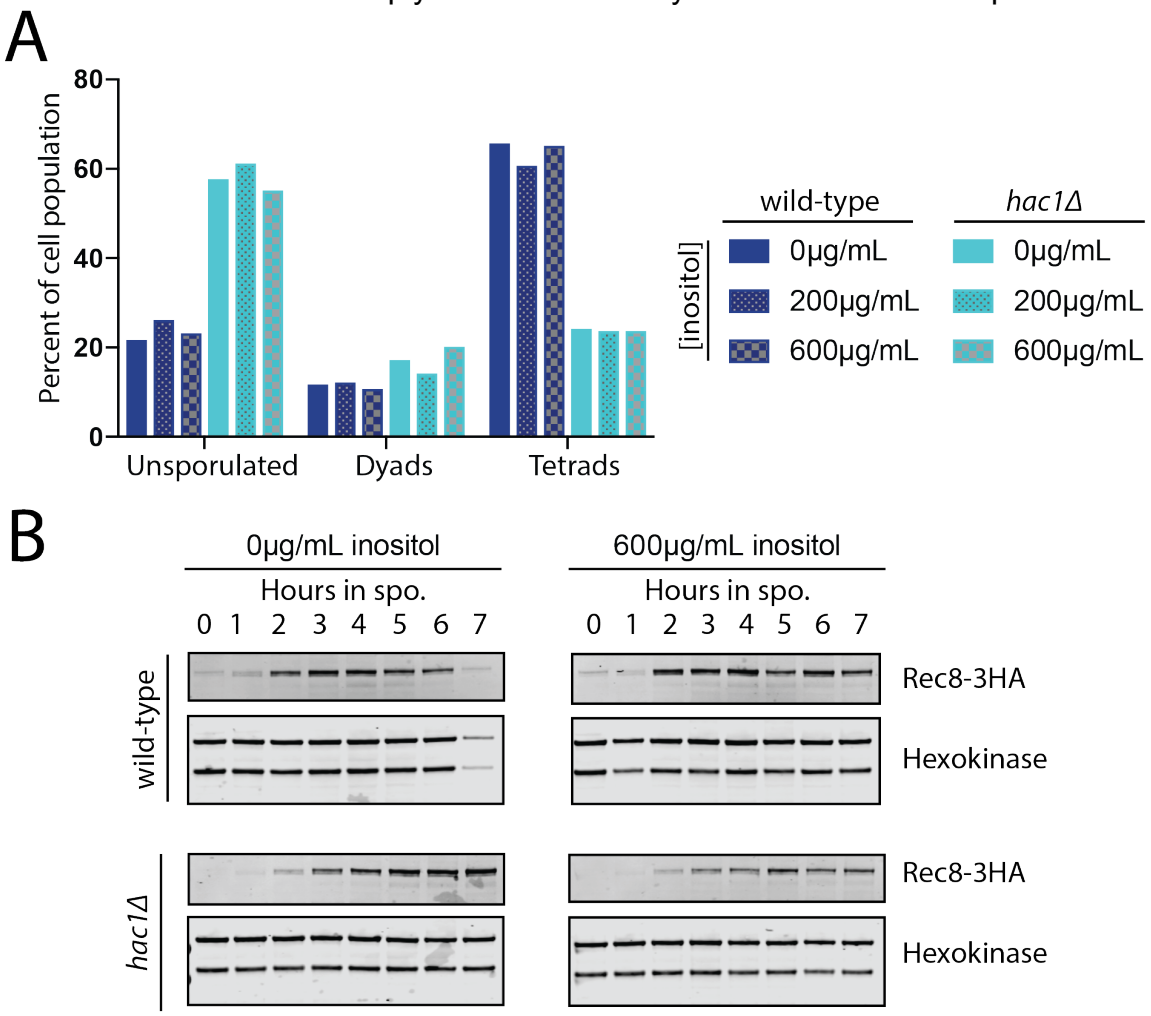

Figure 3.3. Inositol addition fails to rescue the phenotype of UPR^{ER} mutant cells.

A) Sporulation efficiency of wild-type cells (BrÜn 1362) compared to *hac1Δ* cells (BrÜn 4431), with and without 0-600µg/mL inositol supplementing the sporulation media.

B) Rec8 immunoblots (anti-HA) reveal the entry-related defect of *hac1Δ* cells (BrÜn 4431) is not suppressed by even the highest concentration of inositol.

3.2.4 Conditional *HAC1* mutants display phenotypes correlated with *HAC1* expression levels prior to meiosis

We wondered if part of the entry-related defect could be due to the decreased fitness of UPR^{ER} mutant cells prior to meiotic induction. To promote robust, semi-synchronous sporulation in yeast, cells are grown to saturation first in rich medium (YEPD), and then again in a pre-sporulation medium lacking dextrose (BYTA). Both of these nutrient-deprived saturation conditions could result in induction of stress responses, potentially making UPR^{ER} mutant cells less fit prior to entry. In an attempt to mitigate this possible effect, we constructed meiotic null alleles of *HAC1* and *IRE1*, using a common strategy for decreasing meiotic gene expression by replacing the endogenous promoters with that of *CLB2*, a mitosis-specific B-type cyclin (Lee and Amon, 2003). We reasoned that these strains would have the added benefit of allowing us to determine if there is an additional, later defect of UPR^{ER} mutants as these strains should presumably have *HAC1*/*IRE1* expression through meiotic entry. In the case of *pCLB2-IRE1*, the new promoter was integrated into the endogenous *IRE1* locus directly upstream of the *IRE1* coding region. Because of the complicated *HAC1* transcript architecture, an alternate strategy was required. To retain the portion of the 5' UTR important for the translational repression of *HAC1*, we integrated *pCLB2* 38 bp upstream of the *HAC1* coding sequence (Figure 3.4A). Transcripts produced from this allele should therefore contain the sequences necessary for the base-pairing interaction between the intron and the new *CLB2-HAC1* hybrid 5' UTR. We found that *pCLB2*-driven expression of *HAC1* showed a similar defect in comparison to *hac1Δ* cells, but *pCLB2*-driven expression of *IRE1* resulted in wild-type levels of sporulation (Figure 3.4B). We reasoned that the difference in phenotype between *pCLB2-IRE1* and *pCLB2-HAC1* cells could be due to the fact that Ire1 is a stable protein embedded in the ER membrane, likely necessitating more than transcriptional shutoff for its full depletion, while Hac1 protein is thought to be relatively short-lived (Gao et al., 2008; Kawahara et al., 1997).

To determine the degree to which the *HAC1* transcript was repressed in meiosis when regulated by the *CLB2* promoter, we performed a northern blot comparing *HAC1* levels in *pCLB2-HAC1* cells to that in wild-type cells (Figure 3.4C). While the *HAC1* message was virtually undetectable in meiotic cells, it was also strongly repressed in BYTA, the pre-sporulation medium. We concluded that the *CLB2* promoter efficiently repressed *HAC1* expression, but that it did so earlier than desirable.

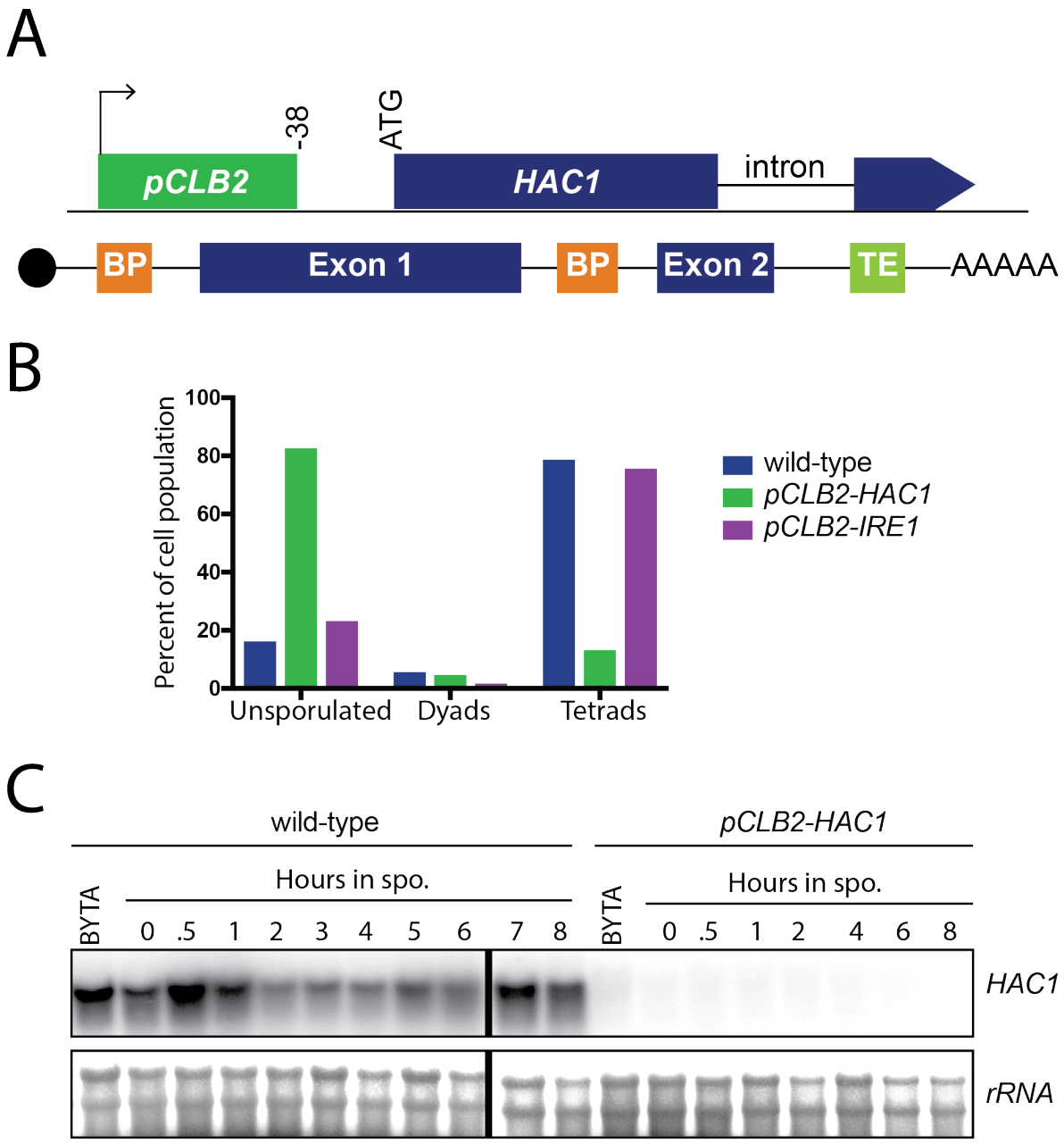

Figure 3.4. Replacing the endogenous *HAC1* promoter with that of *CLB2* results in decreased sporulation efficiency.

A) Schematic of the *pCLB2-HAC1* allele and resulting transcript architecture. Note that the regions required for the base-pairing (BP) interaction that represses *HAC1* translation are retained in this construct, as is the 3' targeting element (TE) required for localization of the *HAC1* transcript.

B) *pCLB2-HAC1* (BrÜn 3939) shows a sporulation defect, while *pCLB2-IRE1 (*BrÜn 3865) behaves like wild-type (BrÜn 1362), as judged by 24 hr sporulation efficiency. 200 cells per strain were counted.

C) *HAC1* expression is strongly repressed in the *pCLB2-HAC1* strain (BrÜn 3939) compared to wild-type (BrÜn 1362), even in pre-meiotic conditions. Note that for this particular northern blot, gel running conditions were insufficient to separate spliced and unspliced *HAC1*. Dark bar represents where the gel image has been spliced, as the gel was loaded in two rows.

Because the level of *HAC1* transcript was so much lower in the pre-meiotic condition when regulated by *pCLB2*, we were concerned that *pCLB2-HAC1* cells may be effective *hac1Δ* cells, thus unable to mitigate the effects of *hac1Δ* prior to and during entry. We therefore sought a promoter that would be repressed closer to the time of the second, strong wave of *HAC1* translation instead of throughout meiosis. Using mRNA-seq and ribosome profiling data available in (Brar et al., 2012), we searched the genome looking for patterns of mRNA expression that were anti-correlated with the timing of *HAC1* translation. Two candidates emerged: *ATC1* and *URA1* (Figure 3.5A). *URA1* encodes an enzyme involved in the synthesis of pyrimidines (Lacroute, 1968), and *ATC1* encodes a nuclear protein of unknown function (Munson et al., 2004). We cloned regions that should contain the promoters of these genes while avoiding nearby genes (taking 1000 bp upstream of the *URA1* coding sequence and 365 bp upstream of the *ATC1* coding sequence) into vectors that could be used to generate cassettes for one-step genomic integration. Cassettes derived from these vectors were integrated ahead of *HAC1* as for *pCLB2*.

We found that *pATC1-HAC1* exhibited a sporulation defect similar to that of *pCLB2-HAC1*, while *pURA1-HAC1* sporulated at levels closer to that of wild-type cells (Figure 3.5B). We wondered if varying amounts of persistent *HAC1* transcript could explain this difference. To determine whether or not this was the case, we first quantified meiotic expression of *ATC1* and *URA1*, comparing the levels of these transcripts to those of *HAC1* and *CLB2* using mRNA-seq data available in (Brar et al., 2012). We found that *URA1* was expressed more similarly to *HAC1* in vegetative growth conditions, pre-meiotic conditions (BYTA), and early in meiosis (0.5 hr post-transfer to sporulation medium), while *CLB2* and *ATC1* levels were consistently lower (Figure 3.5C). To test whether these promoters drove similar expression patterns of *HAC1*, we performed RT-qPCR using RNA isolated from meiotic cells at various time points. We found that the strain containing *pURA1-HAC1* showed higher levels of *HAC1* transcript than did *pCLB2-HAC1* or *pATC1-HAC1* in vegetative growth conditions, pre-meiotic medium (BYTA), and as late as 2 hr into meiosis, suggesting that these cells retained more *HAC1* (Figure 3.5D). The fact that the sporulation efficiency of *pURA1-HAC1* cells was very similar to that of wild-type cells suggested that the major defect of *hac1Δ* cells was primarily due to effects prior to and/or during meiotic entry.

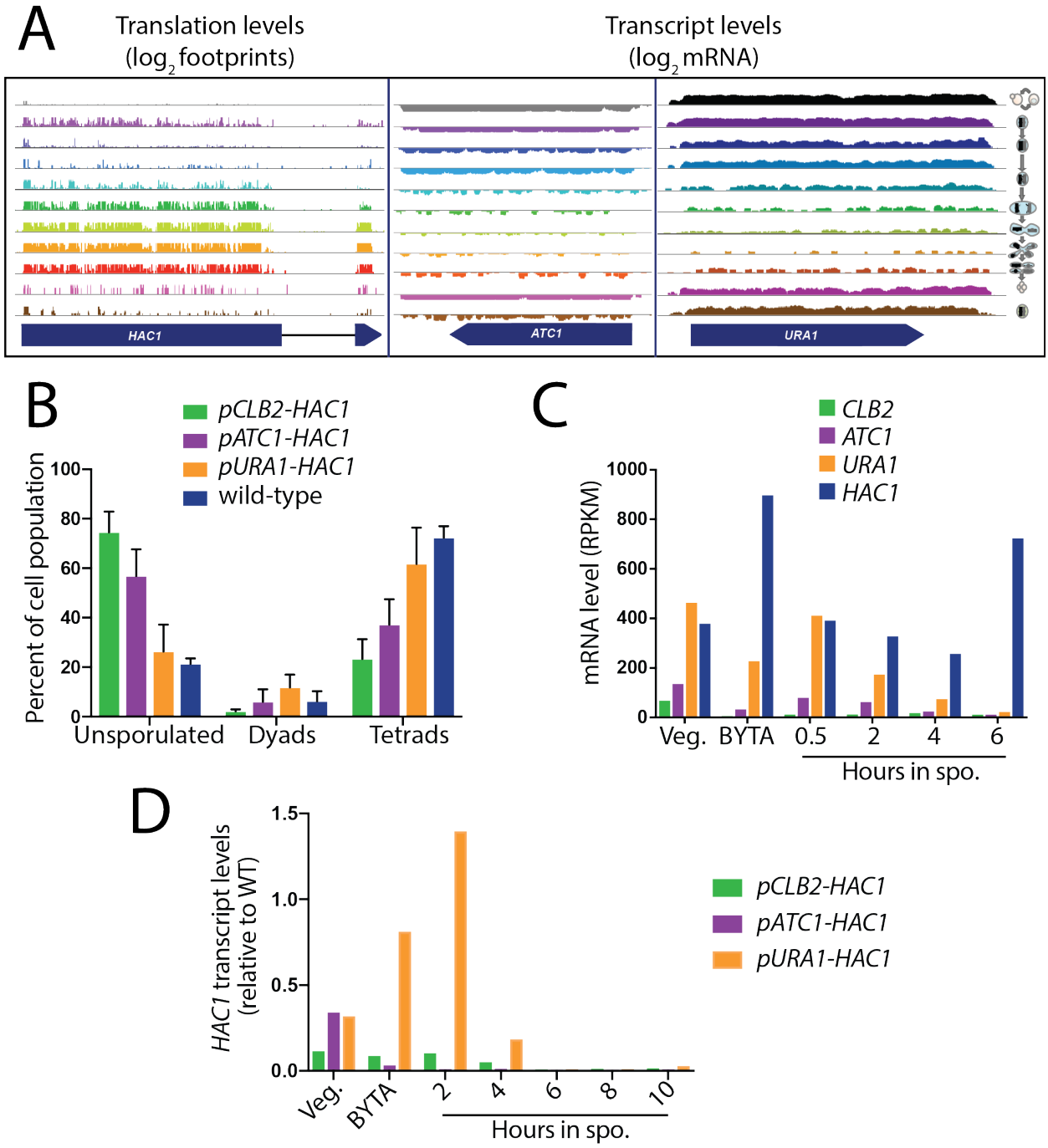

Figure 3.5. Promoter shutoff strategies reveal a requirement for *HAC1* prior to/during meiotic entry.

A) Genome browser tracks showing that *ATC1* and *URA1* mRNA levels (middle and right, respectively) are anti-correlated with *HAC1* translation levels (left). mRNA-seq and ribosome profiling data from (Brar et al., 2012) were used for this analysis.

B) 24 hr sporulation efficiencies of the various promoter shutoff constructs (*pCLB2-HAC1,* BrÜn 5179/5180; *pATC1-HAC1*, BrÜn 5603; *pURA1-HAC1*, BrÜn 5431) compared to that of wild-type cells (BrÜn 15). Average sporulation efficiencies of 3 biological replicates are shown, with error bars representing SD. 200 cells per strain were counted for each replicate.

C) Quantification of *CLB2*, *ATC1*, *URA1*, and *HAC1* mRNA levels (RPKM), obtained in the sequencing experiment described in (Brar et al., 2012).

D) Expression of *HAC1*, as judged by RT-qPCR, in the promoter shutoff constructs (*pCLB2-HAC1,* BrÜn 5179/5180; *pATC1-HAC1*, BrÜn 5603; *pURA1-HAC1*, BrÜn 5431). Note that transcript levels were normalized to matched wild-type samples (BrÜn 15).

3.2.5 The second wave of UPR^{ER} induction depends on expression of *NDT80* and may be related to ER dynamics in meiosis

Although the stronger UPR^{ER} induction that occurs midway through meiosis appeared potentially dispensable for sporulation efficiency, several interesting questions remained about this induction in a physiologically unperturbed context – including how the UPR^{ER} gets activated and what it activates transcriptionally. To begin to determine what might turn on the UPR^{ER} during meiosis, we first determined which key meiotic events are required for meiotic UPR^{ER} induction. We created a panel of meiotic mutants containing *AID-HAC1* and evaluated UPR^{ER} induction by assaying Hac1 protein levels during a meiotic time course (Figure 3.6A). The second wave of Hac1 expression was robust even in cells that failed to package spores (*spo21Δ*, which fail to generate prospore membranes [Bajgier et al., 2001]), ruling out the possibility that meiotic UPR^{ER} induction is dependent on mature spore formation. Additionally, the UPR^{ER} was induced in cells that package spores after a single meiotic division (*spo12Δ* [Klapholz and Esposito, 1980]), suggesting meiotic UPR^{ER} induction is independent of meiosis II-specific gene expression and events. Cells arrested at metaphase I (*pCLB2-CDC20*, a meiotic null of the APC/C activator, Cdc20 [Brito et al., 2010]) also showed robust UPR^{ER} activation, suggesting an event independent of progression past metaphase I is required for UPR^{ER} induction. The only mutant tested that showed a defect in UPR^{ER} activation was that of *NDT80*, an early meiotic transcription factor required for exit from the pachytene stage of late prophase (Xu et al., 1995). We concluded that *NDT80*, a direct or indirect target of Ndt80, and/or exit from pachytene is required for meiotic UPR^{ER} induction.

Because UPR^{ER} induction has been reported to be related to altered ER morphology (Manford et al., 2012; reviewed in [Federovitch et al., 2005]), we decided to investigate ER morphology during meiosis. We observed a meiotic “collapse” of the peripheral ER (Figure 3.6B) during late meiosis, similar to that observed by (Suda et al., 2007). Concurrent work in the lab identified a mutant in which the ER fails to collapse during meiosis, and showed that the second wave of meiotic *HAC1* splicing is absent in this strain (George Otto, unpublished data). This suggests that perhaps altered ER morphology is linked to meiotic UPR^{ER} induction. More work will be required to determine the exact nature of the relationship between ER collapse and UPR^{ER} induction.

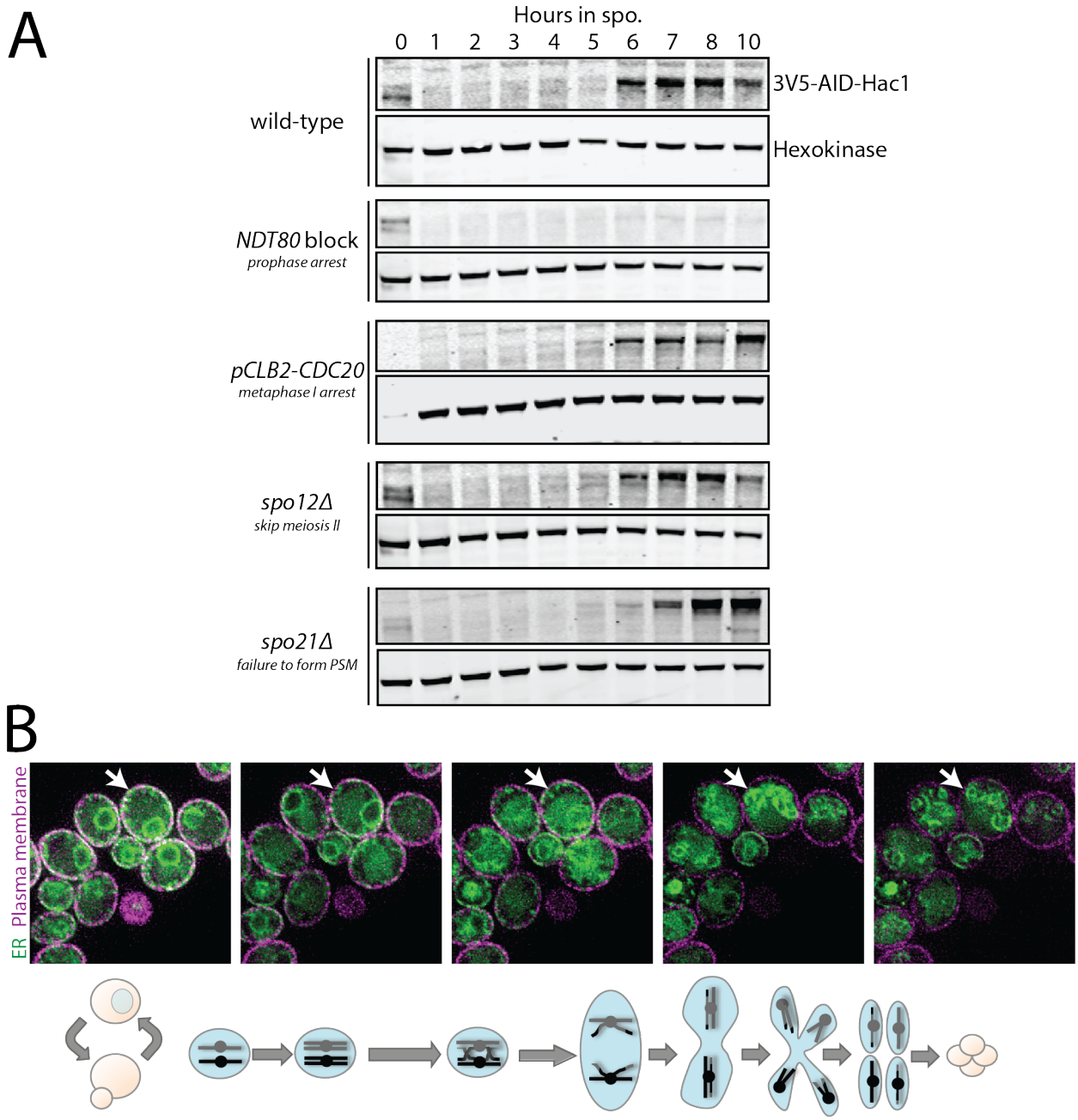

Figure 3.6. Evaluation of meiotic events required for UPR^{ER} induction.

A) Immunoblotting for Hac1 (3V5-AID-Hac1) reveals that the second wave of Hac1 expression is absent in cells in which *NDT80* expression is prevented (BrÜn 13405). Robust UPR^{ER} induction is still seen in mutants that arrest at metaphase I (*pCLB2-CDC20*, BrÜn13401), package spores after meiosis I (*spo12Δ*, BrÜn 13397), and fail to form mature spores (*spo21Δ*, BrÜn 13399). Note that the wild-type (BrÜn 13403) comparison is also shown in Figure 3.1A.

B) Evaluation of ER localization (GFP-HDEL) compared to the plasma membrane (Pil1-mKate) in BrÜn 5616 shows a collapse of cortical ER during the meiotic divisions.

3.2.6 Towards identification of Hac1 transcriptional targets during meiosis

In addition to determining what activates the UPR^{ER} in meiosis, elucidating how expression of Hac1 alters gene expression during meiosis would provide insight into physiologically-relevant UPR^{ER} activation. To begin to determine what the

transcriptional targets of the meiotic UPR^{ER} might be, we first asked whether previously defined drug-induced Hac1 targets (Travers et al., 2000) showed increased transcript levels coincident with either wave of meiotic UPR^{ER} induction. Surprisingly, we observed that two separate subsets of drug-induced Hac1 targets showed increased transcript abundance during the two waves of meiotic *HAC1* translation (Figure 3.7). The fact that the stronger, second wave of *HAC1* translation was correlated with increased levels of some drug-induced targets but not others suggested that Hac1 may have different targets in different contexts. We therefore decided to evaluate Hac1 targets in meiosis, using a similar approach to that of our drug-induced approach described in Chapter 2.

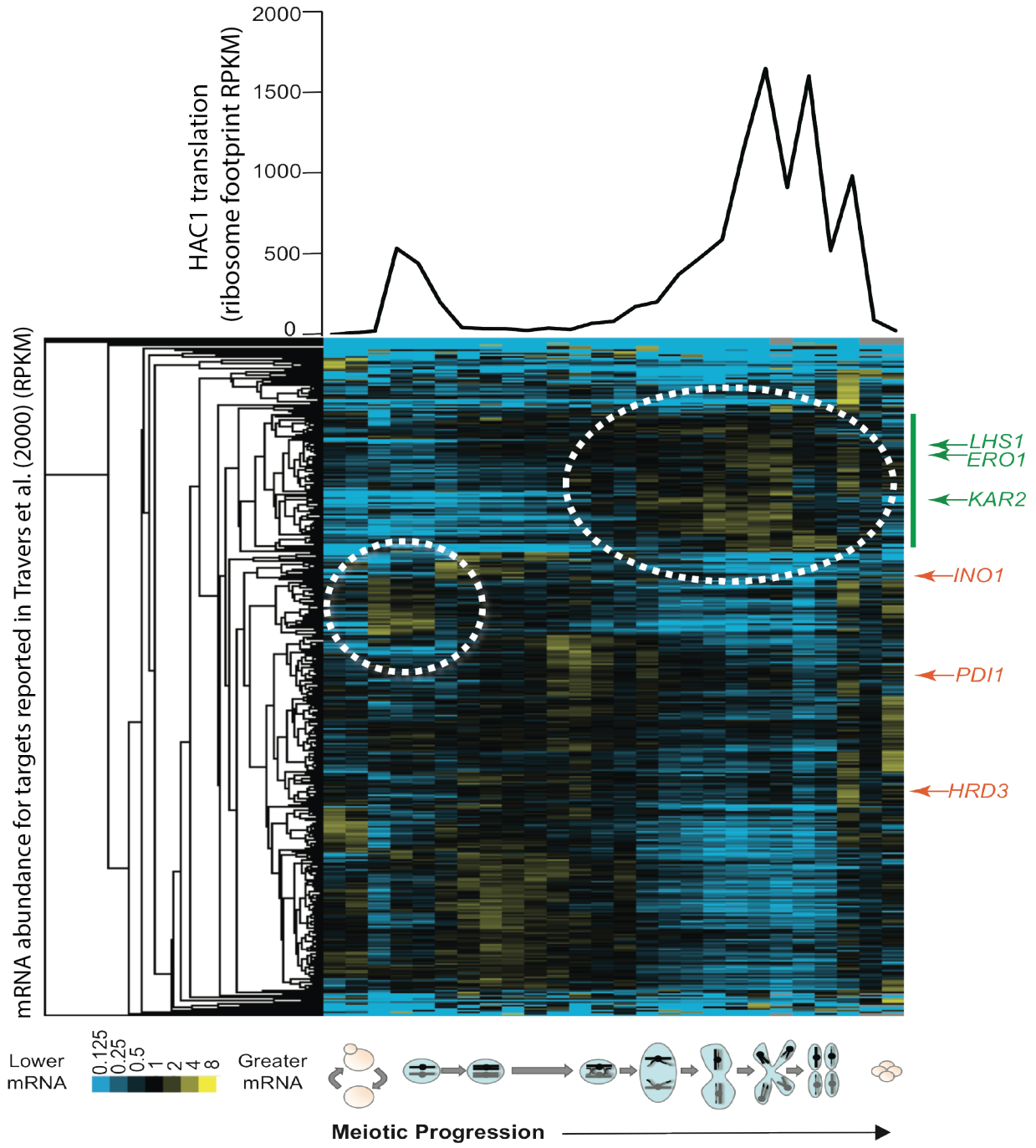

Figure 3.7. Two subsets of reported pharmacological Hac1 targets show increased mRNA expression levels during the two waves of meiotic UPR^{ER} induction.
mRNA expression levels (RPKM) of previously annotated Hac1 targets (rows; [Travers et al., 2000]), shown with the timing of *HAC1* translation indicated above (all data from Brar et al. (2012). White circles indicate groups of previously annotated Hac1 targets that appear to show increased transcript abundance during each wave of meiotic UPR^{ER} activation. The positions of several well-known Hac1 targets are indicated at right.

Our first strategy was to deplete Hac1 upon auxin addition in the *AID-HAC1* background. Because the second wave of *HAC1* translation is stronger than the first (~50% of *HAC1* splicing versus ~10% early in meiosis), we sought to determine Hac1 targets during this wave of induction as the difference in Hac1 content of *AID-HAC1* cells with and without depletion would be larger than it would be if attempting to determine early meiotic targets. We induced meiosis in cells containing the *AID-HAC1* allele, with and without the gene encoding the plant SCF adaptor protein Tir1, under control of a copper inducible promoter (*pCUP1-osTIR1*). Samples were taken at 5 and 6 hr after transfer to sporulation medium, at which point cultures were co-treated with copper and auxin (or DMSO vehicle). Additional samples were then collected at 6.5, 7, and 7.5 hr. We found that the AID-Hac1 protein was efficiently depleted, specifically in the *TIR1* background (Figure 3.8A). Consistent with our earlier findings that the defect of UPR^{ER} mutant strains appears largely related to entry, depleting cells of Hac1 after they had entered meiosis did not affect sporulation efficiency (Figure 3.8B). To determine if there were more subtle effects on meiotic progression that could complicate comparison of gene expression between cultures at the same chronological time point, we analyzed meiotic progression by evaluating spindle morphology (Figure 3.8C). We did not find evidence of altered meiotic progression on this timeline, suggesting that comparing time points between cultures would be reasonable.

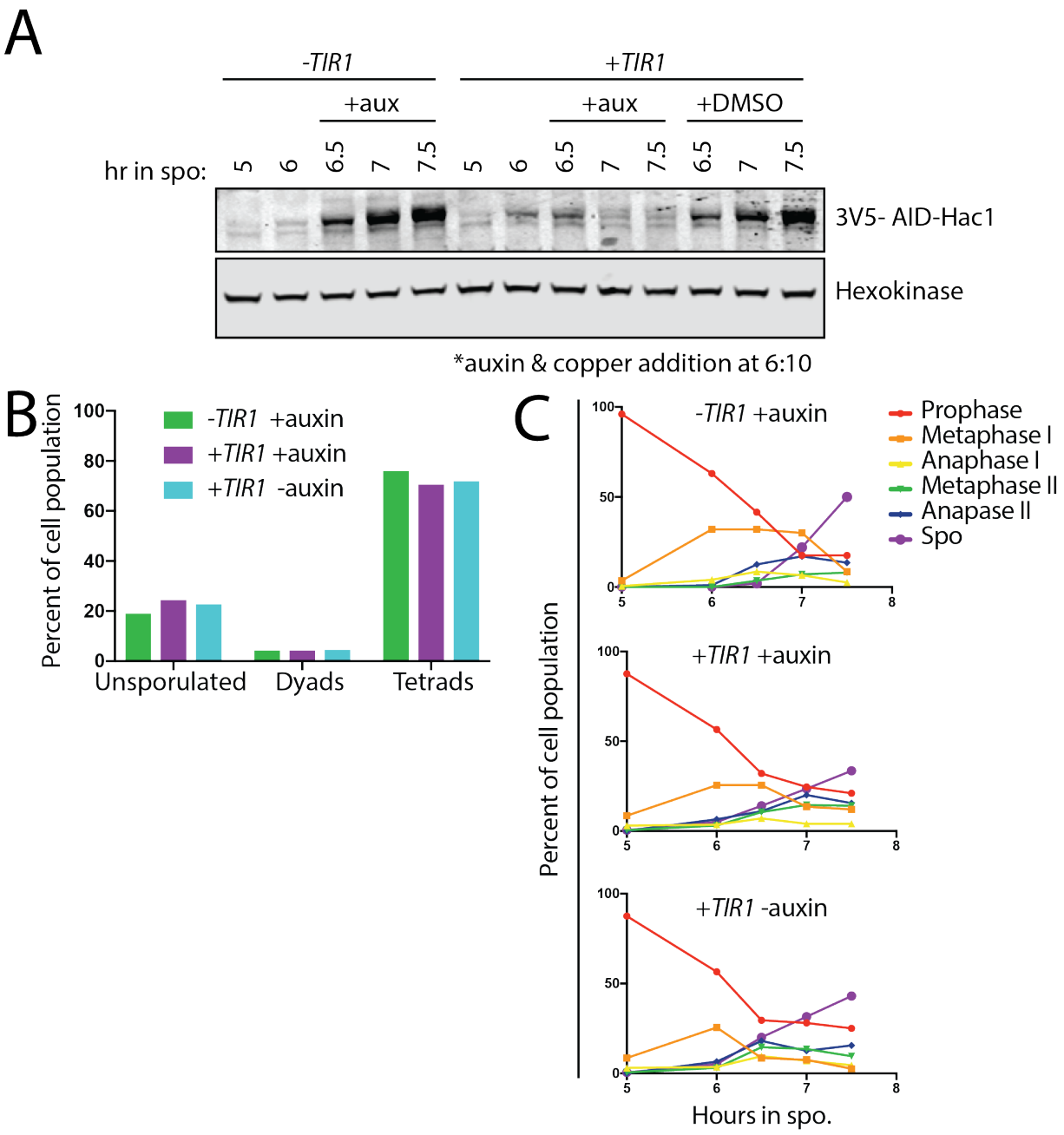

Figure 3.8. AID-Hac1 depletion strategy for meiotic Hac1 target identification.

A) AID-Hac1 is efficiently depleted in meiotic cells, specifically in the *TIR1*-containing background (BrÜn 10744) but not the strain lacking TIR1 (BrÜn 10532). After 6 hr 10 min in sporulation media, 50 μM copper ($CuSO_4$) was added to induce *pCUP1-osTIR1* and 1mM auxin was co-added to degrade AID-Hac1.

B) 24 hr sporulation efficiency of cells with and without AID-Hac1 depletion (as in panel A). 200 cells per condition were counted.

C) Meiotic progression (as judged by spindle morphology) of cells with and without AID-Hac1 depletion (as in panel A). 200 cells were counted per sample.

We additionally sought to determine meiotic targets of Hac1 via an orthologous approach. Instead of depleting Hac1, we decided to inducibly express Hac1 late in meiosis in a meiotic null background. To do this, we employed a bacterial gene expression regulation module relying on the LexA repressor (LexA) and LexA operator (LexO). Previous work (Ottoz et al., 2014) developed a synthetic transcription factor in which the DNA binding domain of the LexA repressor was fused to the bacterial transcriptional activator B112, as well as an estrogen receptor domain. We cloned an intron-less *HAC1* (*sHAC1*, with and without an N-terminal V5 epitope tag) downstream of a previously developed synthetic promoter (Ottoz et al., 2014), containing an array of 8 LexO sites and a minimal *CYC1* promoter (Figure 3.9A). Prior to initiating meiotic studies, we first tested whether or not the addition of β-estradiol resulted in expression of Hac1 protein and induction of canonical Hac1 targets in vegetative cells. Cells were treated with increasing β-estradiol concentrations for 90 min, and protein content was analyzed by immunoblot (Figure 3.9B). Immunoblotting for V5 showed β-estradiol-dependent expression of 3V5-Hac1. Because we were unable to detect untagged Hac1 protein, and because we wondered if downstream targets of Hac1 were induced dependent on β-estradiol, we also performed a Kar2 immunoblot. We observed increases in Kar2 expression using both alleles, but the induction seemed slightly more robust with the untagged Hac1 protein, so we decided to use this allele for our meiotic studies.

The synthetic *pGPD1-LEXA* and *pCYC1-8LEXO-sHAC1* alleles were crossed into a *hac1* meiotic null background. In this background, endogenous *HAC1* was depleted by use of the *pCLB2-HAC1* allele, which we optimized using modified meiotic media and preparation conditions (see methods) to enter meiosis efficiently (Figure 3.9, compared to Figure 3.4). Cells were induced to undergo meiosis, and β-estradiol was added 5 hr 40 min after transfer to sporulation medium. We tested a range of β-estradiol concentrations and saw robust increases in Kar2 protein levels even with the lowest concentration, 30 nM (Figure 3.9C). This was due to expression of *sHAC1*, because this increase in Kar2 protein was not observed in cells containing *pGPD1-LEXA* alone (Figure 3.9D).

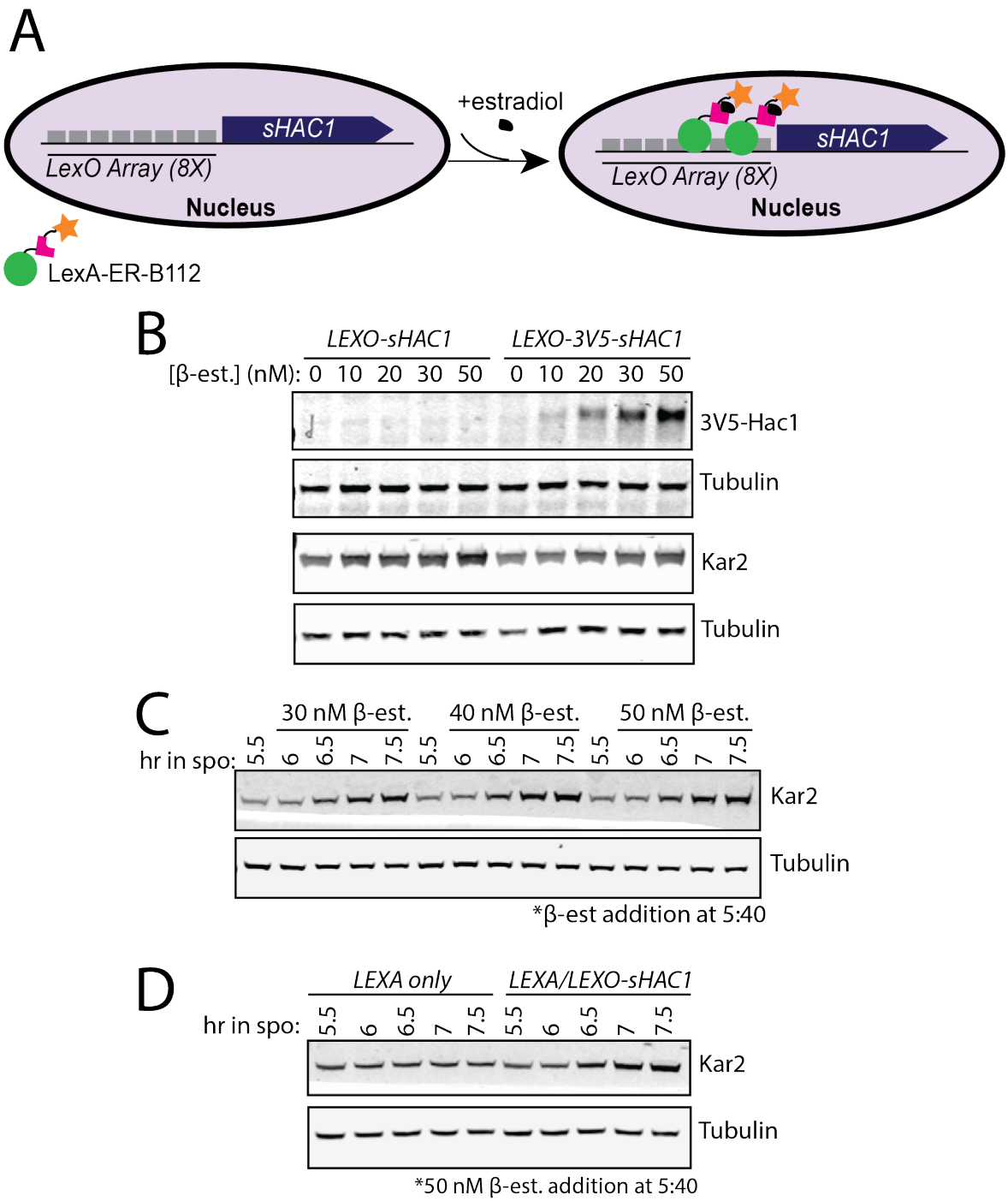

Figure 3.9. LexA/LexO mediated inducible expression of spliced *HAC1* (*sHAC1*).

A) Schematic of LexA/LexO mediated expression of *sHAC1*. In the absence of β-estradiol, the synthetic LexA activator (LexA binding domain fused to an estrogen receptor domain and the B112 transcriptional activator) remains in the cytoplasm. Upon β-estradiol addition, the synthetic LexA transcription factor enters the nucleus where it recognizes an array of LexO sequences driving expression of an intronless *HAC1* (*sHAC1*) from the *CYC1* minimal promoter.

B) Immunoblot (anti-3V5, top; anti-Kar2, bottom) showing that upon 90 min addition of increasing concentrations of β-estradiol, 3V5-Hac1 (specifically in BrÜn 15740) and known Hac1 targets (as judged by Kar2) are expressed (in both BrÜn 15739 and 15740).

C) Addition of β-estradiol after 5 hr 40 min in sporulation media causes an increase in Kar2 protein levels during meiosis, as judged by immunoblot (anti-Kar2). Samples were collected from a meiotic time course of BrÜn 16987.

D) The β-estradiol-dependent increase in Kar2 during meiosis is restricted to cells containing the LexO construct (BrÜn 16987) and is not observed in cells carrying only the LexA construct (BrÜn 16989).

For global analysis of gene expression changes in this background to complement our *AID-HAC1* depletion studies, we transferred cells to sporulation medium and added 30nM β-estradiol immediately after collection of samples at 5.5hr post-meiotic induction. Additional samples were collected through 7hr. We again observed an increase in Kar2 protein following β-estradiol addition, dependent on the *pCYC1-8LEXO-sHAC1* allele (Figure 3.10A). We confirmed that expression of *sHAC1* did not appear to impact meiotic success, as judged by sporulation efficiency (Figure 3.10B, note that we observed a β-estradiol-dependent decrease in sporulation efficiency in both strains, likely due to nonspecific effects of nuclear LexA). Expression of *sHAC1* also did not result in any additional meiotic defects that we observed, again suggesting that comparisons between cultures would not be muddled by differences in the speed of meiotic progression (Figure 3.10C). Samples were collected for parallel analysis of mRNA, translation, and protein levels.

Libraries were prepared to analyze mRNA expression levels by mRNA-seq and prepared as in Chapter 2 for samples collected from the two complementary target identification approaches. We are currently analyzing the data obtained from sequencing the *AID-HAC1* libraries. Future work in the lab will integrate both datasets to identify transcriptional targets of Hac1 during meiosis.

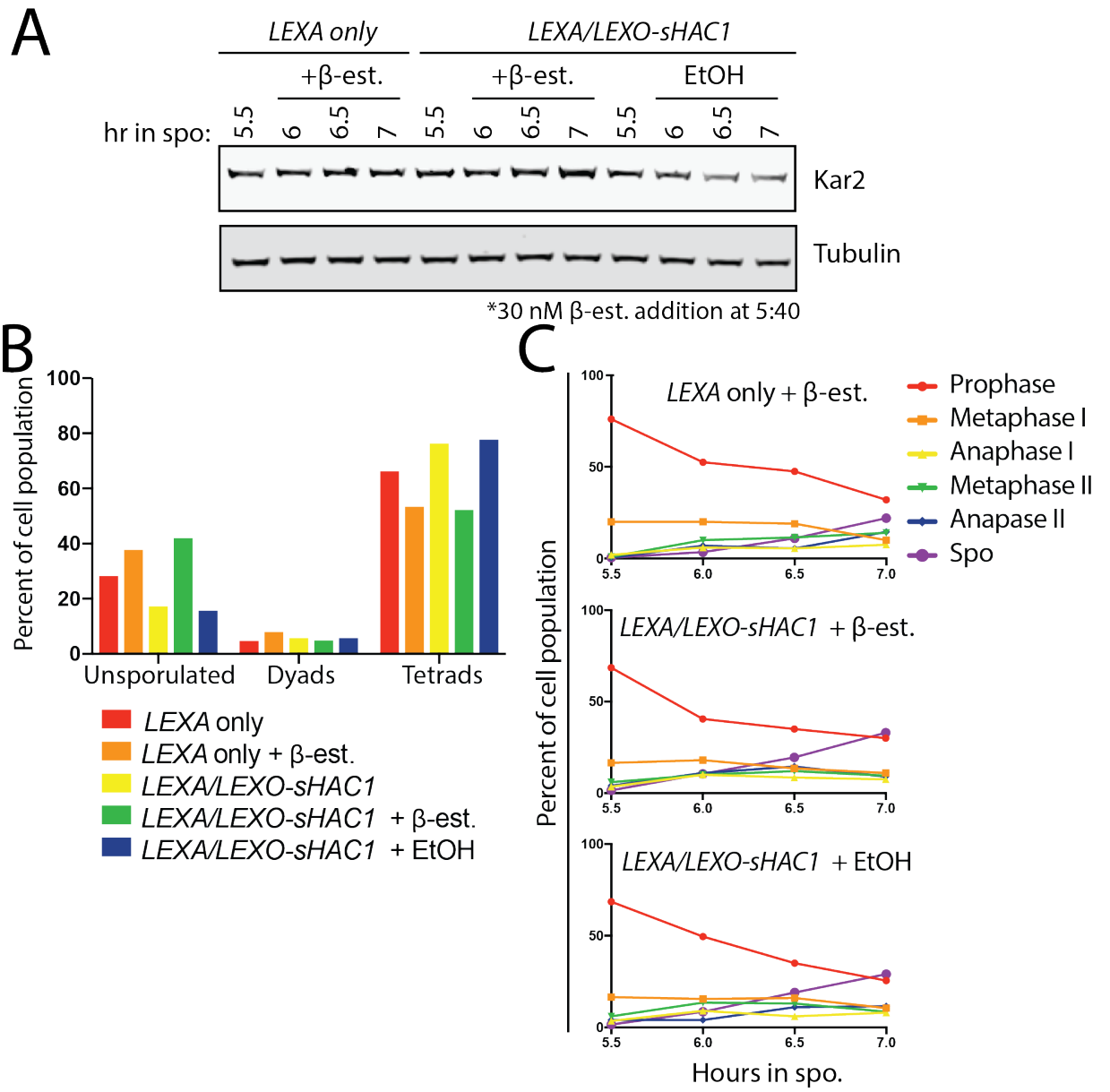

Figure 3.10. The inducible Hac1 expression strategy for meiotic Hac1 target identification.

A) Addition of 30 nM β-estradiol to meiotic cultures results in increased Kar2 protein levels, as judged by immunoblot, in the extract collected for global gene expression analysis. This increase is observed in cells carrying both the LexA and LexO constructs (BrÜn 16987) and is absent in control cells containing only the LexA construct (BrÜn 16989).

B) Inducing *sHAC1* expression with β-estradiol addition (as in panel A) does not alter 24 hr sporulation efficiency (beyond the defect associated with β-estradiol addition alone). 200 cells were counted per condition.

C) Meiotic progression (as judged by spindle morphology) of cells with and without β-estradiol-dependent induction of *sHAC1* (as in panel A).

3.3 Discussion

The UPR^{ER} is a cellular stress response pathway known to be important in a wide variety of contexts, from B-cell differentiation to cancer cell biology (reviewed in [Walter and Ron, 2011]). The functional relevance of UPR^{ER} activation to development and disease is well-recognized in metazoans, but much of the mechanistic detail of the signaling involved in this pathway was first elucidated in budding yeast. Despite this fact, and its high degree of conservation, the importance of the URR^{ER} in normal yeast physiology remains largely unclear. In this study, we further characterized a previously reported physiological context in which UPR^{ER} activation occurs without external perturbation – the meiotic program in yeast (Brar et al., 2012).

We showed that *HAC1* splicing during meiosis results in two waves of stable Hac1 protein expression. The nuclear localization pattern of Hac1 in meiosis is similar to that during drug induction of the UPR^{ER}, and analysis of wild-type mRNA-seq through meiosis suggests that the best-studied UPR^{ER} targets, including BiP (*KAR2* in yeast) are also activated in meiosis (Figure 3.7). We found that an intact UPR^{ER} is required for meiotic success, with UPR^{ER} mutants showing entry-related defects that ultimately manifest in reduced sporulation efficiency. The observation that providing more *HAC1* prior to and during entry (by using promoter shutoff constructs and auxin depletion strategies) could suppress this defect was quite surprising, given that the higher degree of sustained UPR^{ER} activation occurs much later in meiosis.

It remains to be determined why having Hac1 very early in meiosis is so important despite the lower level and shorter period of UPR^{ER} induction at that time compared to later in meiosis, and is an area that warrants future investigation. One possibility is that the early induction of the UPR^{ER} occurs in response to nutritional deprivation. Therefore, having an intact UPR^{ER} at this time helps overcome this initial stress, allowing cells to efficiently enter the differentiation program. This possibility is supported by the fact that *MAT**a**/MAT**a*** cells unable to enter meiosis also turn on the UPR^{ER} under the conditions required to induce sporulation in normal *MAT**a**/MAT**α*** diploids (as judged by *HAC1* translation), suggesting the initial wave of UPR^{ER} induction may not be meiosis-specific (Brar et al., 2012). It will thus be important to determine if altering entry conditions might suppress the defects of *hac1Δ* and *ire1Δ* cells. We noted that addition of inositol was not sufficient to achieve this suppression, but perhaps using genetic techniques to allow for induction of meiosis in rich media (Weidberg et al., 2016) might.

While our data suggest that the UPR^{ER} is important for robust entry, at least in the laboratory conditions used to induce meiosis, meiotic UPR^{ER} induction provides an interesting, physiological context in which to study two outstanding questions in the yeast UPR^{ER} field: namely, how does this pathway get activated and what transcriptional targets does it, in turn, activate? In the case of the former, there are several potential stimuli for induction. The first wave could be due to the starvation conditions used to induce meiosis, as altered nutrient sources have been reported to result in UPR^{ER} induction (Kuhn et al., 2001), though even in this case the specific activating signal remains elusive. The second wave of UPR^{ER} activation is unlikely to be

due to this effect, as the media conditions do not change between the first and second waves of UPR^{ER} induction. One possibility is that immediately prior to the later wave of meiotic UPR^{ER} activation, one or more proteins are synthesized that require additional ER folding machinery, leading to the accumulation of misfolded species that lumenally activate Ire1 in a manner similar to that reported for model misfolded peptides (Gardner et al., 2011). This would be, to our knowledge, the first case of an endogenous misfolded protein activating Ire1. Another possibility is that the UPR^{ER} is activated by an unknown mechanism in anticipation of the demand for new membrane production during sporulation, similar in principle to the proposed anticipatory induction in immune cells (van Anken et al., 2003; Hu et al., 2009). It is worth noting, however, that our results show that spore formation is not required for activation. This of course does not rule out an anticipatory mechanism, but is an intriguing observation. A third potential cause of meiotic UPR^{ER} induction is that a physical change to the ER membrane causes Ire1 activation. It has been reported that altering ER membrane composition causes UPR^{ER} activation independent of Ire1's lumenal domain through a currently poorly understood mechanism (Promlek et al., 2011). Additionally, previous work has shown that when cortical ER is synthetically "collapsed" (by deleting genes encoding proteins responsible for tethering the ER to the plasma membrane) the UPR^{ER} is constitutively active, suggesting such a collapse in meiosis could be related to UPR^{ER} induction (Manford et al., 2012). Also in support of this model are the results of parallel work in the lab, showing that preventing ER collapse genetically (by deleting genes encoding reticulon proteins important for ER structure) additionally prevents the second wave of UPR^{ER} induction, despite continued meiotic progression (George Otto, unpublished data).

The second outstanding question made accessible by meiotic UPR^{ER} induction is that of what Hac1 turns on in a more physiologically relevant context than DTT or tunicamycin treatment. We show evidence that it is unlikely that all drug-induced targets are induced during the meiotic UPR^{ER}. The idea that Hac1 may have different targets in different contexts is an interesting one. While analyses of the global expression data that we collected will be required to determine if this is the case, further experimentation will be needed to understand how this might be achieved. It is worth noting that during the course of constructing the *AID-HAC1* strain (first presented in Chapter 2), we obtained strains with varying copy numbers of this allele. Work by others in the lab showed that upon pharmacological activation of the pathway, the same genes were transcriptionally induced when there was a single copy of the allele as when there were multiple copies. This suggests that the different levels of Hac1 protein in meiosis as compared to drug-activated cells are unlikely to be sufficient to reprogram its transcriptional targets. We did, however, note that the major Hac1 species in meiosis appeared to migrate differently between the two waves of induction (Figure 3.1A), raising the possibility that the Hac1 protein is post-translationally modified in meiosis. Hac1 has been reported to be post-translationally modified, though thus far only in the context of its degradation (Pal et al., 2007). Perhaps there is an unrecognized role for other post-translational modifications that could alter DNA binding preferences or result in new protein-protein interactions that could reprogram Hac1 to regulate different targets in meiosis. Alternatively, differences in chromatin structure or expression of meiosis-specific DNA

binding partners may explain the shift in Hac1 target specificity during meiosis that we propose.

It will be interesting to determine if Hac1 has any LUTI-based targets in meiosis, or if the phenomenon of induction of long, repressive transcript isoforms is specific to the drug-induced UPR^{ER}, as described in Chapter 2. Over 380 LUTI transcripts are expressed in meiosis, some of which are expressed during the second wave of meiotic UPR^{ER} induction (Cheng et al., 2018; Brar et al., 2012). Whether or not Hac1 coordinates up- and downregulation of distinct gene sets in a more physiological context like meiosis remains an open question.

Our results elucidate a previously unrecognized role for the UPR^{ER} in budding yeast meiosis. We further characterized a context in which the UPR^{ER} is induced without external perturbation, allowing for future studies to evaluate the activation mode of and gene expression program related to physiological UPR^{ER} activation. Perhaps most importantly, we generated valuable datasets that, when combined with computational approaches, can be used to answer the longstanding question of what gene expression changes are associated with physiological induction of the UPR^{ER}.

3.4 Materials and methods

Strain	Relevant genotype	Source
BrÜn 15	*MATa/α, wild-type*	Brar-Ünal Lab
BrÜn 1362	*MATa/α, rec8::REC8-HA::URA3/REC8*	Brar-Ünal Lab
BrÜn 3865	*MATa/α, ire1::pCLB2-IRE1::kanMX/ ire1::pCLB2-IRE1::kanMX*	This study
BrÜn 3939	*MATa/α, hac1::pCLB2-HAC1::kanMX/ hac1::pCLB2-HAC1::kanMX*	This study
BrÜn 4431	*MATa/α, hac1::kanMX/hac1::natMX; rec8::REC8-3HA::URA3/REC8*	Chapter 2
BrÜn 5179	*MATa/α, hac1::pCLB2-HAC1::kanMX/ hac1::pCLB2-HAC1::kanMX*	This study
BrÜn 5180	*MATa/α, hac1::pCLB2-HAC1::kanMX/ hac1::pCLB2-HAC1::kanMX*	This study
BrÜn 5431	*MATa/α, hac1::pURA1-HAC1::kanMX/ hac1::pURA1-HAC1::kanMX*	This study
BrÜn 5603	*MATa/α, hac1::pATC1-HAC1::kanMX/ hac1::pATC1-HAC1::kanMX*	This study
BrÜn 5616	*MATa/α, trp1::GFP-HDEL::TRP1/trp1, pil1::PIL1-mKATE::URA3/PIL1*	This study
BrÜn 8669	*MATa/α, hac1::natMX/hac1::natMX, leu2::pHAC1-3V5-IAA7-HAC1::LEU2*/ leu2::pHAC1-3V5-IAA7-HAC1::LEU2* (*single integrant)*	This study
BrÜn 10532	*MATa/α, hac1::natMX/ hac1::natMX, leu2::pHAC1-3V5-IAA7-HAC1::LEU2*/ leu2::pHAC1-3V5-IAA7-HAC1::LEU2* (*multiple integrant)*	Chapter 2
BrÜn 10744	*MATa/α, hac1::natMX/;hac1::natMX, his3::pCUP1-osTIR1::HIS3/ his3::pCUP1-osTIR1::HIS3, leu2::pHAC1-3V5-IAA7-HAC1::LEU2*/ leu2::pHAC1-3V5-IAA7-HAC1::LEU2* (*multiple integrant)*	Chapter 2
BrÜn 13397	*MATa/α, spo12::kanMX/spo12::kanMX, leu2::pHAC1- 3V5-IAA7-HAC1::LEU2*/ leu2::pHAC1-3V5-IAA7-HAC1::LEU2* (*multiple integrant)*	This study
BrÜn 13399	*MATa/α, spo21::hygMX/spo21::hygMX, leu2::pHAC1- 3V5-IAA7-HAC1::LEU2*/ leu2::pHAC1-3V5-IAA7-HAC1::LEU2* (*multiple integrant)*	This study
BrÜn 13401	*MATa/α, cdc20::pCLB2-CDC20::kanMX/cdc20::pCLB2-CDC20::kanMX, leu2::pHAC1-3V5-IAA7-HAC1::LEU2*/ leu2::pHAC1-3V5-IAA7-HAC1::LEU2* (*multiple integrant)*	This study
BrÜn 13403	*MATa/α, leu2::pHAC1-3V5-IAA7-HAC1::LEU2*/ leu2::pHAC1-3V5-IAA7-HAC1::LEU2* (*multiple integrant)*	This study
BrÜn 13405	*MATa/α, ndt80::pGAL-NDT80::TRP1/ndt80::pGAL-NDT80::TRP1, ura3::pGPD1-GAL4(848).ER::URA3/ ura3::pGPD1-GAL4(848).ER::URA3, leu2::pHAC1- V5-IAA7-HAC1::LEU2*/ leu2::pHAC1-3V5-IAA7-HAC1::LEU2* (*multiple integrant)*	This study
BrÜn 15739	*MATa/α, leu2::8LEXO-splicedHAC1::LEU2/leu2, trp1::pGPD1-LexA-ER-HA-*	This study

	B112::TRP1/trp1	
BrÜn 15740	*MATa/α, leu2:: 8LEXO-3V5-splicedHAC1::LEU2/leu2, trp1::pGPD1-LexA-ER-HA-B112::TRP1/trp1*	This study
BrÜn 15924	*MATa/α, ire1::natMX/ire1::kanMX*	Chapter 2
BrÜn 16987	*MATa/α, leu2:: 8LEXO-splicedHAC1::LEU2/ leu2:: 8LEXO-splicedHAC1::LEU, trp1::pGPD1-LexA-ER-HA-B112::TRP1/ trp1::pGPD1-LexA-ER-HA-B112::TRP1, hac1::pCLB2-HAC1::kanMX/hac1::pCLB2-HAC1::kanMX*	This study
BrÜn 16989	*MATa/α, trp1::pGPD1-LexA-ER-HA-B112::TRP1/ trp1::pGPD1-LexA-ER-HA-B112::TRP1, hac1::pCLB2-HAC1::kanMX/hac1::pCLB2-HAC1::kanMX*	This study

Table 3.1. Yeast strains used in Chapter 3.

Plasmid	Backbone	Description
pAA501	pFA6a	*kanMX6-pCLB2*
pÜB715	pFA6a	*kanMX6-pATC1*
pÜB716	pFA6a	*kanMX6-pURA1*
pÜB926	pNH604	*pGPD1-LEXA-ER-B112 TRP1*
pÜB996	pLC605	*pHAC1-3V5-IAA7-HAC1 LEU2*
pÜB1073	pRS305	*pHAC1-3V5-IAA7-HAC1 LEU2*
pÜB1376	pLC605	*p8LEXO-pCYC1-3V5-splicedHAC1 LEU2*
pÜB1377	pLC605	*p8LEXO-pCYC1-splicedHAC1 LEU2*

Table 3.2. Plasmids used in Chapter 3.

Name	Sequence (5'-3')
oÜB1310	cgcgtcggaccaagagacttcatgggagctgcagatgtttaagac
oÜB1311	taatacgactcactataggacgccaattgtcaagatcaattgaattgtcaaagggtagac

Table 3.3. Oligonucleotides used in Chapter 3.

3.4.1 Yeast strain construction

All strains are derivatives of SK1. Gene deletion and promoter swap strains were constructed by one-step gene replacement, as described in (Longtine et al., 1998). For promoter swap constructs, cassettes were integrated into the endogenous *HAC1* locus, replacing -39 to -219 relative to the start of the *HAC1* coding sequence.

3.4.2 Meiotic time courses

Cells were inoculated into YEPD and grown for 24 hr at RT, shaking. Cells were diluted to OD_{600}0.25 in buffered YTA (BYTA) and grown for ~16hr at 30C, shaking. Cells were washed with water and resuspended to OD_{600}1.85 in sporulation medium (0.3% potassium acetate + 0.02% raffinose). Samples were collected at the indicated time points and treated as follows. For meiotic time courses with inositol, inositol (Sigma) was added to the sporulation medium at the indicated concentrations from a 25mg/mL stock.

Tubulin immunofluorescence/DAPI nuclear morphology:
450µl meiotic culture was added to 50µl 37% formaldehyde and fixed overnight at 4C. Spindle and nuclear morphology were scored by immunofluorescence, as described in (Chen et al., 2017). Briefly, cells were washed and spheroplasts were prepared by digestion with zymolyase and glusolase. Spheroplasts were methanol/acetone permeabilized prior to adhering them to poly-L-lysine coated slides. Antibodies used were rat anti-tubulin at 1:200, 4C overnight (MCA78G, BioRad) and pre-adsorbed FITC-conjugated anti-rat at 1:200, room temperature 2+ hr (712-095-153, Jackson ImmunoResearch Laboratories). Wells were coated with DAPI-mount (Vector) prior to imaging. At least 200 cells were counted per condition.

Samples for immunoblotting:
1.8mL meiotic culture was added to 200µl 50% trichloroacetic acid (TCA) and incubated at 4C for at least 10 min. Extracts were prepared for immunoblotting as in Chapter 2.

Sporulation efficiency:
Following 24 hr in sporulation media, cells were examined microscopically and characterized by the number of packaged spores present. At least 200 cells were counted per condition.

3.4.3 Immunoblotting

Immunoblots were performed as in Chapter 2. Antibodies used were mouse anti-HA.11 (1:1,000; Covance), rabbit anti-Zip1 (1:500; Santa Cruz Biotechnology), mouse anti-V5 (1:2,000; Invitrogen), rabbit anti-Kar2 (1:100,000; gift of Mark Rose), mouse anti-PGK (1:10,000; Molecular Probes) rabbit anti-hexokinase (1:10,000; US Biological), and IRDye secondaries (all 1:15,000; LiCOR). All primary incubations were completed overnight at 4C, and all secondary incubations were completed for at least 1 hr at RT.

3.4.4 RT-qPCR

RNA was isolated by the hot acid phenol method. cDNA was prepared as follows: 5µg of total RNA was treated with DNAse I (Ambion) to remove DNA. RNA concentrations were adjusted to 50 ng/µl and 3 µl RNA was added to 9 µl water and 0.5µl 2mg/mL random hexamers (Roche). Samples were incubated at 65C for 5 min, then put on ice. First strand buffer (Invitrogen), DTT (2µl, 0.1M) and dNTPs (1µl,10mM) were added and samples were incubated at room temperature for 2 min. The reverse transcriptase was added (Superscript III; Invitrogen) and the RT reaction was allowed to proceed as follows: 25C, 10 min; 42C, 50 min; 70C, 10 min. The resulting cDNA was diluted 1:50. SYBR green ROX mix (ThermoFisher) mix was added and qPCR was performed using oÜB 1051/1052. It is important to note that at the time of these experiments, there was no reasonable internal standard to use for normalization (based on genome-wide expression analyses from [Brar et al., 2012]). In all cases, resulting C_T values were normalized to a wild-type control instead. Values should therefore be considered rough approximations.

3.4.5 Northern blotting

Northern blots were performed as described in (Cheng et al., 2018). Briefly, 6-10µg of RNA (wild-type, BrÜn 1362; *pCLB2-HAC1*, BrÜn 3939) was run on a 1% MOPS/formaldehyde gel at 90V for 1 hr (note that this did not result in sufficient separation to distinguished spliced and unspliced transcript isoforms). Nucleic acids were transferred to a nitrocellulose membrane (Hybond H+; GE). Following cross-linking and methylene blue staining, the membrane was pre-hybridized for at least 30 min at 68C using UltraHyb Buffer (Invitrogen). Probes were prepared as in Chapter 2, transcribing the hot probe from a template amplified from wild-type yeast genomic DNA using oÜB1310/1311 (see Table 3.3).

3.4.6 AID-Hac1 immunofluorescence

Samples were acquired as follows. For vegetative cells, BrÜn 8669 was treated with 5mM DTT for 1 hr (as in Chapter 2). For meiotic cells, BrÜn 8669 was induced to undergo meiosis (as above) and 450 µl of culture was collected. In both experiments, cells were fixed at room temperature for 30 min in 3.7% formaldehyde. The immunofluorescence protocol was then the same as that for tubulin, except using 1:800 pre-adsorbed mouse anti-V5 (Invitrogen) and 1:800 pre-adsorbed Cy3-conjugated anti-mouse (Jackson ImmunoResearch Laboratories) and performing extra washes between antibody incubations. Cells were imaged with a DeltaVision 100x/1.40 oil-immersion objective (GE Healthcare), and acquired in softWoRx (GE Healthcare).

3.4.7 Flow cytometry

Cells (wild-type, BrÜn 1362; *hac1Δ,* BrÜn4431) were grown in YEPD and harvested at OD_{600}=~0.8. Samples (1mL) were spun at 1,000 RCF at room temperature for 3 min, prior to fixing in 70% ethanol for 1 hr at room temperature. Fixed samples were washed in 50 mM sodium citrate pH7.2 and resuspended in 500 µl 50 mM sodium citrate pH7.2 supplemented with 0.25mg/mL RNase A (Fermentas). and 0.03% Tween. Samples were incubated overnight at 37C prior to addition of 5µl of 20mg/mL proteinase K (Roche). Samples were then incubated at 50C for 1.5 hr. Prior to flow cytometry, samples were sonicated 30 sec and rotated in the dark for 7 min with 500 µl of SYTOX green (Molecular Probes). Flow cytometry was performed on a Guava easyCyte flow cytometer (Millipore). Quantification was performed with FlowJo software (FlowJo, LLC).

3.4.8 Live cell imaging

Meiotic cultures were prepared as above, except using a 1:1 mixture of fresh sporulation medium and conditioned sporulation medium (filtered at the conclusion of a standard meiosis experiment, as we found cells meiosed more efficiently in conditioned medium). BrÜn 5616 (*GFP-HDEL* and *PIL1-MKATE*, marking the ER and plasma membrane, respectively) was used. Prior to imaging, cells were loaded onto CellASIC ONIX Y04D microfluidics plate (CellASIC Corp.). Chambers were supplied with sporulation medium throughout the experiment by a CellASIC ONIX Microfluidic Perfusion System (CellASIC Corp.). Images were taken with a DeltaVision 60x/1.42 oil-immersion objective (GE Healthcare), and acquired in softWoRx (GE Healthcare).

3.4.9 AID-Hac1 depletion

A standard meiosis was set up using BrÜn 10532 and BrÜn 10744. After collection of the 6 hr time point, auxin (Sigma) was added at a final concentration of 1mM and copper ($CuSO_4$) was added at a final concentration of 50µM. Samples were collected at the indicated time points for tubulin IF and TCA extract as above. 250mL samples were then collected as for the global gene expression experiments in Chapter 2, allowing for mRNA-seq, ribosome profiling, and mass spectrometry analysis.

3.4.10 LexA/LexO inducible *sHAC1* expression

For the vegetative pilot experiments, BrÜn 15739 and BrÜn 15740 were grown overnight in YEPD at 30C, with shaking. Cultures were diluted to OD_{600}=0.05 in fresh YEPD. Following ~2 doublings, cells were treated with β-estradiol (ranging in final concentration from 0-50nM, or ethanol control). After 90 min, samples were harvested and TCA extracts were prepared.

For the meiotic pilot experiments, meiotic cultures were prepared using BrÜn 16987 and BrÜn 16989, with the following modifications. All media was prepared with bottled water (Arrowhead) and sterile filtered into non-autoclaved sterile plastic containers. YEPD and BYTA cultures were grown in non-autoclaved, sterile plastic Erlenmeyer flasks. Spo cultures were set up in non-autoclaved fernbach flasks. Samples for TCA extract were collected at the indicated time points, with β-estradiol (ranging in final concentration from 30-50nM, or ethanol control) addition at 5 hr 40 min post-inoculation into sporulation medium.

For the large-scale collection enabling global analysis of gene expression, collection was the same as for the pilot meiosis experiment with the following modifications. At each time point, samples were collected for tubulin IF and TCA extract. 250mL samples were then collected as for the global gene expression experiments in Chapter 2, allowing for mRNA-seq, ribosome profiling, and mass spectrometry analysis.

3.4.11 mRNA-sequencing

Samples were prepared for mRNA-sequencing as in Chapter 2. Sequencing was done at the UC-Berkeley Vincent J. Coates QB3 Sequencing Facility. Libraries were sequenced on an Illumina HiSeq 2500, 50 single read, with multiplexing.

Chapter 4: Summary and future directions

4.1 Summary of key findings of this dissertation

In my dissertation work, I showed that the previous understanding of transcriptional targets during the UPR^{ER} in budding yeast was incomplete. In addition to the well-characterized positive transcriptional targets of Hac1 (including chaperones and ERAD components [Travers et al., 2000]), Hac1 also has a set of negative targets (Chapter 2). Negative regulation is achieved in part through expression of Hac1-driven long undecoded transcript isoforms (LUTIs), which allow for coordinated up- and downregulation of distinct protein sets. My work therefore identified an additional mechanism by which gene repression occurs during the conserved UPR^{ER}. Many of Hac1's negative targets appear to be mitochondrial, suggesting a link between UPR^{ER} activation and altered mitochondrial function.

Because the finding that Hac1 has LUTI-based negative targets was made via pharmacological induction of the pathway and therefore could be muddled by off-target effects of the drugs used, I also investigated physiological induction of the UPR^{ER} in budding yeast meiosis, working to characterize this induction more completely (Chapter 3). I found that meiotic entry appears sensitive to *HAC1* levels, but that later stages of meiosis do not seem to show this sensitivity. This was surprising, given that the wave of meiotic UPR^{ER} induction during early meiosis is much less robust than the second, stronger wave of induction. I found that the second wave of induction depends on expression of *NDT80*, a gene encoding an important meiotic transcription factor, but is independent of many other key meiotic events. I developed strategies that can be applied to identify Hac1 targets in meiosis, which will allow for analysis of Hac1 targets under physiological conditions and enable determination of whether or not Hac1 has negative targets under physiological conditions as well.

4.2 Unanswered questions and future directions

4.2.1 What roles might other non-canonical transcriptional targets play in the response to ER stress?

In Chapter 2, I generated several rich datasets, but focused mainly on my finding that Hac1 has a set of LUTI-based negative targets. In addition to these LUTI targets, I also noticed other classes of pharmacological targets, though I did not investigate these further. For example, I found cases where a truncated version of a canonical transcript was expressed, dependent on Hac1. There was evidence of translation of these truncated transcripts, in the same frame as translation of full-length transcripts. If the proteins produced from such truncated transcripts impact the function of full-length protein (for example, by titrating away binding partners, etc.), then perhaps expression of truncated transcripts could serve to negatively regulate the function of an existing, full-length protein pool (similar to [Karimi et al., 2014]). In this sense, expression of truncated transcript isoforms could be another mechanism by which Hac1 could achieve negative regulation via transcriptional induction. Whether protein products resulting from

translation of the observed truncated transcripts have any function, however, remains to be determined. Additionally, more systematic analysis will be required to determine how widespread this phenomenon of transcriptional induction of truncated transcripts is. This will likely rely on using an alternate ribosome profiling protocol in which a translation inhibitor that acts on initiating ribosomes, such as lactidomycin, is used to more easily see internal initiation events (e.g. Lee et al., 2012). In the cases I noticed by eye, only a truncated transcript was present, enabling detection without being masked by a co-expressed canonical transcript. In principle, however, this type truncated transcript could be co-expressed with a canonical transcript, which severely complicates identification of different isoforms. Using a ribosome profiling method designed to specifically detect initiation events and/or an mRNA-seq method designed to capture 5' ends (such as transcript leader sequencing [Arribere and Gilbert, 2013]) will enable a more systematic analysis of this type of regulation.

I also observed some cases where a canonical transcript was induced in response to ER stress, dependent on Hac1, overriding what appeared to be a LUTI transcript that was expressed in the absence of ER stress. If in under unstressed conditions the default state of these genes is tight repression via expression of a LUTI transcript, it will be very interesting to study why expression of the resulting protein must be restricted to times of ER stress.

4.2.2 What activates Ire1 during physiological ER stress?

This is one of the most interesting open questions, as the mechanism of ER stress sensing by Ire1 is a topic of much speculation in the UPR^{ER} field. Meiosis provides an untapped context in which to investigate Ire1's mechanism of stress sensing. It will be informative to employ a mutational analysis of *IRE1* to determine which regions of the protein are required for its activation in meiosis. This could be achieved through an unbiased random mutagenesis screen, perhaps designed to recover *IRE1* mutants that fail to activate a *HAC1* splicing reporter (described in [Pincus et al., 2010]). Alternately, a candidate-based approach could be used, testing previously described mutants for their ability to splice *HAC1* in meiosis. Given the possible connection between ER collapse and the second wave of UPR^{ER} induction, determining whether meiotic *HAC1* splicing depends on Ire1's lumenal domain or its cytoplasmic linker region will give further insight into this relationship. If ER collapse promotes UPR^{ER} activation by causing membrane aberrancy, I would predict that UPR^{ER} activation would be independent of Ire1's lumenal domain, but dependent on its cytoplasmic linker region. If UPR^{ER} induction is altered in cells in which the Ire1-BiP or Ire1-peptide interaction interfaces have been mutated, this will indicate that interactions with misfolded proteins and/or altered BiP binding may be responsible for meiotic UPR^{ER} activation, similar to the "classic" view of Ire1 stress sensing.

If it turns out that the Ire1-peptide interaction interface is required for robust UPR^{ER} activation in meiosis, this would suggest that an endogenous protein in the ER lumen activates the pathway. Development of screens aimed at recovering such a protein could be employed to finally identify a specific, endogenous Ire1 activator.

4.2.3 How is ER stress mitigated between waves of UPR^{ER} activation in meiosis?

Previous reports of meiotic UPR^{ER} induction (Brar et al., 2012), as well as my own work in Chapter 3, show that *HAC1* splicing and protein expression are absent in between the two waves of meiotic UPR^{ER} induction. Because the induction of the pathway is rapidly turned off early in meiosis, but remains on at low levels in meiotically incompetent *MAT**a**/MAT**a*** cells in sporulation medium (Brar et al., 2012), it appears that UPR^{ER} induction itself does not mitigate ER stress such that the pathway returns to the "off" state. Rather, this suggests that there could be meiosis-specific repression of pathway signaling in between waves of activation. Further experimentation is necessary to determine whether this is the case. It will be interesting to determine at what point in the UPR^{ER} signaling pathway this putative negative regulation is achieved. Does Ire1 remains clustered in between waves of activation or does it return to the monomeric state? If it returns to the monomeric state, this would suggest that the pathway is inhibited at the level of Ire1 activation. Alternately, if Ire1 remains clustered, perhaps *HAC1* transcript recruitment to Ire1 clusters is somehow impaired. Evaluating these possibilities by performing immunofluorescence against Ire1 through a meiotic time course to determine its clustering pattern and using single molecule fluorescence in situ hybridization (as in [Chen et al., 2017]) to identify *HAC1* transcript localization will be informative. Understanding how this repression works will be important given previous reports in other strain backgrounds that overexpression of *HAC1* impedes expression of some early meiotic genes (Schröder et al., 2000). It is possible that having an intact UPR^{ER} prior to/during entry is important for meiotic success, but that it is critical to repress the pathway in between waves of UPR^{ER} activation to ensure proper timing of expression of some early genes, for example.

4.2.4 What are the physiological targets of Hac1 during meiosis, and are a set of LUTI targets important during this case of UPR^{ER} induction?

Determining the transcriptional targets of Hac1 during physiological ER stress was a technically challenging aspect of my dissertation work. Ultimately, I developed two strategies that will be useful to this end, namely depletion of AID-Hac1 and overexpression of spliced *HAC1* (Chapter 3). A systematic, computational analysis integrating information from both datasets will be required to confidently identify Hac1 targets during the response to physiological levels of ER stress during meiosis. Determining sites that Hac1 binds to in the genome during meiotic UPR^{ER} induction by chromatin immunoprecipitation (ChIP) will also be informative, though previous attempts to perform Hac1-ChIP have been largely unsuccessful.

All analyses of Hac1-dependent LUTI targets were performed under pharmacological activation of the UPR^{ER} (Chapter 2), leaving whether Hac1 has LUTI targets during the physiological induction observed in meiosis an open question. Preliminary evidence (Helen Vander Wende, unpublished results) suggests that Hac1 may regulate a LUTI transcript of superoxide dismutase (*SOD1*) in meiosis. Interestingly, *SOD1* did not emerge as a LUTI candidate in my work (Chapter 2). Why Hac1 might have one set of

LUTI targets under pharmacological conditions of ER stress and another set during physiological conditions remains to be determined.

4.2.5 Does LUTI-based repression of gene expression play a role in the UPR^{ER} in other eukaryotes?

All of my studies of the UPR^{ER} were performed in the budding yeast *Saccharomyces cerevisiae*. While most aspects of UPR^{ER} signaling via Ire1 are well-conserved from yeast to human, it will be interesting to determine if LUTI-based repression of gene expression also plays a role in the response to ER stress in other eukaryotes. In contrast to budding yeast, metazoans have multiple mechanisms other than LUTI-based regulation by which negative regulation during the UPR^{ER} is achieved. For example, through the PERK pathway (a UPR^{ER} signaling branch not conserved in yeast), widespread translational repression is achieved via phosphorylation of eIF2α (reviewed in [Walter and Ron, 2011]). Additionally, regulated Ire1-dependent decay (RIDD) allows for the selective degradation of some ER-localized mRNAs, resulting in downregulation of the proteins they encode (Hollien and Weissman, 2006). Importantly, many of the LUTI-based negative targets that my work identified encode mitochondrial proteins, which would not be expected to be targets of RIDD, suggesting that there could be a class of targets that RIDD cannot negatively regulate but that a LUTI-based mechanism could. Determining whether there are LUTI-based targets during the UPR^{ER} in metazoans is a formidable task, however, because metazoans have more complex transcript architectures due to ubiquitous splicing. Identification of possible LUTI mRNAs will likely require 5' end mapping, such as through the cap analysis of gene expression (CAGE) method (Kodzius et al., 2006). Importantly, recent work (Hollerer et al., 2018) has identified that LUTI-based regulation occurs in mammals (though not during the UPR^{ER}), suggesting that the mechanism of gene repression is conserved and therefore should be possible in the context of UPR^{ER} signaling in other eukaryotes.

References

Akopian, D., Shen, K., Zhang, X., and Shan, S. (2013). Signal Recognition Particle: An Essential Protein-Targeting Machine. *Annual Review of Biochemistry*, 82(1), 693–721.

Aragón, T., van Anken, E., Pincus, D., Serafimova, I.M., Korennykh, A.V., Rubio, C.A., and Walter, P. (2009). Messenger RNA targeting to endoplasmic reticulum stress signalling sites. *Nature,* 457, 736–740.

Arribere, J. A., and Gilbert, W. V. (2013). Roles for transcript leaders in translation and mRNA decay revealed by transcript leader sequencing. *Genome Research*, 23(6), 977–987.

Bajgier, B. K., Malzone, M., Nickas, M., and Neiman, A. M. (2001). SPO21 Is Required for Meiosis-specific Modification of the Spindle Pole Body in Yeast. *Molecular Biology of the Cell*, 12(6), 1611–1621.

Baxter, B. K., James, P., Evans, T., and Craig, E. A. (1996). SSI1 Encodes a Novel Hsp70 of the Saccharomyces cerevisiae Endoplasmic Reticulum. *Molecular and cellular biology*, 16(11), 6444–6456.

Bertolotti, A., Zhang, Y., Hendershot, L. M., Harding, H. P., and Ron, D. (2000). Dynamic interaction of BiP and ER stress transducers in the unfolded-protein response. *Nature Cell Biology*, 2(6), 326–332.

Bicknell, A. A., Babour, A., Federovitch, C. M., and Niwa, M. (2007). A novel role in cytokinesis reveals a housekeeping function for the unfolded protein response. *The Journal of Cell Biology*, 177(6), 1017–1027.

Bowring, C.E., and Llewellyn, D.H. (2001). Differences in HAC1 mRNA processing and translation between yeast and mammalian cells indicate divergence of the eukaryotic ER stress response. *Biochem. Biophys. Res. Commun.,* 287, 789–800.

Braakman, I., Helenius, J., and Helenius, A. (1992). Manipulating disulfide bond formation and protein folding in the endoplasmic reticulum. *The EMBO Journal*, 11(5), 1717–1722.

Brar, G. A., Yassour, M., Friedman, N., Regev, A., Ingolia, N. T., and Weissman, J. S. (2012). High-resolution view of the yeast meiotic program revealed by ribosome profiling. *Science*, 335(6068), 552–557.

Brito, I. L., Yu, H.-G., and Amon, A. (2010). Condensins promote coorientation of sister chromatids during meiosis I in budding yeast. *Genetics*, 185(1), 55–64.

Brodsky, J. L., and Skach, W. R. (2011). Protein folding and quality control in the endoplasmic reticulum: Recent lessons from yeast and mammalian cell systems. *Current Opinion in Cell Biology*, 23(4), 464–475.

Brunsing, R., Omori, S. A., Weber, F., Bicknell, A., Friend, L., Rickert, R., and Niwa, M. (2008). B- and T-cell Development Both Involve Activity of the Unfolded Protein Response Pathway. *Journal of Biological Chemistry*, 283(26), 17954–17961.

Cao, Y., Knöchel, S., Oswald, F., Donow, C., Zhao, H., and Knöchel, W. (2006). XBP1 forms a regulatory loop with BMP-4 and suppresses mesodermal and neural differentiation in Xenopus embryos. *Mechanisms of Development*, 123(1), 84–96.

Carvalho, P., Goder, V., and Rapoport, T. A. (2006). Distinct Ubiquitin-Ligase Complexes Define Convergent Pathways for the Degradation of ER Proteins. *Cell*, 126(2), 361–373.

Chan, L.Y., Mugler, C.F., Heinrich, S., Vallotton, P., and Weis, K. (2017). Non-invasive measurement of mRNA decay reveals translation initiation as the major determinant of mRNA stability. *bioRxiv* https://doi.org/10.1101/214775.

Chapman, R., Sidrauski, C., and Walter, P. (1998). Intracellular signaling from the endoplasmic reticulum to the nucleus. *Annu. Rev. Cell Dev. Biol.,* 14, 459–485.

Chapman, R. E., and Walter, P. (1997). Translational attenuation mediated by an mRNA intron. *Current Biology*, 7(11), 850–859.

Chen, J., Tresenrider, A., Chia, M., McSwiggen, D.T., Spedale, G., Jorgensen, V., Liao, H., van Werven, F.J., and Ünal, E. (2017). Kinetochore inactivation by expression of a repressive mRNA. *eLife* 6.

Cheng, Z., Otto, G.M., Powers, E.N., Keskin, A., Mertins, P., Carr, S., Jovanovic, M., and Brar, G.A. (2018). Pervasive, coordinated protein level changes driven by transcript isoform switching during meiosis. *Cell,* 172, 910–923.

Chia, M., Tresenrider, A., Chen, J., Spedale, G., Jorgensen, V., Ünal, E., and van Werven, F.J. (2017). Transcription of a 5' extended mRNA isoform directs dynamic chromatin changes and interference of a downstream promoter. *eLife* 6.

Church, C., Chapon, C., and Poyton, R.O. (1996). Cloning and characterization of PET100, a gene required for the assembly of yeast cytochrome c oxidase. *J. Biol. Chem.,* 271, 18499–18507.

Cohen, N., Breker, M., Bakunts, A., Pesek, K., Chas, A., Argemí, J., … Schuldiner, M. (2017). Iron affects Ire1 clustering propensity and the amplitude of endoplasmic reticulum stress signaling. *Journal of Cell Science*, 130(19), 3222–3233.

Cox, J., and Mann, M. (2008). MaxQuant enables high peptide identification rates, individualized p.p.b.-range mass accuracies and proteome-wide protein quantification. *Nat. Biotechnol.,* 26, 1367–1372.

Cox, J. S., Chapman, R. E., and Walter, P. (1997). The Unfolded Protein Response Coordinates the Production of Endoplasmic Reticulum Protein and Endoplasmic Reticulum Membrane. *Molecular Biology of the Cell*, 8, 1805–1814.

Cox, J. S., Shamu, C. E., and Walter, P. (1993). Transcriptional induction of genes encoding endoplasmic reticulum resident proteins requires a transmembrane protein kinase. *Cell*, 73(6), 1197–1206.

Cox, J.S., and Walter, P. (1996). A novel mechanism for regulating activity of a transcription factor that controls the unfolded protein response. *Cell,* 87, 391–404.

Credle, J. J., Finer-Moore, J. S., Papa, F. R., Stroud, R. M., and Walter, P. (2005). On the mechanism of sensing unfolded protein in the endoplasmic reticulum. *PNAS* 102(52), 18773-84.

Cullen, B.R., Lomedico, P.T., and Ju, G. (1984). Transcriptional interference in avian retroviruses--implications for the promoter insertion model of leukaemogenesis. *Nature*, 307, 241–245.

De Hoon, M.J.L., Imoto, S., Nolan, J., and Miyano, S. (2004). Open source clustering software*. Bioinforma. Oxf. Engl*., 20, 1453–1454.

Di Santo, R., Aboulhouda, S., and Weinberg, D. E. (2016). The fail-safe mechanism of post-transcriptional silencing of unspliced HAC1 mRNA. *ELife*, 5, e20069.

Esko, J. D., Bertozzi, C., and Schnaar, R. L. (2015). Chemical Tools for Inhibiting Glycosylation. Essentials of Glycobiology. *Cold Spring Harbor Laboratory Press*.

Farquhar, R., Honey, N., Murant, S. J., Bossier, P., Schultz, L., Montgomery, D., … Tuite, M. F. (1991). Protein disulfide isomerase is essential for viability in Saccharomyces cerevisiae. *Gene*, *108*(1), 81–89.

Federovitch, C. M., Ron, D., and Hampton, R. Y. (2005). The dynamic ER: experimental approaches and current questions. *Current Opinion in Cell Biology*, 17(4), 409–414.

Fordyce, P. M., Pincus, D., Kimmig, P., Nelson, C. S., El-Samad, H., Walter, P., and Derisi, J. L. (2012). Basic leucine zipper transcription factor Hac1 binds DNA in two distinct modes as revealed by microfluidic analyses. *PNAS*, 09(45):E3084-93.

Frakes, A. E., and Dillin, A. (2017). The UPRER: Sensor and Coordinator of Organismal Homeostasis. *Molecular Cell*, 66(6), 761–771.

Gao, B., Lee, S.-M., Chen, A., Zhang, J., Zhang, D. D., Kannan, K., … Fang, D. (2008). Synoviolin promotes IRE1 ubiquitination and degradation in synovial fibroblasts from mice with collagen-induced arthritis. *EMBO Reports*, 9(5), 480–485.

Gardner, B. M., Pincus, D., Gotthardt, K., Gallagher, C. M., and Walter, P. (2013). Endoplasmic reticulum stress sensing in the unfolded protein response. *Cold Spring Harbor Perspectives in Biology*, 5(3), a013169.

Gardner, B. M., and Walter, P. (2011). Unfolded Proteins Are Ire1-Activating Ligands That Directly Induce the Unfolded Protein Response. *Science*, 333(6051), 1891–1894.

Gass, J. N., Gifford, N. M., and Brewer, J. W. (2002). Activation of an unfolded protein response during differentiation of antibody-secreting B cells. *The Journal of Biological Chemistry*, 277(50), 49047–49054.

Gething, M. J., McCammon, K., and Sambrook, J. (1986). Expression of wild-type and mutant forms of influenza hemagglutinin: the role of folding in intracellular transport. *Cell*, 46(6), 939–950.

Goder, V., and Spiess, M. (2003). Molecular mechanism of signal sequence orientation in the endoplasmic reticulum. *The EMBO Journal*, 22(14), 3645–3653.

Gonzalez, T. N., Sidrauski, C., Dörfler, S., Walter, P., and Silverman, R. H. (1999). Mechanism of non-spliceosomal mRNA splicing in the unfolded protein response pathway. *The EMBO Journal*, 18(11), 3119–3132.

Halbleib, K., Pesek, K., Covino, R., Hofbauer, H. F., Wunnicke, D., Hänelt, I., … Ernst, R. (2017). Activation of the Unfolded Protein Response by Lipid Bilayer Stress. *Molecular Cell*, 67(4), 673–684.e8.

Han, J., and Kaufman, R.J. (2017). Physiological/pathological ramifications of transcription factors in the unfolded protein response. *Genes Dev.*, 31, 1417–1438.

Hanson, S. R., Culyba, E. K., Hsu, T.-L., Wong, C.-H., Kelly, J. W., and Powers, E. T. (2009). The core trisaccharide of an N-linked glycoprotein intrinsically accelerates folding and enhances stability. *PNAS*, 6(9), 3131-3136.

Hell, K., Tzagoloff, A., Neupert, W., and Stuart, R.A. (2000). Identification of Cox20p, a novel protein involved in the maturation and assembly of cytochrome oxidase subunit 2. *J. Biol. Chem.,* 275, 4571–4578.

Hollerer, I., Barker, J. C., Jorgensen, V., Tresenrider, A., Dugast-Darzacq, C., Darzacq, X., … Brar, G. A. (2018). mRNA expression-mediated gene repression in human cells. *BioRxiv*, 264721.

Hollien, J., Lin, J.H., Li, H., Stevens, N., Walter, P., and Weissman, J.S. (2009). Regulated Ire1-dependent decay of messenger RNAs in mammalian cells. *J. Cell Biol.,* 186, 323–331.

Hollien, J., and Weissman, J. S. (2006). Decay of Endoplasmic Reticulum-Localized mRNAs During the Unfolded Protein Response*. Science*, 313(5783), 104–107.

Homann, O.R., and Johnson, A.D. (2010). MochiView: versatile software for genome browsing and DNA motif analysis. *BMC Biol*, 8, 49.

Hu, C.-C. A., Dougan, S. K., Mcgehee, A. M., Love, J. C., and Ploegh, H. L. (2009). XBP-1 regulates signal transduction, transcription factors and bone marrow colonization in B cells. *The EMBO Journal*, 28.

Ingolia, N.T., Ghaemmaghami, S., Newman, J.R.S., and Weissman, J.S. (2009). Genome-wide analysis in vivo of translation with nucleotide resolution using ribosome profiling. *Science,* 324, 218–223.

Iwakoshi, N. N., Lee, A.-H., Vallabhajosyula, P., Otipoby, K. L., Rajewsky, K., and Glimcher, L. H. (2003). Plasma cell differentiation and the unfolded protein response intersect at the transcription factor XBP-1. *Nature Immunology*, 4(4), 321–329.

Iwawaki, T., Akai, R., Yamanaka, S., and Kohno, K. (2009). Function of IRE1 alpha in the placenta is essential for placental development and embryonic viability. *Proceedings of the National Academy of Sciences*, 106(39), 16657–16662.

Jiang, Y., Cheng, Z., Mandon, E. C., and Gilmore, R. (2008). An interaction between the SRP receptor and the translocon is critical during cotranslational protein translocation. *The Journal of Cell Biology*, 180(6), 1149–1161.

Jomaa, A., Fu, Y.-H. H., Boehringer, D., Leibundgut, M., Shan, S., and Ban, N. (2017). Structure of the quaternary complex between SRP, SR, and translocon bound to the translating ribosome*. Nature Communications*, 8, 15470.

Jonikas, M.C., Collins, S.R., Denic, V., Oh, E., Quan, E.M., Schmid, V., Weibezahn, J., Schwappach, B., Walter, P., Weissman, J.S., et al. (2009). Comprehensive characterization of genes required for protein folding in the endoplasmic reticulum. *Science,* 323, 1693–1697.

Karagöz, G. E., Acosta-Alvear, D., Nguyen, H. T., Lee, C. P., Chu, F., and Walter, P.

(2017). An unfolded protein-induced conformational switch activates mammalian IRE1. *ELife*, 6, e30700.

Karimi, M. A., Aguilar, O., Zou, B., Bachmann, M. H., Carlyle, J. R., Baldwin, C. L., and Kambayashi, T. (2014). A truncated human NKG2D splice isoform negatively regulates NKG2D-mediated function. *Journal of Immunology*, 193(6), 2764–2771.

Kawahara, T., Yanagi, H., Yura, T., and Mori, K. (1997). Endoplasmic Reticulum Stress-induced mRNA Splicing Permits Synthesis of Transcription Factor Hac1p/Ern4p That Activates the Unfolded Protein Response. *Molecular Biology of the Cell*, 8, 1845–1862.

Keshishian, H., Burgess, M.W., Gillette, M.A., Mertins, P., Clauser, K.R., Mani, D.R., Kuhn, E.W., Farrell, L.A., Gerszten, R.E., and Carr, S.A. (2015). Multiplexed, Quantitative Workflow for Sensitive Biomarker Discovery in Plasma Yields Novel Candidates for Early Myocardial Injury. *Mol. Cell. Proteomics MCP,* 14, 2375–2393.

Kim, W., Spear, E. D., and Ng, D. T. W. (2005). Yos9p Detects and Targets Misfolded Glycoproteins for ER-Associated Degradation. *Molecular Cell*, 19(6), 753–764.

Kimata, Y., Ishiwata-Kimata, Y., Ito, T., Hirata, A., Suzuki, T., Oikawa, D., … Kohno, K. (2007). Two regulatory steps of ER-stress sensor Ire1 involving its cluster formation and interaction with unfolded proteins. *The Journal of Cell Biology*, 179(1), 75–86.

Kimata, Y., Oikawa, D., Shimizu, Y., Ishiwata-Kimata, Y., and Kohno, K. (2004). A role for BiP as an adjustor for the endoplasmic reticulum stress-sensing protein Ire1. *The Journal of Cell Biology*, 167(3), 445–456.

Kimura, T., Hosoda, Y., Sato, Y., Kitamura, Y., Ikeda, T., Horibe, T., and Kikuchi, M. (2005). Interactions among yeast protein-disulfide isomerase proteins and endoplasmic reticulum chaperone proteins influence their activities. *The Journal of Biological Chemistry*, 280(36), 31438–31441.

Kiss, D.L., Waters, C.E., Ouda, I.M., Saldivar, J.C., Karras, J.R., Amin, Z.A., Mahrous, S., Druck, T., Bundschuh, R.A., Schoenberg, D.R., et al. (2017a). Identification of Fhit as a post-transcriptional effector of Thymidine Kinase 1 expression. *Biochim. Biophys. Acta*, 1860, 374–382.

Kiss, D.L., Baez, W., Huebner, K., Bundschuh, R., and Schoenberg, D.R. (2017b). Impact of FHIT loss on the translation of cancer-associated mRNAs. *Mol. Cancer*, 16, 179.

Klapholz, S., and Esposito, R. E. (1980). Isolation of SPO12-1 and SPO13-1 from a

natural variant of yeast that undergoes a single meiotic division. *Genetics*, 96(3), 567–588.

Kodzius, R., Kojima, M., Nishiyori, H., Nakamura, M., Fukuda, S., Tagami, M., … Carninci, P. (2006). CAGE: cap analysis of gene expression. *Nature Methods*, 3(3), 211–222.

Kohno, K., Normington, K., Sambrook, J., Gething, M. J., and Mori, K. (1993). The promoter region of the yeast KAR2 (BiP) gene contains a regulatory domain that responds to the presence of unfolded proteins in the endoplasmic reticulum. *Molecular and Cellular Biology*, 13(2), 877–890.

Korennykh, A. V., Egea, P. F., Korostelev, A. A., Finer-Moore, J., Zhang, C., Shokat, K. M., … Walter, P. (2009). The unfolded protein response signals through high-order assembly of Ire1. *Nature*, 457(7230), 687–693.

Kozutsumi, Y., Segal, M., Normington, K., Gething, M.-J., and Sambrook, J. (1988). The presence of malfolded proteins in the endoplasmic reticulum signals the induction of glucose-regulated proteins. *Nature*, 332(6163), 462–464.

Krishnan, K., Ren, Z., Losada, L., Nierman, W.C., Lu, L.J., and Askew, D.S. (2014). Polysome profiling reveals broad translatome remodeling during endoplasmic reticulum (ER) stress in the pathogenic fungus Aspergillus fumigatus. *BMC Genomics,* 15, 159.

Kuhn, K. M., DeRisi, J. L., Brown, P. O., and Sarnow, P. (2001). Global and specific translational regulation in the genomic response of Saccharomyces cerevisiae to a rapid transfer from a fermentable to a nonfermentable carbon source. *Molecular and Cellular Biology*, 21(3), 916–927.

Labunskyy, V.M., Gerashchenko, M.V., Delaney, J.R., Kaya, A., Kennedy, B.K., Kaeberlein, M., and Gladyshev, V.N. (2014). Lifespan extension conferred by endoplasmic reticulum secretory pathway deficiency requires induction of the unfolded protein response. *PLoS Genet*., 10, e1004019.

Lacroute, F. (1968). Regulation of pyrimidine biosynthesis in Saccharomyces cerevisiae. *Journal of Bacteriology*, 95(3), 824–832.

Langmead, B., and Salzberg, S.L. (2012). Fast gapped-read alignment with Bowtie 2. *Nat. Methods*, 9, 357–359.

Law, G.L., Bickel, K.S., MacKay, V.L., and Morris, D.R. (2005). The undertranslated transcriptome reveals widespread translational silencing by alternative 5' transcript leaders. *Genome Biol.,* 6, R111.

Laufen, T., Mayer, M. P., Beisel, C., Klostermeier, D., Mogk, A., Reinstein, J., and

Bukau, B. (1999). Mechanism of regulation of Hsp70 chaperones by DnaJ cochaperones. *PNAS*, 96, 5452–5457.

Lee, B. H., and Amon, A. (2003). Role of Polo-like Kinase CDC5 in Programming Meiosis I Chromosome Segregation. *Science*, 300(5618), 482–486.

Lee, J.E., Oney, M., Frizzell, K., Phadnis, N., and Hollien, J. (2015). Drosophila melanogaster activating transcription factor 4 regulates glycolysis during endoplasmic reticulum stress. *G3*, 5, 667–675.

Lee, K., Neigeborn, L., and Kaufman, R.J. (2003). The unfolded protein response is required for haploid tolerance in yeast. *J. Biol. Chem*., 278, 11818–11827.

Lee, S., Liu, B., Lee, S., Huang, S.-X., Shen, B., and Qian, S.-B. (2012). Global mapping of translation initiation sites in mammalian cells at single-nucleotide resolution. *PNAS,* 109(37), E2424-32

Liu, Y., Stuparevic, I., Xie, B., Becker, E., Law, M. J., and Primig, M. (2015). The conserved histone deacetylase Rpd3 and the DNA binding regulator Ume6 repress BOI 1 's meiotic transcript isoform during vegetative growth in Saccharomyces cerevisiae. *Molecular Microbiology*, 96(4), 861–874.

Longtine, M.S., McKenzie, A., Demarini, D.J., Shah, N.G., Wach, A., Brachat, A., Philippsen, P., and Pringle, J.R. (1998). Additional modules for versatile and economical PCR-based gene deletion and modification in Saccharomyces cerevisiae. *Yeast*,14, 953–961.

Louie, S.M., Grossman, E.A., Crawford, L.A., Ding, L., Camarda, R., Huffman, T.R., Miyamoto, D.K., Goga, A., Weerapana, E., and Nomura, D.K. (2016). GSTP1 Is a Driver of Triple-Negative Breast Cancer Cell Metabolism and Pathogenicity. *Cell Chem. Biol.,* 23, 567–578.

Maier, T., Güell, M., and Serrano, L. (2009). Correlation of mRNA and protein in complex biological samples*. FEBS Letters*, 583(24), 3966–3973.

Manford, A. G., Stefan, C. J., Yuan, H. L., MacGurn, J. A., and Emr, S. D. (2012). ER-to-Plasma Membrane Tethering Proteins Regulate Cell Signaling and ER Morphology. *Developmental Cell*, 23(6), 1129–1140.

Martens, J.A., Laprade, L., and Winston, F. (2004). Intergenic transcription is required to repress the Saccharomyces cerevisiae SER3 gene. *Nature,* 429, 571–574.

Maurel, M., Chevet, E., Tavernier, J., and Gerlo, S. (2014). Getting RIDD of RNA: IRE1 in cell fate regulation. *Trends Biochem. Sci.,* 39, 245–254.

Mayer, M. P., and Bukau, B. (2005). Hsp70 chaperones: cellular functions and

molecular mechanism. *Cellular and Molecular Life Sciences : CMLS*, 62(6), 670–684.

Metzger, M.B., and Michaelis, S. (2008). Analysis of Quality Control Substrates in Distinct Cellular Compartments Reveals a Unique Role for Rpn4p in Tolerating Misfolded Membrane Proteins. *Mol. Biol. Cell*, 20, 1006–1019.

Mori, K., Kawahara, T., Yoshida, H., Yanagi, H., and Yura, T. (1996). Signalling from endoplasmic reticulum to nucleus: transcription factor with a basic-leucine zipper motif is required for the unfolded protein-response pathway. *Genes Cells*, 1, 803–817.

Mori, K., Ma, W., Gething, M. J., and Sambrook, J. (1993). A transmembrane protein with a cdc2+/CDC28-related kinase activity is required for signaling from the ER to the nucleus. *Cell*, 74(4), 743–756.

Mori, K., Ogawa, N., Kawahara, T., Yanagi, H., and Yura, T. (1998). Palindrome with spacer of one nucleotide is characteristic of the cis-acting unfolded protein response element in Saccharomyces cerevisiae. *The Journal of Biological Chemistry*, 273(16), 9912–9920.

Mori, K., Sant, A., Kohno, K., Normington, K., Gething, M. J., and Sambrook, J. F. (1992). A 22 bp cis-acting element is necessary and sufficient for the induction of the yeast KAR2 (BiP) gene by unfolded proteins. *The EMBO Journal*, 11(7), 2583–2593.

Moseley, J.L., Page, M.D., Alder, N.P., Eriksson, M., Quinn, J., Soto, F., Theg, S.M., Hippler, M., and Merchant, S. (2002). Reciprocal Expression of Two Candidate Di-Iron Enzymes Affecting Photosystem I and Light-Harvesting Complex Accumulation. *Plant Cell*, 14, 673–688.

Munro, S., and Pelham, H. R. (1986). An Hsp70-like protein in the ER: identity with the 78 kd glucose-regulated protein and immunoglobulin heavy chain binding protein. *Cell*, 46(2), 291–300.

Munson, A. M., Love, S. L., Shu, J., Palanivel, V. R., and Rosenwald, A. G. (2004). ARL1 participates with ATC1/LIC4 to regulate responses of yeast cells to ions. *Biochemical and Biophysical Research Communications*, 315(3), 617–623.

Nishimura, K., Fukagawa, T., Takisawa, H., Kakimoto, T., and Kanemaki, M. (2009). An auxin-based degron system for the rapid depletion of proteins in nonplant cells. *Nat. Methods*, 6, 917–922.

Normington, K., Kohno, K., Kozutsumi, Y., Gething, M. J., and Sambrook, J. (1989). S. cerevisiae encodes an essential protein homologous in sequence and function to mammalian BiP. *Cell*, 57(7), 1223–1236.

Ogawa, N., and Mori, K. (2004). Autoregulation of the HAC1 gene is required for sustained activation of the yeast unfolded protein response. *Genes Cells Devoted Mol. Cell. Mech.,* 9, 95–104.

Okamura, K., Kimata, Y., Higashio, H., Tsuru, A., and Kohno, K. (2000). Dissociation of Kar2p/BiP from an ER Sensory Molecule, Ire1p, Triggers the Unfolded Protein Response in Yeast. *Biochemical and Biophysical Research Communications*, 279(2), 445–450.

Otto, G.M., and Brar, G.A. (2018). Seq-ing answers: uncovering the unexpected in global gene regulation. *Curr. Genet.*

Ottoz, D. S. M., Rudolf, F., and Stelling, J. (2014). Inducible, tightly regulated and growth condition-independent transcription factor in Saccharomyces cerevisiae. *Nucleic Acids Research*, 42(17), e130–e130.

Pal, B., Chan, N. C., Helfenbaum, L., Tan, K., Tansey, W. P., and Gething, M.-J. (2007). SCFCdc4-mediated degradation of the Hac1p transcription factor regulates the unfolded protein response in Saccharomyces cerevisiae. *Molecular Biology of the Cell*, 18(2), 426–440.

Papa, F. R., Zhang, C., Shokat, K., and Walter, P. (2003). Bypassing a Kinase Activity with an ATP-Competitive Drug. *Science*, 302(5650), 1533–1537.

Parlati, F., Dominguez, M., Bergeron, J. J., and Thomas, D. Y. (1995). Saccharomyces cerevisiae CNE1 encodes an endoplasmic reticulum (ER) membrane protein with sequence similarity to calnexin and calreticulin and functions as a constituent of the ER quality control apparatus. *The Journal of Biological Chemistry*, 270(1), 244–253.

Patil, C.K., Li, H., and Walter, P. (2004). Gcn4p and novel upstream activating sequences regulate targets of the unfolded protein response. *PLoS Biol.,* 2, E246.

Payne, T., Hanfrey, C., Bishop, A.L., Michael, A.J., Avery, S.V., and Archer, D.B. (2008). Transcript-specific translational regulation in the unfolded protein response of Saccharomyces cerevisiae. *FEBS Lett.,* 582, 503–509.

Pearse, B. R., and Hebert, D. N. (2010). Lectin chaperones help direct the maturation of glycoproteins in the endoplasmic reticulum. *Biochimica et Biophysica Acta*, 1803(6), 684–693.

Pincus, D., Chevalier, M. W., Aragón, T., van Anken, E., Vidal, S. E., El-Samad, H., and

Walter, P. (2010). BiP Binding to the ER-Stress Sensor Ire1 Tunes the Homeostatic Behavior of the Unfolded Protein Response. *PLoS Biology*, 8(7), e1000415.

Pollard, M. G., Travers, K. J., and Weissman, J. S. (1998). Ero1p: A Novel and Ubiquitous Protein with an Essential Role in Oxidative Protein Folding in the Endoplasmic Reticulum. *Molecular Cell*, 1(2), 171–182.

Promlek, T., Ishiwata-Kimata, Y., Shido, M., Sakuramoto, M., Kohno, K., and Kimata, Y. (2011). Membrane aberrancy and unfolded proteins activate the endoplasmic reticulum stress sensor Ire1 in different ways. *Molecular Biology of the Cell*, 22(18), 3520–3532.

Rappsilber, J., Mann, M., and Ishihama, Y. (2007). Protocol for micro-purification, enrichment, pre-fractionation and storage of peptides for proteomics using StageTips. *Nat Protoc.,* 2, 1896–1906.

Reimold, A. M., Etkin, A., Clauss, I., Perkins, A., Friend, D. S., Zhang, J., … Glimcher, L. H. (2000). An essential role in liver development for transcription factor XBP-1. *Genes and Development*, 14(2), 152–157.

Reimold, A. M., Iwakoshi, N. N., Manis, J., Vallabhajosyula, P., Szomolanyi-Tsuda, E., Gravallese, E. M., … Glimcher, L. H. (2001). Plasma cell differentiation requires the transcription factor XBP-1. *Nature*, 412(6844), 300–307.

Rüegsegger, U., Leber, J. H., and Walter, P. (2001). Block of HAC1 mRNA translation by long-range base pairing is released by cytoplasmic splicing upon induction of the unfolded protein response. *Cell*, 107(1), 103–114.

Rutkowski, D. T., and Hegde, R. S. (2010). Regulation of basal cellular physiology by the homeostatic unfolded protein response. *The Journal of Cell Biology*, 189(5), 783–794.

Saldanha, A.J. (2004). Java Treeview--extensible visualization of microarray data. *Bioinforma. Oxf. Engl.,* 20, 3246–3248.

Sathe, L., Bolinger, C., Mannan, M.A., Dever, T.E., and Dey, M. (2015). Evidence That Base-pairing Interaction between Intron and mRNA Leader Sequences Inhibits Initiation of HAC1 mRNA Translation in Yeast. *J. Biol. Chem.*, 290, 21821–21832.

Schröder, M., Chang, J. S., and Kaufman, R. J. (2000). The unfolded protein response represses nitrogen-starvation induced developmental differentiation in yeast. *Genes and Development*, 14(23), 2962–2975.

Schuldiner, M., and Weissman, J.S. (2013). The Contribution of Systematic Approaches

to Characterizing the Proteins and Functions of the Endoplasmic Reticulum. *Cold Spring Harb. Perspect. Biol.,* 5, a013284–a013284.

Sehgal, A., Hughes, B.T., and Espenshade, P.J. (2008). Oxygen-dependent, alternative promoter controls translation of tco1 + in fission yeast. *Nucleic Acids Res.,* 36, 2024–2031.

Séraphin, B. (1992). The HIT protein family: a new family of proteins present in prokaryotes, yeast and mammals. *DNA Seq. J. DNA Seq. Mapp.,* 3, 177–179.

Sevier, C. S., and Kaiser, C. A. (2002). Formation and transfer of disulphide bonds in living cells. *Nature Reviews Molecular Cell Biology*, 3(11), 836–847.

Shamu, C. E., and Walter, P. (1996). Oligomerization and phosphorylation of the Ire1p kinase during intracellular signaling from the endoplasmic reticulum to the nucleus. *The EMBO Journal*, 15(12), 3028–3039.

Shearwin, K., Callen, B., and Egan, J. (2005). Transcriptional interference – a crash course*. Trends in Genetics*, 21(6), 339–345.

Shental-Bechor, D., and Levy, Y. (2008). Effect of glycosylation on protein folding: A close look at thermodynamic stabilization. *PNAS,* 105(24), 8256-61.

Sidrauski, C., Cox, J.S., and Walter, P. (1996). tRNA ligase is required for regulated mRNA splicing in the unfolded protein response. *Cell*, 87, 405–413.

Sidrauski, C., and Walter, P. (1997). The Transmembrane Kinase Ire1p Is a Site-Specific Endonuclease That Initiates mRNA Splicing in the Unfolded Protein Response. *Cell*, 90(6), 1031–1039.

Silberstein, S., Schlenstedt, G., Silver, P. A., and Gilmore, R. (1998). A role for the DnaJ homologue Scj1p in protein folding in the yeast endoplasmic reticulum. *The Journal of Cell Biology*, 143(4), 921–933.

Stevenson, J., Huang, E. Y., and Olzmann, J. A. (2016). Endoplasmic Reticulum-Associated Degradation and Lipid Homeostasis. *Ann. Rev. Nutr.,* 36, 511-542.

Suda, Y., Nakanishi, H., Mathieson, E. M., and Neiman, A. M. (2007). Alternative modes of organellar segregation during sporulation in Saccharomyces cerevisiae. *Eukaryotic Cell*, 6(11), 2009–2017.

Taggart, J., MacDiarmid, C. W., Haws, S., and Eide, D. J. (2017). Zap1-dependent transcription from an alternative upstream promoter controls translation of RTC4 mRNA in zinc-deficient Saccharomyces cerevisiae. *Molecular Microbiology*, 106(5), 678–689.

Tellier, J., Shi, W., Minnich, M., Liao, Y., Crawford, S., Smyth, G. K., … Nutt, S. L. (2016). Blimp-1 controls plasma cell function through the regulation of immunoglobulin secretion and the unfolded protein response. *Nature Immunology*, 17(3), 323–330.

Titov, D.V., Cracan, V., Goodman, R.P., Peng, J., Grabarek, Z., and Mootha, V.K. (2016). Complementation of mitochondrial electron transport chain by manipulation of the NAD+/NADH ratio. *Science*, 352, 231–235.

Travers, K.J., Patil, C.K., Wodicka, L., Lockhart, D.J., Weissman, J.S., and Walter, P. (2000). Functional and genomic analyses reveal an essential coordination between the unfolded protein response and ER-associated degradation. *Cell*, 101, 249–258.

Tresenrider, A., and Ünal, E. (2018). One-two punch mechanism of gene repression: a fresh perspective on gene regulation. *Curr. Genet.*, 64(3) 581-588.

van Anken, E., Pincus, D., Coyle, S., Aragón, T., Osman, C., Lari, F., … Walter, P. (2014). Specificity in endoplasmic reticulum-stress signaling in yeast entails a step-wise engagement of HAC1 mRNA to clusters of the stress sensor Ire1. *ELife*, 3, e05031.

van Anken, E., Romijn, E. P., Maggioni, C., Mezghrani, A., Sitia, R., Braakman, I., and Heck, A. J. . (2003). Sequential Waves of Functionally Related Proteins Are Expressed When B Cells Prepare for Antibody Secretion. *Immunity*, 18(2), 243–253.

van Werven, F. J., and Amon, A. (2011). Regulation of entry into gametogenesis. *Philosophical Transactions of the Royal Society of London. Series B, Biological Sciences*, 366(1584), 3521–3531.

Vander Heiden, M.G., Cantley, L.C., and Thompson, C.B. (2009). Understanding the Warburg effect: the metabolic requirements of cell proliferation. *Science*, 324, 1029–1033.

van Werven, F. J., Neuert, G., Hendrick, N., Lardenois, A., Buratowski, S., van Oudenaarden, A., … Amon, A. (2012). Transcription of Two Long Noncoding RNAs Mediates Mating-Type Control of Gametogenesis in Budding Yeast. *Cell*, 150(6), 1170–1181.

Volmer, R., Van Der Ploeg, K., and Ron, D. (2013). Membrane lipid saturation activates endoplasmic reticulum unfolded protein response transducers through their transmembrane domains. *PNAS*, 110(12), 4628-4633.

Voorhees, R. M., and Hegde, R. S. (2016). Toward a structural understanding of co-translational protein translocation. *Current Opinion in Cell Biology*, 41, 91–99.

Walter, P., and Ron, D. (2011). The unfolded protein response: from stress pathway to homeostatic regulation. *Science*, 334, 1081–1086.

Warburg, O. (1956). On the Origin of Cancer Cells. Science 123, 309–314.

Weidberg, H., Moretto, F., Spedale, G., Amon, A., and van Werven, F. J. (2016). Nutrient Control of Yeast Gametogenesis Is Mediated by TORC1, PKA and Energy Availability. *PLoS Genetics*, 12(6), e1006075.

Welihinda, A. A., and Kaufman, R. J. (1996). The unfolded protein response pathway in Saccharomyces cerevisiae. Oligomerization and trans-phosphorylation of Ire1p (Ern1p) are required for kinase activation. *The Journal of Biological Chemistry*, 271(30), 18181–18187.

Wenger, C.D., Lee, M.V., Hebert, A.S., McAlister, G.C., Phanstiel, D.H., Westphall, M.S., and Coon, J.J. (2011). Gas-phase purification enables accurate, multiplexed proteome quantification with isobaric tagging. *Nat. Methods*, 8, 933–935.

Xie, B., Horecka, J., Chu, A., Davis, R. W., Becker, E., and Primig, M. (2016). Ndt80 activates the meiotic ORC1 transcript isoform and SMA2 via a bi-directional middle sporulation element in Saccharomyces cerevisiae. *RNA Biology*, 13(9), 772–782.

Xu, L., Ajimura, M., Padmore, R., Klein, C., and Kleckner, N. (1995). NDT80, a meiosis-specific gene required for exit from pachytene in Saccharomyces cerevisiae. *Molecular and Cellular Biology*, 15(12), 6572–6581.